OPTIMIZED DESIGN OF A COMPOSITE HELICOPTER STRUCTURE BY RESIN TRANSFER MOULDING

By

France Thériault

May, 2007

Composite Materials Group

Department of Mechanical Engineering

McGill University, Montreal, QC, Canada, H3A 2K6

A Thesis Submitted to

McGill University

in Partial Fulfillment of the Requirements of the Degree of

Master of Engineering

Your file Votre référence
ISBN: 978-0-494-32623-7
Our file Notre référence
ISBN: 978-0-494-32623-7

ABSTRACT

This research project is partnership project involving industrial, university and government collaborators. The overall objective is to develop and enhance tools for use in Resin Transfer Moulding (RTM) design technology in order to re-design existing metallic parts using composite materials.

The specific objective of this work is to present preliminary research findings of the development of an optimized design of a leading edge slat (horizontal stabilizer component) from the Bell Model 407 Helicopter. The results presented here focus on the static stress analysis and the structure design aspects. The findings will serve as a basis for future design optimization as well as further developments in the use of RTM technology in re-designing metallic aeronautic components and can be considered to be "semi-optimized".

This research is based on extensive finite element analysis (FEA) of several composite material configurations, with a comparison made with the original metallic design. Different key criteria of the part design such as ply lay-up, bracket geometry, angle and configuration are tested using FEA technology with the objective of selecting the design which is minimizing stress concentrations. The influence of the modification of model-related parameters was also studied.

Preliminary comparative studies show that the slat configuration with half brackets opened towards the inside with an angle of 70 degrees (angle between the top of the airfoil and the side of the bracket) is the best option according to minimum stress concentration and structural flexibility. This choice is confirmed by other factors such as material savings and ease of processing.

RÉSUMÉ

Ce projet de recherche est un partenariat impliquant plusieurs collaborateurs de secteurs industriel, universitaire et gouvernemental. L'objectif général est le développement et l'amélioration des outils technologiques utilisés dans la conception du moulage à injection sur renfort (resin transfer moulding - RTM) dans le but de reconcevoir des pièces métallique existantes en utilisant des matériaux composites.

L'objectif spécifique de ce travail est de présenter les résultats de l'étude préliminaire du développement d'un modèle optimisé d'un bec de bord d'attaque (composante de l'empennage horizontal) du modèle 407 de Bell Hélicoptère. Les résultats présentés se concentrent sur les aspects de l'analyse statique et la conception structurale. Les conclusions serviront de point de départ pour les optimisations futures ainsi que les développements additionnels de l'utilisation de la technologie RTM dans la re-conception de composantes aéronautiques métalliques. Elles peuvent donc être considérées comme étant « semi-optimisées ».

Cette recherche est fondée sur des analyses par éléments finis (finite element analysis FEA) exhaustives réalisées avec plusieurs configurations de matériaux composites et comparées avec le modèle métallique original. Différents critères déterminants de la conception de la pièce tels que la disposition des couches, la géométrie des supports d'attache et leur configuration sont testés utilisant la technologie FEA dans l'objectif de sélectionner le modèle minimisant la concentration de contraintes. L'influence des modifications des paramètres reliés à la conception des modèles ont également été étudiés.

Les études comparatives préliminaires démontrent que la configuration du bec de bord d'attaque avec les demi-supports d'attache ouverts vers l'intérieur avec un angle de 70 degrés (angle entre le dessus du profil d'aile et le côté des supports d'attache) est la meilleure option selon la concentration de contraintes minimale et la flexibilité de la structure. Ce choix est confirmé par d'autres facteurs tels que l'économie du matériau et la facilité de production.

ACKNOWLEGMENTS

I would like to thank **Professor Larry Lessard** for giving me the great opportunity to live the Master's experience at McGill. He opened the door to a truly enriching experience I will always remember. Thanks to:

- **Loleï Khoun**, **Meysam Rahmat**, **Kamal Adhikari**, **Geneviève Palardy**, **Julian O'Flynn**, **Zemfira Khisaeva**, **Guru Sosale**, **Behnam Ashrafi** and everybody else from **FDA 015** and the **Composite group** for their support and patience throughout hard times and all the wonderful unforgettable memories
- **Professor Pascal Hubert** for his advice and professionalism
- **Simon Bernier** and **Pieter Minderhoud** from Bell Helicopter for their FEA expertise and valuable help
- **Yannick Banaszak** for teaching me everything I know on Patran/Nastran
- **Marc-André Octeau** for sharing his experience and ideas
- **Jonathan Laliberté** and **François Diquinzio** for their availability and software skills
- All the collaborators in the **R&D-CRIAQ1.15** project for their advice and knowledge
- **Gabrielle Migner-Laurin**, **David Marcel**, **Annie Mantha**, **Marie-Hélène Savard** and **Mai Tran** for being there for me
- My family, **Donald**, **Marie-May**, **Stéphane** and **Chantal** for always believing in me
- **Pierre Grimaud** for being the loveliest "lapaon" I know

I would also like to thank the **Natural Sciences and Engineering Research Council of Canada (NSERC)** for their financial support.

TABLE OF CONTENTS

LIST OF TABLES

LIST OF FIGURES

1. INTRODUCTION

Helicopters were amongst the first types of aircraft to incorporate composites in their primary structure. Composite material's stiffness, lightweight and unique design capabilities have made them appealing materials for both structural and non-structural components. In military rotorcraft, where the application of technology is more audacious, composites now constitute 50 to 80 percent of the airframe, by weight [1]. However, in the civil aviation sector, composite application is more conservative due to several factors such as lack of experience, established manufacturing philosophy and available R&D budget.

Bell Helicopter Textron has been one of the few companies able to extend military experience into composites-intensive civil helicopters [1]. The non-negligible advantages of composites are the main motivation for such changes. These materials allow designers to reduce the number of parts, thus reducing manufacturing cost [2].

This work is associated with the Consortium for Research and Innovation in Aerospace in Quebec (CRIAQ). It is part of a larger project involving collaboration between two universities (McGill and École Polytechnique), two industrial partners (Bell Helicopter Textron Canada and Delastek) and government organizations (Aerospace Manufacturing Technology Centre (AMTC), National Research Council of Canada (NRC), Natural Sciences and Engineering Research Council of Canada (NSERC), and Center for Applied Research on Polymers and Composites (CREPEC)).

This chapter introduces the objectives of the project, similar previous applications, a description and constraints of the slat, and an overview of the project.

1.1 Objectives of the project

The ultimate goal of this collaboration project is to develop and enhance tools for use in Resin Transfer Moulding (RTM) design technology in order to re-design existing metallic parts [3]. To do so, a more specific task is determined: develop an optimized design of a leading edge slat from the Bell Model 407 Helicopter. This task is to be completed using composite materials and the RTM process. This document presents the preliminary findings that will serve as a basis for future optimization of this helicopter component. This work should then be considered to be "semi-optimized".

The project can be divided in three main sections: Analysis, Optimization and Verification (Figure 1.1). The analysis section has three subsections: static stress and failure, RTM flow simulation and fatigue failure. These subsections lead to the optimization process that is followed by two subsections: structural design and RTM manufacturing design. All of these operations lead ultimately to the verification process.

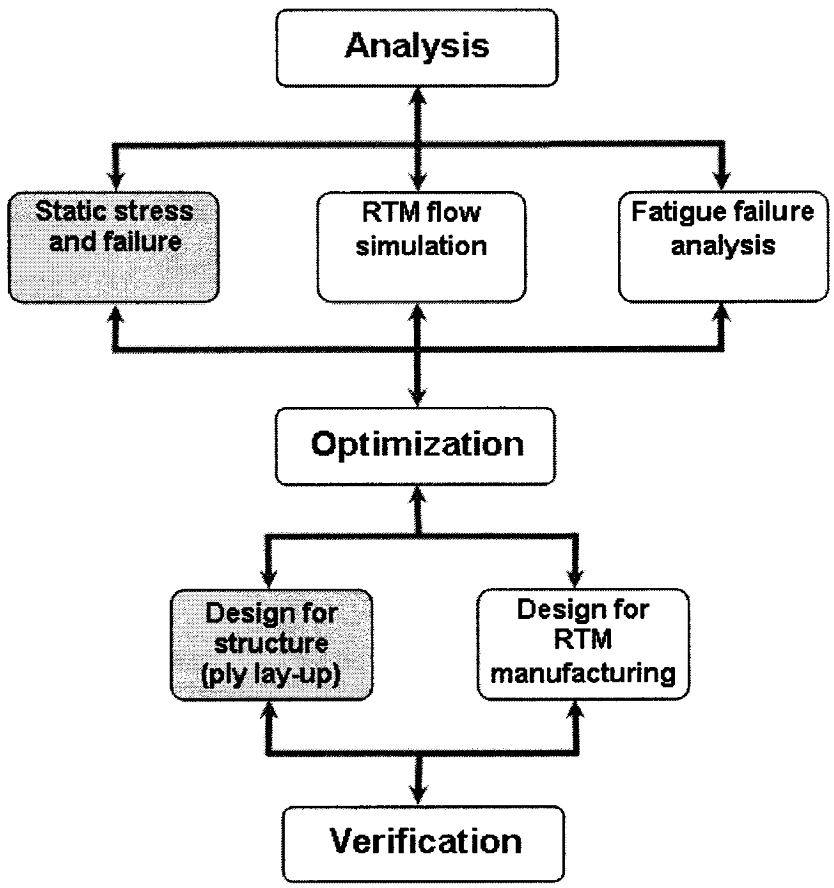

Figure 1.1: Flowchart of the different sections of the project

This work is part of the preliminary steps of the project and focuses on the static stress analysis and the structure design (See shaded areas in the flowchart of Figure 1.1). The fatigue failure analysis and the RTM design aspects (manufacturing process, mould design) are studied by other collaborators at McGill. The flow simulation part is covered by a group at École Polytechnique.

Delastek and the Aerospace Manufacturing Technology Centre (AMTC) will contribute to the verification process by manufacturing the moulds and process the part, respectively. Bell Helicopter is involved in all aspects of the project.

1.2 Similar applications

A Bell Helicopter Textron division in United States (Hurst, TX) in collaboration with Fiber Innovations (Walpole, MA) [4-6] investigated the development of a one-piece, low-cost horizontal stabilizer using composite materials (carbon fibres and bismaleimide (BMI) resin). A hybrid approach combining the benefits of tailored braids with unidirectional and woven fabrics was used. The part was designed to fly on a Modular Affordable Product Line (MAPL) demonstrator aircraft. The main aspects of this trade study are weight savings, recurring (material purchase) and non-recurring cost (mould), design complexity and reparability. The constant section horizontal stabilizer was manufactured using RTM process with the objective of reducing the costs by reducing parts count, subassemblies and associated surface preparation, bonding and inspection steps as well as simplifying the attachment to the fuselage.

Another Bell Helicopter Textron division in United States (Fort Worth, TX) [7, 8] replaced an aluminium horizontal stabilizer of an OH-58D aircraft by a re-designed fibre reinforced thermoplastic (FTRP) part. The objectives of this work were to demonstrate the durability of a thermoplastic component and achieving a 40% cost reduction. The concept was also minimizing part count. Carbon-fibre reinforced aromatic polymer composite was used for the spars and skins. The injection moulded lugs and ribs were made with polyetheretherketone (PEEK) resin with 30% discontinuous carbon fibre filler.

The Design and Manufacture of Low-Cost Composite Bonded Wing (DMLCC—BW) project involving Bell Helicopter (Fort Worth, TX) and American Air Force was a research and development program with the objective of identifying and developing new structural design concepts and manufacturing technologies to reduce production costs of advanced composite aircraft structures [9]. Within the scope of this study, Bell's V-22 Full Scale Development (FSD) wing structure was redesigned using composite materials [10]. This research focused on reducing part count, improving part integration and repeatability as well as minimizing recurring costs. Carbon/epoxy based material and RTM process technology were used. The strength of the component was demonstrated through several tests including full-scale static. Following this study, a second generation of designs was investigated: Bell/Agusta Aerospace (Fort Worth, TX) fabricated a composite wing skin for the world's first civil tilt rotor, the BA609 [10, 11]. The piece was made out of a mix of carbon/epoxy plain weave fabric and unidirectional fibres. Low cost process and minimized manufacturing time were the main design goals of this component.

Bell Helicopter Textron Canada in Mirabel, Quebec [12] designed a one piece composite slat for Bell 427 model. The part is made of carbon fibre fabric reinforced BMI and its brackets are single-sided. The lay-up is composed of a mix of 45 degree (for flexibility) and 0 degree (for edge stability) plies [13]. The deformation incompatibility between the horizontal stabilizer (in aluminium) and the composite slat is the main design challenge in this case.

Sikorsky Aircraft [14, 15] have integrated composites in horizontal stabilizers of the Sikorsky S-76 helicopter model for about 25 years already. In fact, it was the first airframe manufacturer to acquire certification on a primary structure of a commercial aircraft [16]. The parts are designed for static loads and elevated temperature and are mainly constructed of Kevlar/epoxy with graphite/epoxy beam caps. In the 1990's, a fibre placed Kevlar/epoxy horizontal stabilizer (with graphite spar caps) was designed for the Boeing Sikorsky RAH-66 Comanche military rotorcraft [10, 17, 18]. This part was designed in order to successfully achieve design-to-cost goals as well as meeting aggressive performance and increased militarization requirements. More recently, a lightweight carbon / epoxy stabilator has been designed for the H-60 Black Hawk / Seahawk family of military helicopters [19, 20]. Once again, weight savings was the main motivation of this project. To evaluate the design, static tests were performed.

The Agusta Company [21] has extended the use of composite materials to stabilizers for more than two decades. The motivations of this transition were weight and cost reduction as well as the improvement of the dynamic characteristics in term of natural frequencies. Graphite, Kevlar and glass fibre epoxy resin pre-impregnated items were used for the design of the stabilizer for the Agusta A 109 helicopter. A form of computer-based mathematic optimization was used to obtain the required stiffness and strength characteristics while keeping weight as low as possible. The optimization module was containing all calculations covering the mass and stiffness characteristics as well as a section stress. The optimization variables for this study were material selection, laminate thickness and flow. The designed and manufactured assembly had to meet the requirements of interchangeability with the metal stabilizer currently installed.

Bell Helicopter Xworx organization's Advanced Concepts Engineering group [22] recently developed a composite elevator (horizontal stabilizer) for the H-1 upgrade aircraft. The interest in this design was the weight reduction of the tail boom and the cut down in the part count. The new design utilized Bismaleimide (BMI) composite materials and Kevlar honeycomb core. The composite prototype significantly reduced part count and reached an 18% reduction in weight compared to the previous metal elevator.

McDonnell Douglas Helicopter Company (merged with Boeing in 1997) [23, 24] redesigned a horizontal stabilizer for the AH-64A in the early 1990's using graphite-reinforced thermoplastic composites (carbon/PEEK). The main objectives of this primary structure design were to decrease the weight by around 20% over the existing metallic part and to reduce the major parts count by 50%. Low cost manufacturing was also an important aspect of this project. It was also demonstrating the application of thermoplastic composites to primary airframe structures. The stabilator was designed to match the characteristics of the existing metal structure, and to be fully interchangeable with the baseline unit. Static testing and finite element modeling techniques have been used.

Thus, several companies have experimented with composites for slat and stabilizer components. The various designs have used a variety of materials and manufacturing methods, but no clear optimal design exists. It seems that the establishment of a clear and organized methodology is necessary in order to improve and optimize future re-design processes.

This project focuses on means to facilitate the design of structures made of composite materials. Like the majority of the previous applications mentioned above, low cost manufacturing and an improved end product are common to most projects involving composite materials. This work brings a different perspective by establishing a link between the different key aspects of the design process (design, analysis and manufacturing). In this case, optimization schemes are integrated by focussing more on the preliminary design side using the leading edge slat as a demonstrator. The objectives are to greatly reduce design time and establish a critical competency for conception-to-production of primary aerospace composite components. This is done by using RTM, a low cost process with great optimization potential [3].

1.3 Slat: general description

The leading edge slat is a small airfoil-shaped wing rigidly installed on the leading edge of the stabilizer wing of the Bell Model 407 Helicopter (Figure 1.2). This seven-seat, single-engine helicopter is designated as "the sports car in the air" because it delivers one the best speed, payload, and travel range in its class [25].

Figure 1.2: Bell Model 407 Helicopter [25]

The stabilizer wing (see Figure 1.3 and Figure 1.4) is located on the helicopter's tail boom and eases flaring during autorotation landings by producing a downward lift. Endplates fixed on the tip of the stabilizer wing reduce the tip vortex by blocking the flow around the tip from top to bottom [26].

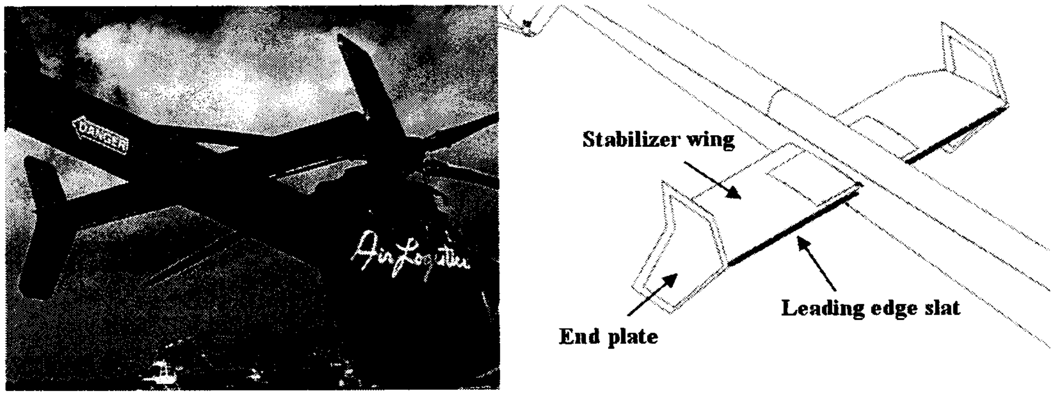

Figure 1.3: Rear view of the stabilizer wing assembly on the Bell 407 model (left) and localization of the stabilizer wing and the leading edge slat on the tail boom (right) [27]

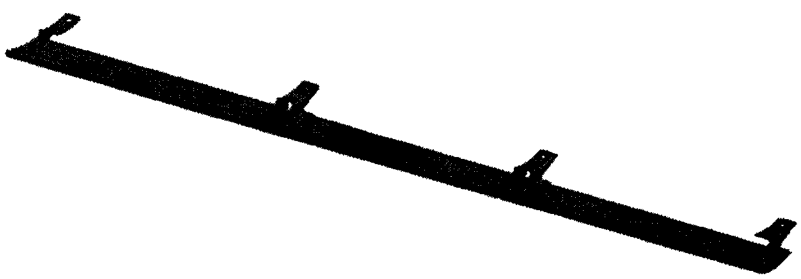

Figure 1.4: 3-D view of the leading edge slat.

By energizing the boundary layer below the wing, the slat delays the stall, thus improving the airflow conditions at greater angle of attack and slower speeds (Figure 1.5) [6, 27].

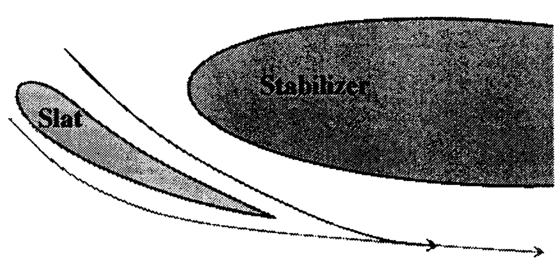

Figure 1.5: Air flowing between the slat and the stabilizer

In spite of its small dimensions (about 889 mm length and 76.2 mm width), the slat can cause non-insignificant damage when it fails in service.

Several times in the past, it has been recorded that this part has demonstrated premature cracking at the radiuses (shaded area of Figure 1.6). The top radius is the more critical of the two.

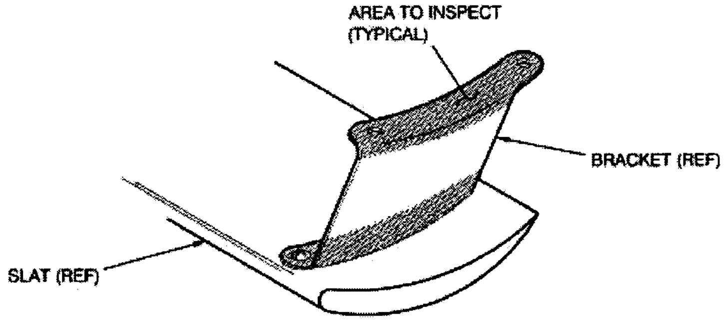

Figure 1.6: Areas at risk for premature cracking (shaded) [28]

The consequences of a slat failure could be serious, causing the part to strike the tail rotor blade as it departs the structure [29]. Thus, other components of the helicopter could be subsequently damaged, causing a non-negligible safety issue.

1.4 Current model and history

The model currently in use on the Bell Model 407 is made out of aluminium. The airfoil is divided in three sections to add flexibility to the structure (see Figure 1.7). In fact, the previous model with a one-piece airfoil has demonstrated to develop fatigue cracking because of its lack of compliance.

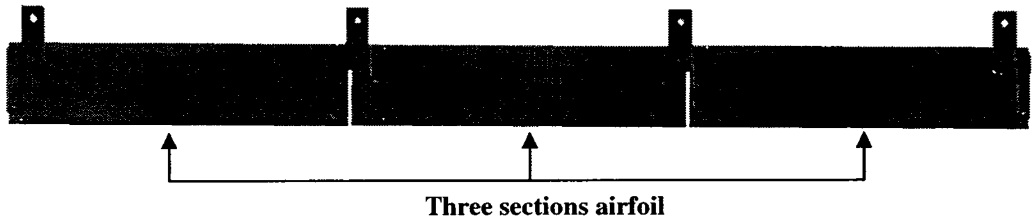

Figure 1.7: Current aluminium model

The four brackets are made out of machined aluminium 2024-T3511 and the airfoil is made out of extruded aluminium 6061-T6 [12]. The inside brackets are two-sided brackets (to join the airfoil sections together) and the outside ones are single-sided. The airfoil has a reinforcement rib across its section to strengthen the structure. Several models with different types of material, geometry and processing options have been tested before choosing the current model. The brackets are attached to the airfoil with blind rivets and are fixed on the stabilizer wing with screws and washers as shown in Figure 1.8 below.

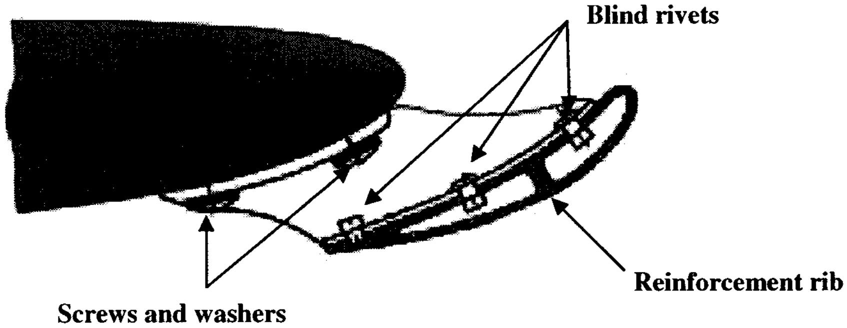

Figure 1.8: Cross-section of the current slat [28]

1.5 Composite slat requirements

The objective of this design optimization study is to remodel the metallic leading slat using the benefits of composite materials. The one-piece model is expected to be able to sustain the operational constraints dictated by its function at the same time as respecting the design limitations imposed by industrial partners and processing issues.

1.5.1 Operational constraints

The composite slat is actually the only re-designed component of the horizontal stabilizer assembly. This is why it should be fixed on the stabilizer with the same screws and washers used for the current model. Some access holes have to be drilled through the airfoil to allow the tool to reach the front screw (see Figure 1.9). These holes will be filled with sealant after installation [28].

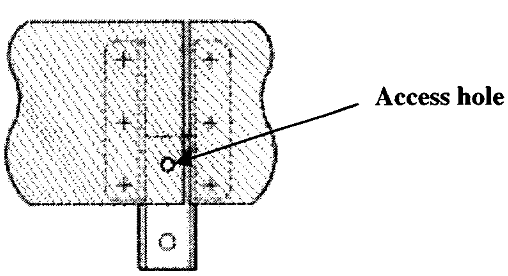

Figure 1.9: Bottom view of a section of the slat [28]

Since the performance of the slat is dependent on the airflow between the stabilizer wing and itself, the aerodynamic shape of the airfoil and its relative position with respect to the stabilizer should also remain the same. This is why flexibility is important. The slat should follow the stabilizer's deformations at all times.

The wing assembly is subjected to a combination of loads caused by complex flight conditions. Upward/downward lift, drag of the end plate and vibration modes of the assembly create twist and bending stresses on the structure. The composite model should have sufficient strength under flexural and torsion loads to withstand flight specifications without losing too much of its flexibility. The challenge here is to find the best ratio between flexibility and strength which consists in maximizing the flexibility of the airfoil section and the strength of the brackets.

The operating temperature of the slat is around 100°C (212 °F) [12] (p. 4) because a majority of the air in contact with the slat comes directly from the engine's exhaust pushed by the rotor downwash [4]. The matrix and reinforcement materials of the composite model should then be able to keep their needed properties under such high temperatures.

The horizontal stabilizer assembly is subjected to repetitively applied stresses from flight conditions (lift and drag). These stresses never exceed the ultimate static strength of the material, but their cyclic action is unavoidable in service. Resistance to fatigue is thus critical to a successful design of the leading edge slat.

1.5.2 Design constraints

Several limitations imposed by industrial partners and processing issues are selected to filter the alternatives. The main ones are:

- Geometry of the current aluminium model
    - Aerodynamic geometry of the airfoil and placement of the attachment holes - the top of the brackets should be wide enough for screw installation

    - Length of the airfoil determining the place left for bonding area of the plies
- Resin transfer moulding technology
    - Material selection
    - Lay-up strategy (integration of the brackets on the airfoil)
    - Rounded edges on the bracket

1.6 Project overview

In summary, this collaborative project involving university, governmental and industrial partners deals with the re-design of an existing metallic part using composite materials. The new part has to meet certain requirements in order to successfully replace the original one in service. This project focuses on means to ease the design and optimize the overall process using RTM manufacturing techniques. Several companies have been experimenting for years on similar helicopter parts (horizontal stabilizer wing components), but no organized strategy is established. This preliminary design work involving the leading edge slat will then contribute to improve and optimize future re-design processes.

The paragraphs below contain a brief outline of the subjects covered by each chapter of this work.

Chapter 2 presents the advantages and disadvantages of composite materials, introduces the resin transfer moulding manufacturing method, discusses material selection, describes the different designs studied and coordinates the determinant aspects influencing their evolution process.

Chapter 3 shows an overview of the finite element models of the horizontal stabilizer and the various composite slat models. Several aspects are discussed for each design stage: elements, draping and material properties, boundary conditions, loading and analyses.

Chapter 4 deals with the results generated by models from all design stages. The overall deformations, stress failure criteria and stress results are presented and discussed.

Chapter 5 lists the aspects left to be covered in the scope of this project.

Chapter 6 summarizes the objectives of the project and discusses the principal findings and conclusions of this work.

2. COMPOSITE DESIGN

The transition from conventional metallic materials to composites requires a good knowledge of the properties of each material. It is essential to study the impact of such a change on the design to fully understand all the aspects involved. Since composite materials are the association of two types of constituent materials (matrix and reinforcement), it is possible to obtain properties unavailable from naturally occurring materials. The wide combination possibilities of matrices and reinforcements allow a great design potential.

This chapter presents the benefits and drawbacks of composites and introduces the resin transfer moulding (RTM) manufacturing method as well as choices for material selection. The different design stages are presented with the determinant aspects influencing their evolution process.

2.1 Benefits and drawbacks of composites

The main advantage of composites is the possibility to manufacture one-piece parts. By eliminating all the joint components, it reduces considerably the number of parts to manufacture. Consequently, it leads to fewer parts to assemble. The assembly is simplified and faster to install. Labour costs related to all these aspects are cut down, leading to some significant cost savings. The absence of junction components eliminates some structural weaknesses caused by the joint holes, leading to a safer part. Additionally, the resultant sleeker geometry induces drag reduction. Subassemblies and associated surface preparation, bonding and inspection steps are consequently eliminated. The removal of these intermediary steps improves repeatability of the part [30]. Moreover, the new composite part is visually elegant and opens to a certain geometric flexibility.

In the case of the leading edge slat, a composite design would permit the transition from a 4-bracket, 3-section airfoil using 18 rivets to a one-piece part (Figure 2.1).

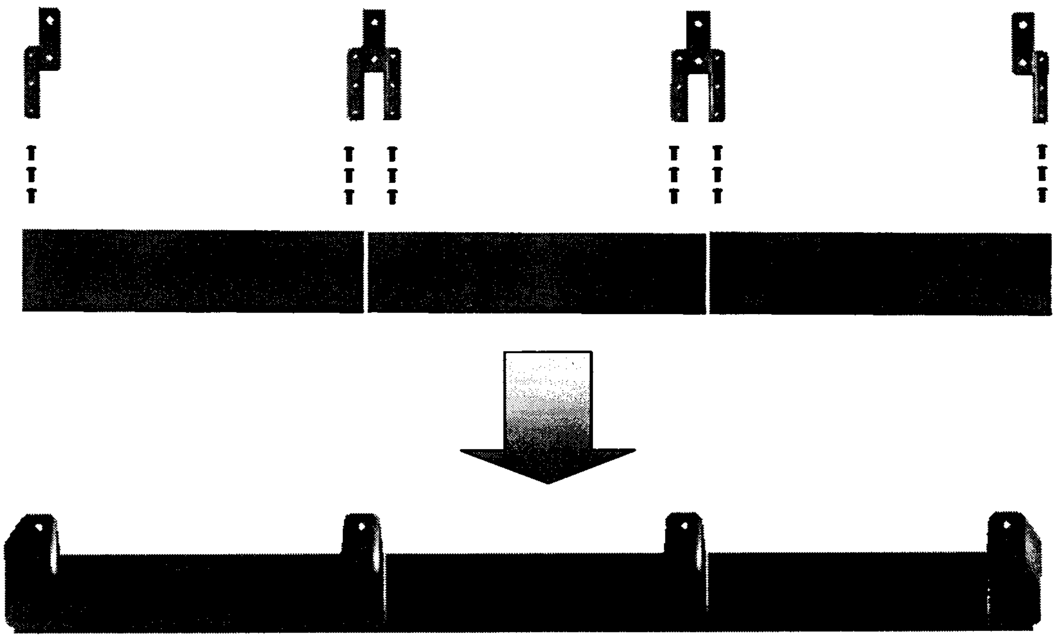

Figure 2.1: Transition from the original 7-piece, 18-rivet aluminium part to a one-piece composite part

Composites ability to get oriented fibres in the direction of loads (directionality) leads to the overall improvement of the quality of the final product. In this case, no superfluous strength in an unsolicited direction will take place, consequently leading to weight savings.

These days, even if they are slowed down by certification requirements, composites are gradually being integrated in the structure of more commercial helicopter models. The aircrafts are getting smaller, lighter and more efficient. To keep up with the highly competitive market of the aerospace sector, the switch to composite design is necessary.

Furthermore, one of the most prominent benefits of composites is their high strength-to-weight and stiffness-to-weight ratios. These materials allow for lighter final parts with the same required properties. The reduced number of parts to assemble also contributes to weight savings.

The design for flexibility of composites allows the use of different combination of materials in specific regions. This leads to expanded design possibilities and a better product with optimized functions.

In metals, the presence of visually detectable damage (cracks) is usually considered as a safety issue because the fissure can quickly expand to final fracture. In composite materials, however, the crack propagation is slowed down by its internal structure. The difference in ply orientation can stop the damage propagation at a ply intersection. The damage in individual plies usually lowers the elastic properties of the laminate, leading to a slower failure process [31]. In this sense, composites are less sensitive in fatigue and are good candidates for parts subjected to repetitive loading such as the leading edge slat.

The major drawback of replacing conventional materials with composites is the high initial costs of the whole procedure. Mould design and fabrication, material purchase (resin and fibres) as well as the expenses related to a geometrical and processing re-design are a few examples of the aspects involved in such a major transition.

Since composites involve fabrics embedded in a matrix, the design approach to adopt will be different to the one used with metallic isotropic materials. The geometry has to be planned and designed in function of draping (lay-up process) and resin injection (see Manufacturing method – Resin Transfer Moulding (RTM)).

Composite design is a relatively new science. Lack of high productivity manufacturing method has the consequence of almost no well-defined and easy-to-employ design rules. This aspect challenges and motivates the development of advanced composite design studies.

Graphite/epoxy fabric has a lower coefficient of thermal expansion (CTE) (1.2E-05 / ^{o}C in Patran database [32]) than aluminium (around 21.6E-06 / ^{o}C in MIL-HDBK-5H [33]). This great difference in CTE is an important aspect to study when a composite part is to be statically combined with metal parts, like the leading edge slat screwed on the horizontal stabilizer in this case. It is then crucial to perform an analysis to make sure this difference in CTE will not generate critical stresses or deformations on the slat.

2.2 Manufacturing method – Resin Transfer Moulding (RTM)

The application of RTM in the aerospace sector has seen major growth in recent years [1]. Used in other sectors such as automotive (car body panels [34]), lightweight structural parts (robotic manipulator [35]) and sport equipment (bicycle frame components [36-38]), the RTM process has a promising future in primary aircraft composite structure applications.

Resin transfer moulding is a process where liquid resin is injected in a closed mould to saturate a dry arrangement of preformed fibres (preform). The mould, generally made of metal, is machined to the outer shape of the part and controls the thickness of the part. As the resin is pushed through the fibres at a relatively low pressure (less than 690 kPa), the air is expulsed through the strategically placed vents to avoid dry spots ("air bubbles" formed in the composite). The injection is stopped when all the air is evacuated through the vents. The part is then heated to cure the resin. When the curing process is completed, the part is ready to be de-moulded [36, 37, 39]. A diagram of the RTM process is shown in Figure 2.2.

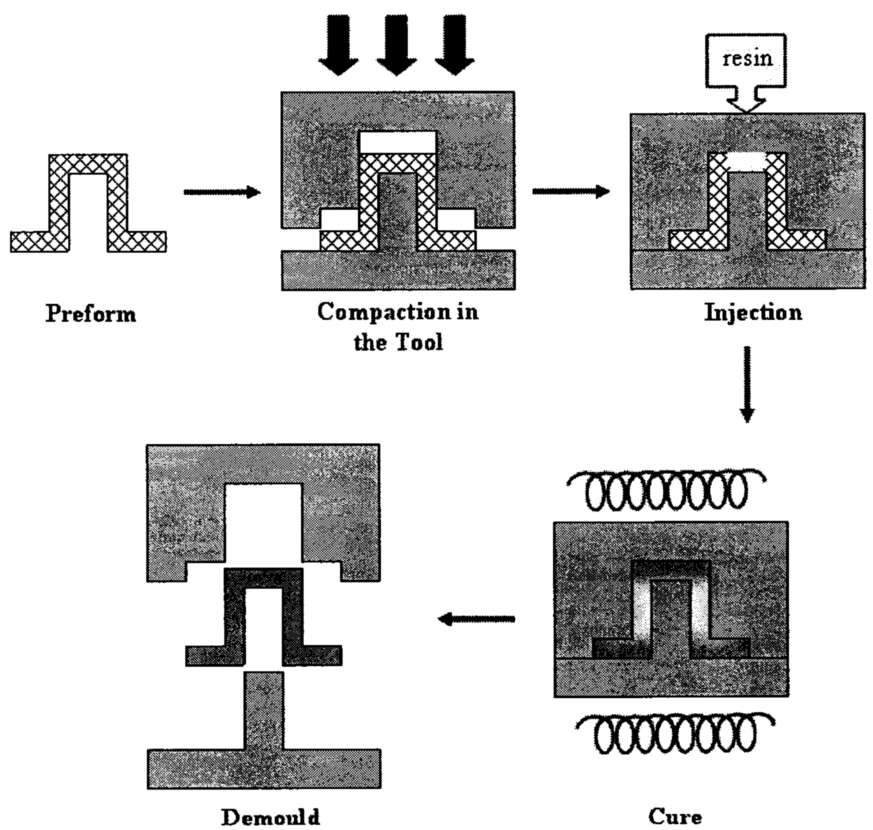

Figure 2.2: RTM process diagram

The choice of using resin transfer moulding (RTM) as a processing method for the leading edge slat has been motivated by several potential benefits. Below is a summary of these main advantages [36, 37, 39, 40]:

Low cost: The most important advantage of using RTM in aerospace applications is cost efficiency. Because it is a low pressure process, it requires inexpensive equipment (pump with pressurized air). It also allows some savings in material purchase since buying resin and dry fibre material in bulk is less expensive than preimpregnated material. Moreover, RTM is a much faster process than lay-up since the production cycles are shorter and some intermediate steps are eliminated. This allows some savings on the labour costs.

Mouldability: Large and complex shapes can be made efficiently and inexpensively. In addition, many mould materials can be used. Dry fibres allow better drapability than pre-impregnated material. Less post-manufacturing trimming is necessary for part integration.

Mechanical properties: Mechanical properties of moulded parts are comparable to other composite fabrication processes. RTM produces parts with high fibre volume fraction, needed for high performance components.

Close tolerance: Parts can be made with better reproducibility than with lay-up. The mould geometry corresponds to the exact dimensions of the external shape of the part. This close-fitting contributes to the structural integrity of the process.

Surface finish: Dependent on the surface quality of the mould, surface finish obtained with RTM is generally superior to lay-up. It requires minimal post-moulding finishing.

Design flexibility: Almost any type of fibre or combination of reinforcements can be used to meet specific properties. It allows a great freedom of design.

Labour skills and safety: The skill level of the operator is less critical. Moreover, since RTM is a closed mould process, the worker is not exposed to chemical vapours or in direct contact with the resin as with the lay-up process.

Like all the other composite processing techniques, RTM has some drawbacks that are important to consider to realize an efficient design. Here is a list of the major aspects to pay close attention to:

Mould design: The design of the mould is a critical step and requires good tools and great skills. Improper gating or venting may result in defects in the composite part. It is very important to have a good mould design since it is difficult to make changes once it is manufactured.

Mould filling and reinforcement movement: Control of flow pattern or resin uniformity is difficult. Radii and edges tend to be resin-rich areas. Change in fibre orientation or wash away of the fibres during resin injection is also a potential problem. It greatly affects greatly the mechanical properties of the composite.

Dry fabric: The manipulation of dry fabric for pre-forming and lay-up can be really awkward for the operator. This is why special care should be taken at this stage of the process.

2.3 Material selection

The main challenge in material selection is finding the best ratio between properties and cost, availability and mechanical/processing properties. The choice of matrix and reinforcement for the re-designed composite leading edge slat needs to be supported by a combination of pertinent criteria such as cost, availability, mechanical properties and processing conditions.

The resin chosen is 890 RTM made by Cycom [41, 42]. Affordable and easily available, it has demonstrated to work well with the process and shows an efficient combination of mechanical and processing properties. Some of its processing conditions are known since the resin has been partially characterized by collaborators working on other projects. The processing time is reasonably short and the curing temperature is within an acceptable range. This epoxy resin shows good mechanical properties such as high toughness under service temperature (about 100°C) and high vibration environment. Finally, it is easy to clean with a low contamination potential.

The fibre material selected is AS4-6K-5HS [43] supplied by Hexcel and Cycom. Easily available at a reasonable cost, it has also demonstrated to work well with the RTM process. This woven carbon fabric material also shows good drapability and mechanical properties.

Glass fibre has also been considered at a certain point during the design process. Its affordable price and high flexibility made it an applicable candidate for the reinforcement part of the composite slat. However, its heavier weight and restricted use in aerospace applications excluded it from being selected for the preliminary design.

2.4 Evolution of design

The transition from a 3-piece aluminium model to a one-piece composite model allows a large number of realizable brackets shapes and configuration possibilities. There are 3 main parameters that can be modified to create a variety of designs: bracket shape, bracket configuration, and the bracket angle between the side of the bracket and the top of the airfoil. This section describes the iterative design process to undergo in order to obtain adequate models for the preliminary finite element analysis.

2.4.1 First design stage

The initial design, (see model 1 in Figure 2.3), for the slat is largely based on the current aluminium model. The first lay-up was chosen in relation with the thickness of the current aluminium part where the airfoil is 1.91 mm (0.075 in) [44] and the brackets are 2.03 mm (0.08 in) thick [45]. The thickness of a ply of woven 890 RTM with AS4-6K-5HS resin is estimated to be 0.42 mm (0.0165 in) [46]. Correspondingly, the even number of plies closer to the thicknesses of the part is 4 plies. This is what justified the lay-up of 4 plies everywhere (on the airfoil and the brackets) for the first design.

Moreover, the stiffness of the composite model should be as close as possible to the current slat, so that the deflections after deformation will remain in the same range. A lay-up with an alternation of 0/90 and ±45 degree fabrics was chosen to get a good balance between flexibility and strength. However, the reinforcement rib is removed of the composite airfoil cross-section to give more flexibility to the structure and ease the processing stage. Moreover, it broadens the manufacturing options of the airfoil by adding the possibility of using braided material formed with a single bladder inside.

A model with four identical brackets was selected to simplify the manufacturing aspect of the composite part. A configuration comparable to the aluminium model with two-sided brackets (or full brackets) inwards and single-sided ones (or half brackets) outwards was too heterogeneous.

Figure 2.3: Overall view of the first design (model 1)

An angle of 85° between the side of the bracket and the top of the airfoil was chosen to increase the radii of the plies at the corners as well as leaving enough bonding area at the tip of the airfoil. The two inside plies of the brackets are composed of braid material while the two outside ones are draped fabric. The void created by the intersection of the plies going inwards and outwards is filled with resin and unidirectional fibres (see Figure 2.4). This adds strength to the part at the same time as preventing the formation of resin-rich areas.

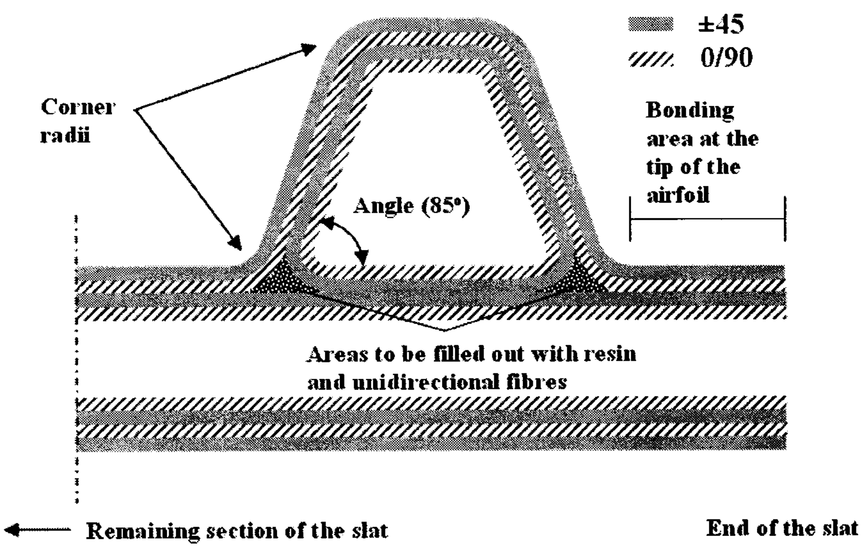

Figure 2.4: Sketch of the cross-section of the first design

2.4.2 Second design stage

The second design stage introduces two pairs of models to be compared in order to study the impact of number of plies and bracket geometry, respectively.

A lay-up of ±45 degree fabric for all plies for every part was chosen because it gives good flexibility in bending as well as shear strength. Moreover, this uniformity in the lay-up eases the comparison between the 4-ply and 6-ply models.

The first pair of models is composed of full brackets for all 4 brackets (see overall geometry for both models in Figure 2.5). The model 2A has 4 plies of ±45 degree fabric everywhere and the model 2B includes two additional braid plies of ±45 degree fabric inside the brackets. The bracket angle is 85° and the lay-up configuration is as illustrated in Figure 2.6 for each model. This pair of models studies the effect of the number of plies on the slat.

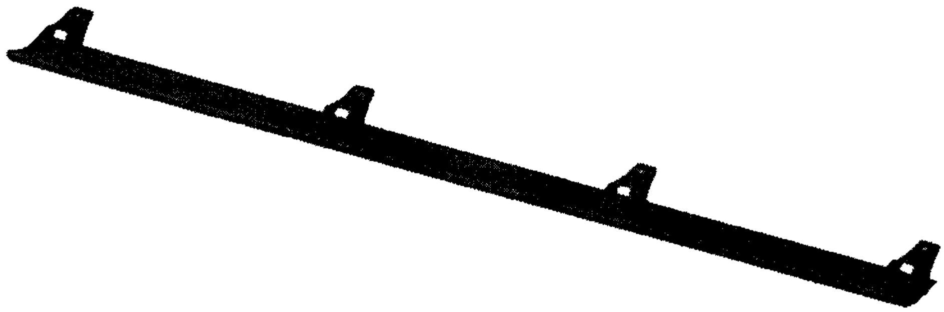

Figure 2.5: Overall geometry of model 2A and 2B

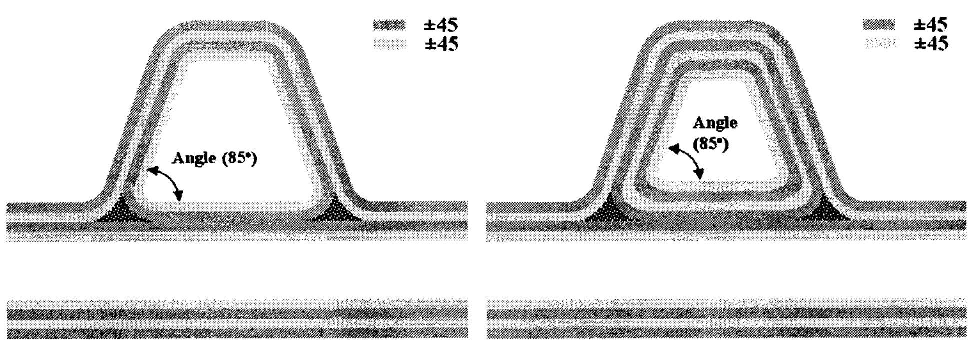

Figure 2.6: Cross-section of model 2A with 4 plies (left) and model 2B with 6 plies (right)

The second pair of models compares the full bracket model with 4 plies (Model 2A) of the first pair with a half bracket geometry (See overall view of Model 2C in Figure 2.7) which is composed of simply bonded plies on the top of the airfoil. The half bracket geometry was considered because of its advantages over the full bracket configuration. Half brackets are easier to process since the inserts would slide in and out more freely than with the full bracket geometry.

Moreover, it uses less material and has the potential to be more flexible (half brackets tend to deform more than full brackets).

To prevent delamination, the plies are splitting up inwards and outwards, creating a void filled with resin and unidirectional fibres (illustrated in the right side of Figure 2.8). This is an important issue since delamination is the primary mode of failure of laminated composites [47]. The bonding area of the bracket plies with the airfoil is equal to the top bracket width on one side and to the remaining distance between the side of the bracket and the end of the slat on the other side.

To ease the comparative analysis, the new geometry has the same lay-up than the full bracket model. The bracket angle is 85^{o} for both models. The lay-up configuration is shown in Figure 2.8. This pair of models (models 2A and 2C) investigates the effect of bracket geometry on the slat.

Figure 2.7: Overall view of model 2C with half brackets

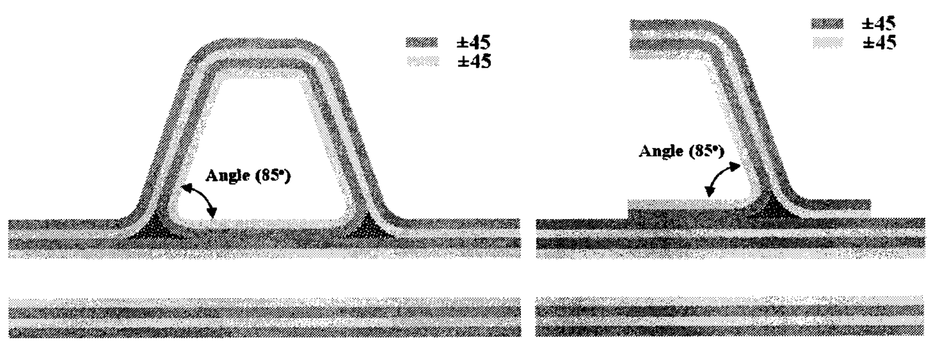

Figure 2.8: Cross-section of Model 2A with full brackets (left) and model 2C with half bracket (right)

2.4.3 Third design stage

More geometries are compared in the third phase of the design. In total, 17 models are studied to consider the impact of geometry (bracket angle and shape) number of plies and gradual lay-up on the slat. Once again, a lay-up of ±45 degree fabric for all plies was chosen to simplify the comparative analysis for the number of plies.

The main motivation for studying the impact of bracket angles on the slat is the potential to reduce stress concentrations located at the corners of the brackets (bigger radius, less risk of stress concentration). However, brackets with larger radii are more likely to deform. Thus, it is necessary to find a satisfactory compromise between stress and deformation when considering the angle.

The first 8 models are all 4-ply models with same lay-up as model 2A for full brackets and model 2C for half brackets (illustrated in Figure 2.8). In total, 8 geometries are considered: 2 full bracket models (models 3A and 3B), 3 half bracket models opened towards the outside (models 3C, 3D and 3E) and 3 half bracket models opened toward the inside (model 3F, 3G and 3H). Figure 2.9, Figure 2.10 and Figure 2.11 show the overall geometry of each model.

The 2 full bracket models have bracket angles of 90 degrees (model 3A) and 85 degrees (model 3B). The choice of 90 degree brackets was motivated by the geometry of the current aluminium model. The choice of 85 degree angle was influenced by the space available on the edge of the slat's airfoil to leave enough bonding area at the tip of the airfoil. Figure 2.9 illustrates the overall geometry of the two full bracket models.

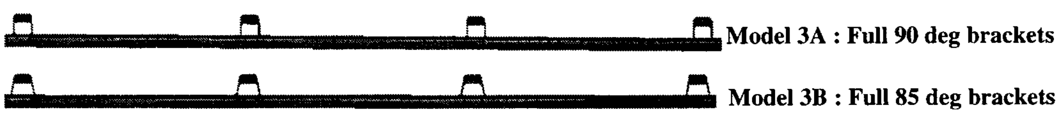

Figure 2.9: Overall geometry of model 3A (top) and 3B (bottom)

The 3 subsequent models have half brackets opened towards the outside of the slat with a symmetrical configuration (illustrated in Figure 2.10). This type of configuration has the advantage to allow a wide range of angles because the space available for ply bonding is no longer an issue. Bracket angles of 90 degrees (model 3C) and 85 degrees (model 3D) were chosen for comparison purpose and a much smaller angle of 60 degrees (model 3E) was added to study the impact of a sharp bracket angle.

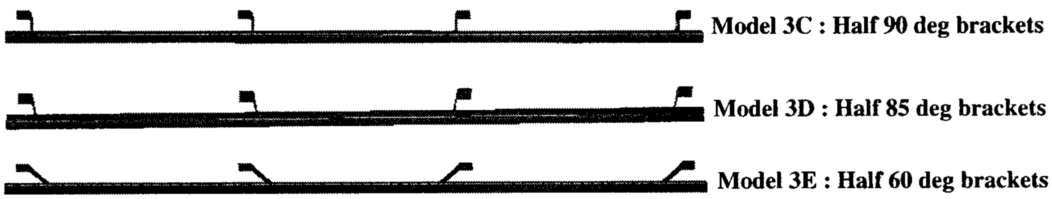

Figure 2.10: Overall geometry of model 3C (top), 3D (middle) and 3E (bottom)

The 3 following models are half brackets opened towards the inside of the slat, again with a symmetrical configuration. The two first configurations have bracket angle of 90 degrees (model 3F) and 85 degrees (model 3G). Once more, the space available on the edge of the slat's airfoil influences the maximum bracket angle allowed. However, a third configuration is possible (model 3H). It features outer brackets that are integrated with the airfoil lay-up by having material extended to the very edge of the slat ends. The bracket angle of 70 degrees is attributable to the angle between the edge of the slat and the top corner of the brackets. It has a symmetrical configuration similar to the models 3F and 3G but with a different lay-up strategy. The respective cross-section of middle brackets and side brackets of model 3H is shown in Figure 2.12.

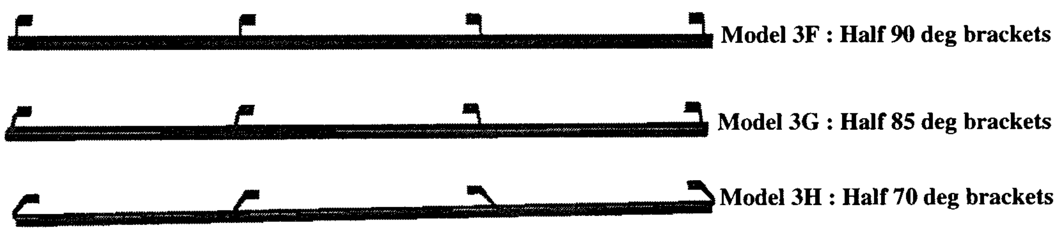

Figure 2.11: Overall geometry of model 3F (top), 3G (middle) and 3H (bottom)

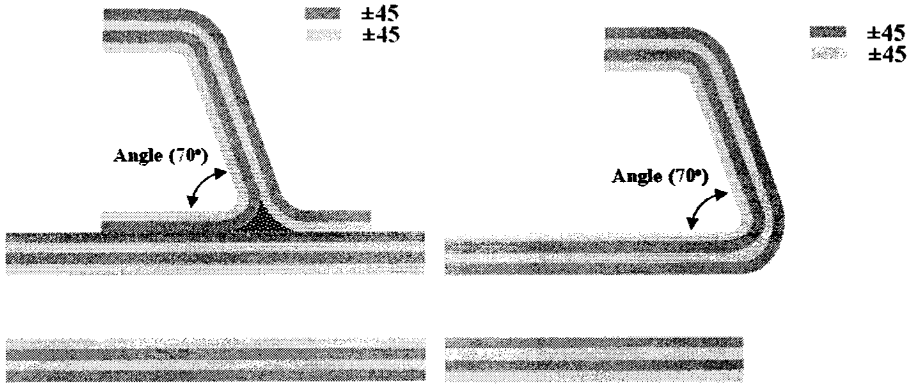

Figure 2.12: Cross-section of a middle bracket (left) and outer bracket (right) of model 3H

The 6 subsequent half brackets models (3I-3N) have the same geometry and configuration as models 3C-3H with 2 additional plies on the brackets (one going inwards and one going outwards). The lay-up of the airfoil remains unchanged with 4 plies. These models were designed in order to study the impact of the lay-up on the slat. Figure 2.13 shows an example of the difference in lay-up between models 3C-3G and middle brackets of model 3H (left) and 3I-3M and middle brackets of model 3N (right).

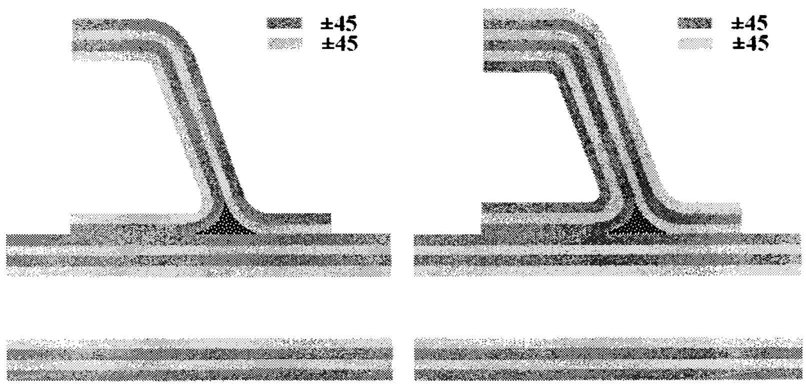

Figure 2.13: Lay-up with 4 plies everywhere (left) and lay-up with 2 additional plies on the brackets, one going inwards and one going outwards (right)

The difference in lay-up for the outer brackets of model 3H and model 3N is as sketched in Figure 2.14 below.

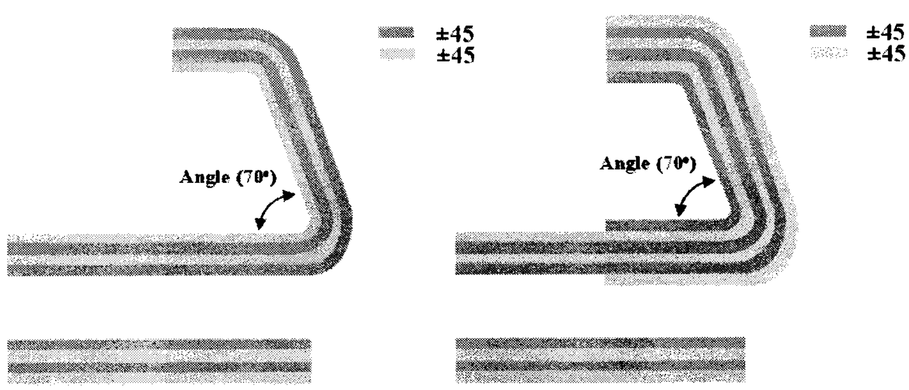

Figure 2.14: Lay-up of outer bracket of model 3H with 4 plies everywhere (left) and model 3N with 2 additional plies on the brackets

The last model of the third design was created to analyze the effect of a more gradual lay-up on the part. Its configuration is similar to the model 3H which is symmetrical with integrated outer brackets forming an angle of 70 degrees (see bottom of Figure 2.11). As for models 3I-3N, model 3P has additional plies on the brackets but only covering the area with a higher potential for stress concentration. For the case of the leading edge slat, this area is located on top of the brackets (return to Figure 1.6 for further justifications). The additional plies are applied on the outside of the brackets and medium plies are covering shorter plies to prevent delamination (see Figure 2.15).

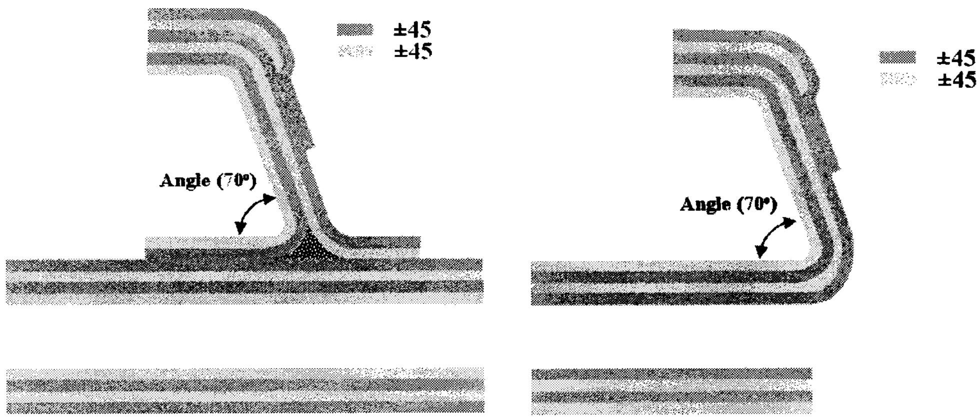

Figure 2.15: Gradual lay-up on the top of middle brackets (left) and outer brackets (right) of model 3P

2.4.4 Fourth design stage

The fourth and last iterative phase of the design is characterized by various geometrical geometrical (bracket angle and configuration) and lay-up (ply orientation, number of plies, ply drop) modifications. A total of 12 geometries are compared at that stage. A modification inspired by the former model 3H (see Figure 2.11) on the outer bracket placement permits a wider selection of configurations. Indeed, all models with full brackets and half brackets opened towards the inside of the slat feature outer brackets with material folding up from the very edge of the slat ends, forming an angle of 70 degrees (angle between the edge of the slat and the top corner of the brackets). This new outer bracket configuration allows a certain liberty of design. Now, each of the 3 main bracket configurations (full, half opened towards the inside and half opened towards the outside) have equal bracket angle possibilities.

To allow a better comparative analysis, 4 bracket angles (90, 80, 70 and 60) have been selected for each of the 3 bracket configurations. Figure 2.16 illustrates 4 different models of full brackets with new outer slat configuration with bracket angles of 90, 80, 70 and 60 degrees (models 4A, 4B, 4C and 4D respectively).

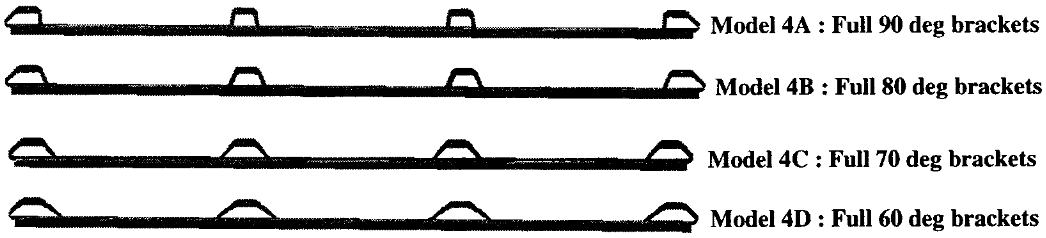

Figure 2.16: Overall geometry of full brackets models: 4A with 90 degree brackets (top), 4B with 80 degree brackets (2nd top), 4C with 70 degree brackets (2nd bottom) and 4D with 60 degree brackets (bottom)

As for the full bracket configuration, Figure 2.17 and Figure 2.18 show 4 different models for half brackets opened towards the outside (models 4E-4H) and the inside (models 4I-4L), respectively.

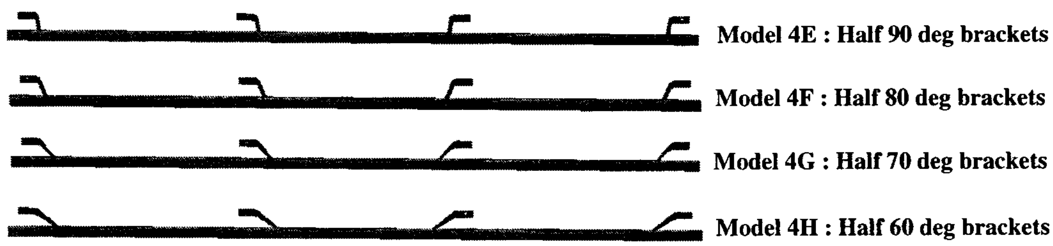

Figure 2.17: Overall geometry of models with half brackets opened towards the outside: 4E with 90 degree brackets (top), 4F with 80 degree brackets (2nd top), 4G with 70 degree brackets (2nd bottom) and 4H with 60 degree brackets (bottom)

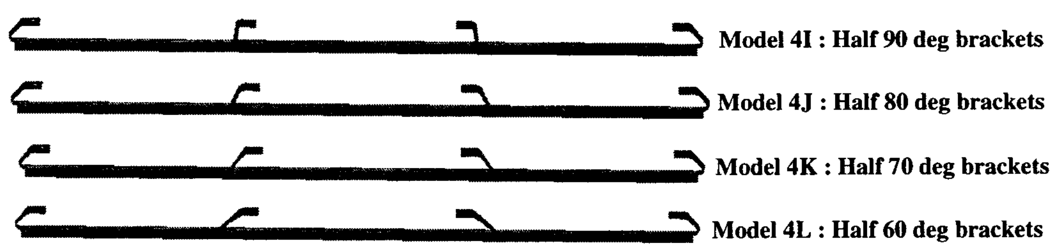

Figure 2.18: Overall geometry of models with half brackets opened towards the inside: 4I with 90 degree brackets (top), 4J with 80 degree brackets (2nd top), 4K with 70 degree brackets (2nd bottom) and 4L with 60 degree brackets (bottom)

Other than new geometries, more modifications have been made at this design phase. The first changes concern the radii of the brackets. The dimensions shown in Figure 2.19 have been selected as a result of the specific requirements brought by its location on the bracket. The top radius of 7.62 mm (0.3 in) is wide enough to be processed easily at the same time as being small enough to leave sufficient space at the top of the bracket. The bottom radius of 2.54 mm (0.1 in) is the smallest radius able to be processed and has been chosen with the objective of minimizing the void to be filled with resin and unidirectional fibres.

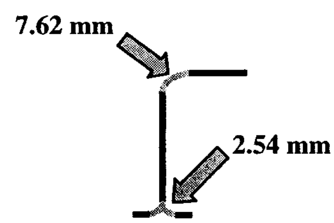

Figure 2.19: Selected dimensions for the top (7.62 mm) and bottom (2.54 mm) radii

The second change consists of a slight change in the bracket angle to ease demoulding. The exact value of the angle has been modified from a straight 90 degrees to a 87 degrees, preventing the fibres from getting damaged or displaced from sliding against the mould during demoulding.

The third change concerns the modification of the side geometry of composite brackets in order to ease the post machining process. Figure 2.20 illustrates the difference between the original metallic brackets riveted to the slat (left) and the composite one-piece design where the brackets must be made slightly larger in preparation for post-manufacturing trimming.

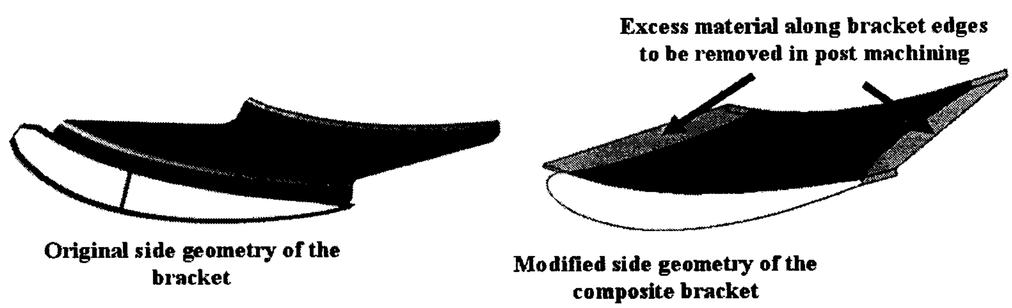

Figure 2.20: Modification of the side geometry of the brackets [48]

A final decision was made about the number of plies. Based on the comparative analysis of the third design phase, a model with 6 plies on the bracket and 4 plies on the airfoil was adopted. Since a final decision was made about the number of plies, it is no longer necessary to have a homogeneous lay-up for comparative purpose. The new lay-up, as shown in Figure 2.21, is $[(0/90)/(\pm45)_2]_s$ for the brackets and $[(\pm45)_2]_s$ for the airfoil. The outer (0/90) plies were added on the brackets to increase stiffness. This new symmetric lay-up configuration has the main advantage of reducing the risk of delamination.

With the previous lay-up of ±45, it was unlikely to obtain a stiffness that would match that of the aluminium slat. Moreover, a lay-up composed of ±45 plies has low stiffness and strength and is mainly used for very low loaded fairings applications. Another drawback of such a lay-up is the large plasticity at higher loads due to the scissoring of fibres. Furthermore, ±45 laminates tend to undergo a great reduction in strength at high temperatures and after moisture absorption (these laminates have matrix controlled properties – the matrix is very sensitive to temperature and moisture). In applications such as the leading edge slat, with a reasonable amount of deformations and stresses, it is preferable to put fibres as much as possible in the principal load direction. In this case, since the slat is bending upwards and downwards to follow the stabilizer's deflections, it seems appropriate to have fibres along the width of the brackets to compensate for the flexibility of the airfoil structure.

Ply drops of the bracket layers bonded on the airfoil have been introduced to lower the risk of delamination around this area. The ply drop is 12.7 mm (0.5 in) for the top plies and 3.175 mm (1/8 in) for the subsequent plies. This ply drop for models is shown in Figure 2.21 for models 4A-4D and in Figure 2.22 for subsequent models.

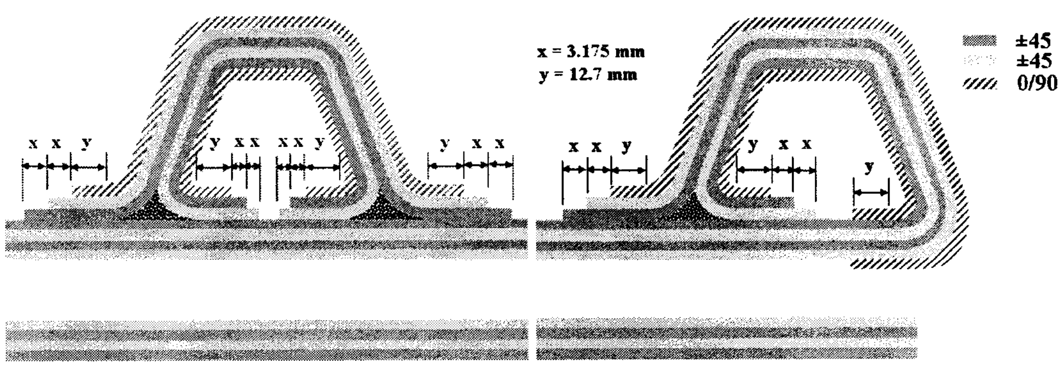

Figure 2.21: Lay-up and ply drop for the middle brackets (left) and outer brackets (right) of models 4A-4D

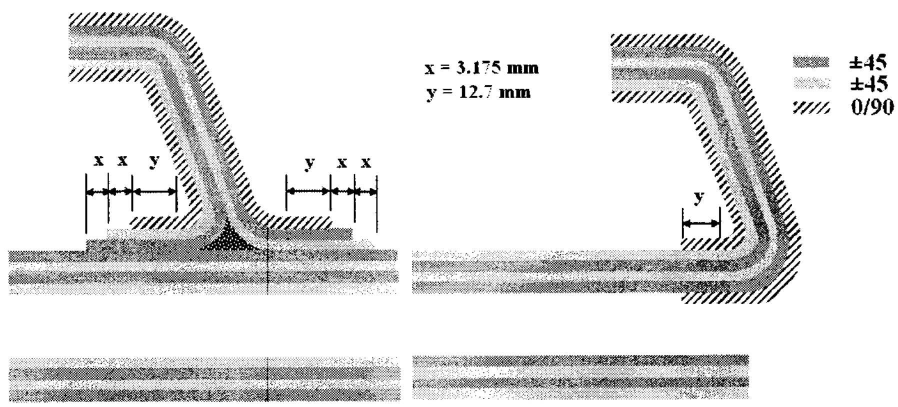

Figure 2.22: Lay-up and ply drop for models 4E-4L (right) and outer brackets of models 4I-4L (left)

2.4.5 Designs for preliminary analyses

The designs selected for preliminary analyses are the designs described in the fourth design stage. The 12 models are easily comparable since each bracket configuration (full, half opened towards the inside, half opened towards the outside) has the same selection of 4 possible bracket angles (90, 80, 70 and 60 degrees).

These models also have improved features compared to designs from other stages. The radii have been modified to ease processing at the same time as optimizing the geometry of the model. Bracket angles are designed to ease demoulding and the side bracket geometry are adapted to post machining. Ply drops of the layers bonded on the airfoil and symmetrical bracket (6 plies - $[(0/90)/(\pm 45)_2]_s$) and airfoil (4 plies - $[(\pm 45)_2]_s$) lay-ups lower the risk of delamination.

2.5 Decisions about composite design

As discussed previously, use of composites to replace isotropic materials such as aluminium involves some challenges. A number of aspects concerning materials and process have to be considered in order to establish an efficient re-design strategy.

Simplicity of processing and installation will also play a determinant role in the choice of design. Since half bracket models seem easier to process than full bracket models, they will be the preferred option if the results of the finite element analyses are comparable. Complementary work performed by collaborators (mould design, flow simulations) will also play a determinant role in the design study since processing complexity could lead to the elimination of some proposed models.

3. FINITE ELEMENT MODEL OVERVIEW

Finite element analysis (FEA) is the best way to efficiently compare different models without having to test any physical samples or structures. Within the scope of this study, FEA is used for preliminary design work only. It is important to specify that it is not meant to generate actual magnitudes of stress or strain to be used in a failure analysis. Indeed, it is arranged to provide means of comparison between possible solutions [12] (p.12).

To achieve this work, Patran 2005 r2 [32] is used as a pre processor (for meshing, selecting boundary conditions, creating load cases, assigning material properties, etc.) and post processor (plotting results). MSC Nastran 2005 [48] is used as finite element analysis software.

It is necessary to point out that both the stabilizer and the slat have to be modeled in order to adequately reproduce the complex loading and boundary conditions under flight environment. However, since a slat is fixed symmetrically on each side of the helicopter, only the left hand side slat assembly has been modeled (the same side used for the hangar test [12] (p.10)) .

This chapter shows an overview of the finite element models of the horizontal stabilizer and the various composite slat models. The following aspects are covered for each design stage: elements, draping and material properties, boundary conditions, loading and analyses.

3.1 Horizontal stabilizer

The model of the horizontal stabilizer used for the comparative analysis remains the same throughout all design stages. It has been inspired from an existing finite element study on the stabilizer's attachment to the tail boom [12] (p. 11) [49]. This model is illustrated in Figure 3.1.

Bilinear quadrilateral (Quad 4) elements are used to model the stabilizer skin. Hexahedral 3D solid elements with 8 nodes (Hex 8) and Wedge solid elements with 6 nodes (Wedge 6) are used to represent the core [50]. There are no contact elements between the 3D elements and the Quad 4 elements. The skin elements are created directly from the surface of the 3D elements, using the same nodes and element face pattern. This prevents overlaps (penetration) of 3D elements into the shell surface.

The skin material used is aluminium 2024-T3 with different thicknesses at strategic areas of the wing surface. The 3D core is made out of aluminium 5056 honeycomb except at the junction between the stabilizer and the tail boom where other properties have been used [51] (p. 15.125).

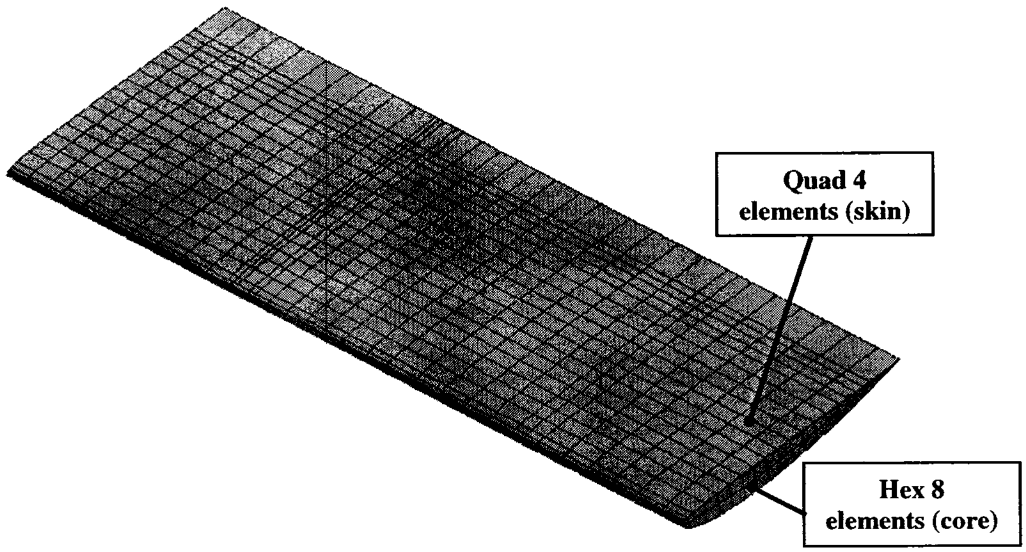

Figure 3.1: Horizontal stabilizer model used for the comparative analysis

3.2 Aluminium leading edge slat

In order to compare the general behaviour of the composite models with the current aluminium part, an FEA model was created. This model was inspired from the same existing finite element study on the stabilizer's attachment to the tail boom used to design the stabilizer model [12] (p. 11). As mentioned previously, magnitudes of the stresses or strains are not compared, but the overall deformations are studied and compared.

3D solid tetrahedral elements with 10 nodes (Tet 10) are used to model the brackets. Bilinear quadrilateral (Quad 4) elements are used to model the 3-section airfoil (see Figure 3.2).

The bracket material used is aluminium 2024-T3511 and the airfoil skin is made out of aluminium 6061-T6 [49].

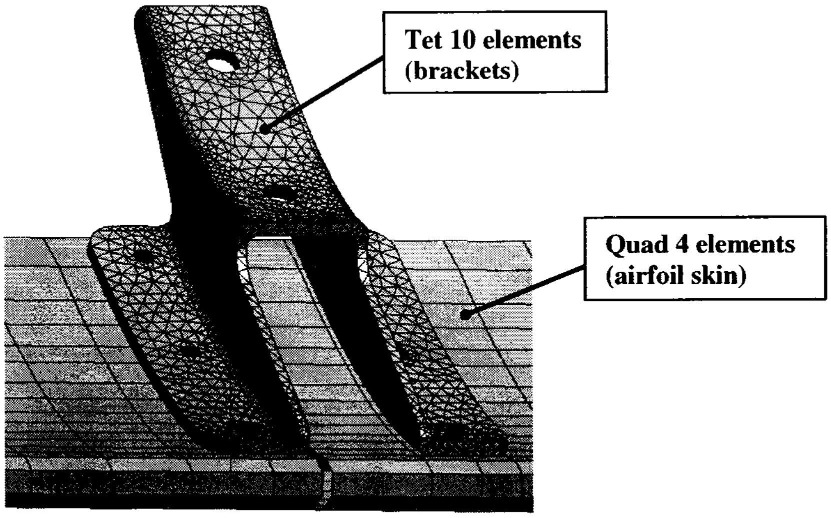

Figure 3.2: Current aluminium leading edge slat model

3.3 Composite slat geometries

All slat geometries are created from the original model developed in CATIA V4 format which are translated in IGES (Initial Graphics Exchange Specification) format. The bracket shapes and geometries are developed from the surface models from the imported IGES files in Pro/Engineer [52]. The slat airfoil shape is kept unchanged from the original geometry as well as its position with respect to the stabilizer. The location of attachment holes is taken from provided drawings [45, 53] and is unaltered since all slat models should be fixed on the stabilizer with the same screws and washers used for the original model. Figure 3.3 shows the template used to create the different slat models according to airfoil geometry and its relative position with the stabilizer.

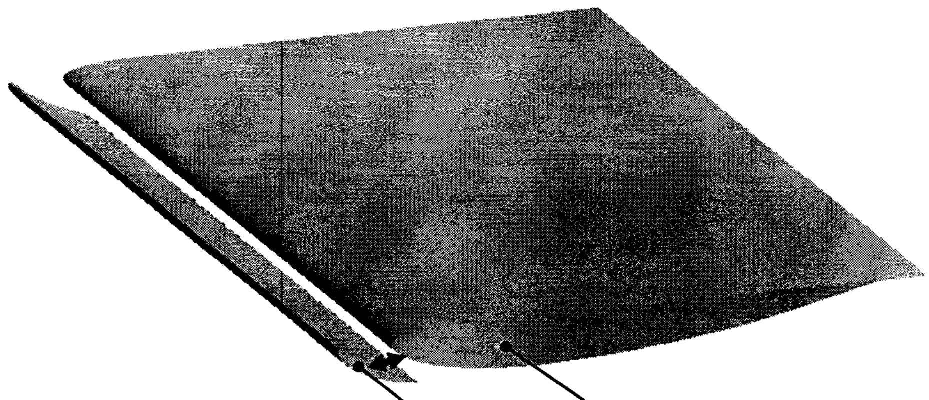

Figure 3.3: Position of the slat airfoil relative to the stabilizer

The surfaces on the airfoil in Figure 3.3 represent the outer most layer of the original aluminium model [12], (p.12). The elements are slightly offset by 0.762 mm (0.030 in) outwards (about half the original airfoil's wall thickness). All geometries are designed in Pro/Engineer using the slat airfoil geometry and its position with respect to the stabilizer as templates. They are then converted back to IGES format and imported in Patran [32] where surfaces are recreated and sewed together in order to obtain adequately connected models.

Holes on top of the brackets are filled for draping purposes (see COMPOSITE SLAT DRAPING section below for more details). One of Patran's modules, called Patran Laminate Modeler, is used to create composite plies on the models. To be able to drape the models adequately, it is required that no hole remains on the surface geometry. These hole surfaces are simply not included in the group submitted to analyses.

The void created by the junction of the plies with the airfoil (splitting up inwards and outwards) to be filled with resin and unidirectional fibres (illustrated in Figure 2.4 of Chapter 2) was left empty in all models. This area is really small and can be neglected in order to simplify the comparative analysis. A sketch of the aspect of the models before and after being fixed is shown below in Figure 3.4.

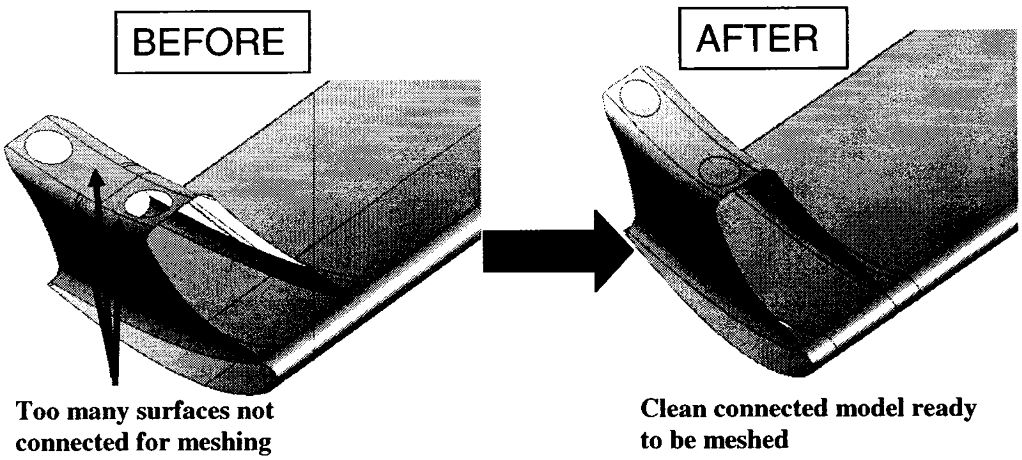

Figure 3.4: Sketch of the models' surfaces before and after being fixed

The elements used for all slat models are 2D shells. These elements seem appropriate since the thickness of the model is small compared to its other overall dimensions. Moreover, shell elements were selected because they allow the modification of the number of plies without having to change the overall thickness of the model. In addition, Patran Laminate Modeler requires shell elements to drape the model.

When using 2D shell elements to model a 3D part, the following assumptions have to be made: 1- transverse normal and shear stresses are small, 2- through-thickness effects are relatively insignificant [32], (p.129). However, it is important to indicate that the possibility of delamination in upper corners of brackets or peeling off at the lower side of the joint between the bracket and the airfoil is a crucial issue in the design of the slat. This issue is discussed in the FUTURE WORK chapter.

3.4 Composite slat draping

All composite models are developed with the "Patran Laminate Modeler" module. Figure 3.5 shows the main components of the draping simulation: starting point, application direction, reference direction and flat pattern of the draped fabric.

First, a material is created with the desired properties and thickness. The draping simulation process starts with the creation of each ply. A ply is a layer of material characterized by the material it is made of, the area it covers, and the way in which it is applied to the surface [50]. The covered area must have no interior holes.

A starting point defining the point at which the ply is first attached to the mould surface during manufacture is then determined. To minimize shear distortion, which usually increases away from the starting point, it is usually best to locate the starting point near the center region.

The application direction defines the side of the surface area on which a subsequent ply is added to form the final lay up. For this case, this direction is always pointing downwards, meaning that the first ply added to the lay-up ends up at the bottom. This concept is very important as composite structures are often built using moulds, limiting the side of application to a single direction.

The reference direction is specifying the initial direction of the fabric. For a fabric at ±45 degrees, a reference angle of 45 is input from the reference direction. However, the direction of the material usually changes away from the starting point when the surface is curved.

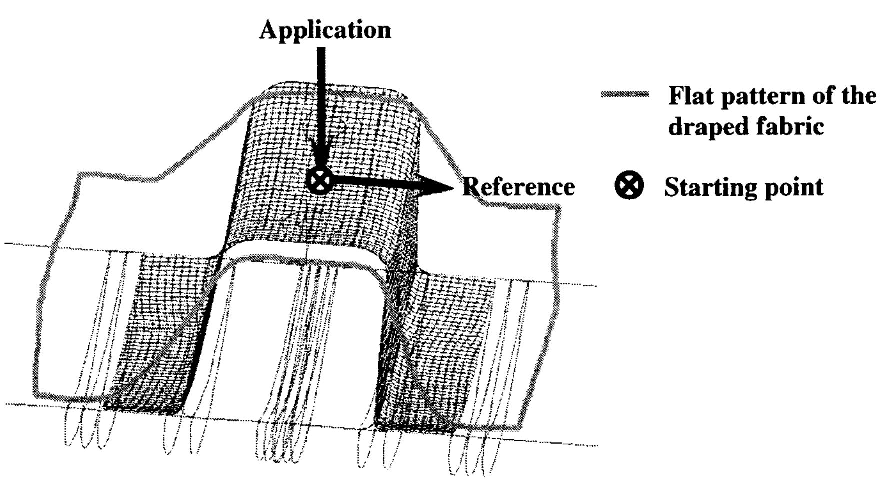

Figure 3.5: Main components of the draping simulation

The remaining part of this chapter presents the iterative modelling process using FEA models in Patran through the four design stages described in Chapter 2. Throughout all stages, modifications are brought to finite element models in order to improve comparative analysis findings. Changes in boundary and loading conditions are also made to refine the relation between simulation conditions and real life behaviour. It is important to note that models from early stages do not produce wrong or inaccurate results. For comparative analysis purposes, the main goal is to provide uniformity between models by imposing the same conditions to all of them, even if the loads and boundary conditions are not perfectly accurate. However, iterative modifications are made with the objective of representing real flight conditions as precisely as possible in order to obtain results that are approaching the real behaviour.

3.5 First design stage

3.5.1 Elements

Since the slat has a fairly complex shape, it was decided that the model would be meshed with Quad 4 elements. These simple elements allow faster analyses than higher order element. Therefore, they make it possible to perform more analyses in less time. Within the scope of this project, Quad 4 elements are estimated to generate results that are accurate enough for a preliminary comparative study. As shown in Figure 3.6, isomesh elements are used to mesh the airfoil surface and the side of the brackets (including the rounds). Isomesh consists of equally-spaced nodes and is usually the best meshing element for parallel features. Paver elements are used for the top of the brackets. Such unparallel elements have been selected because they are best suited for complex surfaces with holes or cut-outs [50].

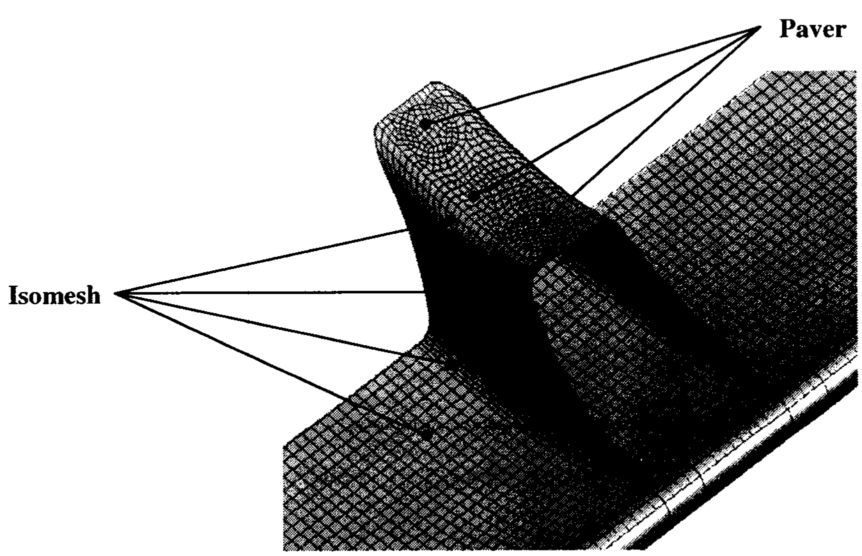

Figure 3.6: Mesh elements used in the different sections of the slat for the first design stage models

3.5.2 Draping and material properties

The lay-up of the model is done with Laminate Modeler. Classical mechanical properties of carbon fabric are used since properties of 890 RTM with AS4-6K-5HS resin are unavailable at that stage. A 2D orthotropic material is created with properties of a graphite/epoxy fabric model (fabric T300/F934) from Patran Laminate Modeler support file [32, 50] and used for the lay-up. Both 0/90 and ±45 degree fabrics can be considered as orthotropic materials since they are symmetrical about the XZ and YZ planes. The model has 4 layers everywhere of 0.25 mm thickness. Figure 3.7 below shows a sketch of the cross-section of the first model as described in Chapter 2 with the exploded view of the modeled lay-up.

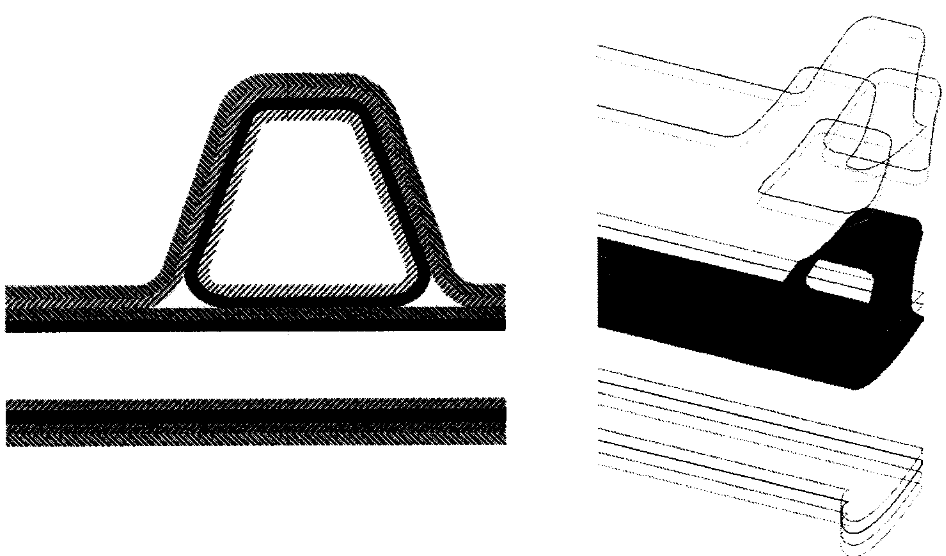

Figure 3.7: Sketch of the cross-section of the 1st model (left) compared with the laminate model in Patran Laminate Modeler (right)

3.5.3 Boundary conditions

As previously mentioned, stresses transmitted to the slat are induced by the stabilizer's deflections. This is why it is crucial to model the stabilizer/slat assembly adequately in order to obtain a sufficiently accurate model.

3.5.3.1 Stabilizer

To simulate the fixation of the stabilizer on the tail boom, all translations are blocked at the nodes along the junction line of the two parts (the locations of these nodes are shown in Figure 3.8). Blocked translations mean no displacement in the X, Y and Z direction (123 blocked in Patran). This boundary condition is applied to both right-hand and left-hand tail boom attachment base lines [12] (p.13) and prevents FEM rigid body motion. In this case, the stabilizer is considered as a cantilever beam fixed on the tail boom.

On the stabilizer model, all rotations are blocked (456 blocked in Patran) at all junction nodes between the core's volume elements (illustrated at the bottom of Figure 3.8). In other words, no rotation is possible around the X, Y and Z axis. This is done to prevent the volume elements from deforming in a way the real core would not.

The endplate is modeled with a rigid body element (RBE) connecting the outboard nodes on the stabilizer skin to an outside node (see Figure 3.8). This corresponds to the interaction between the endplate attachment junction at the end of the stabilizer and the center of gravity of the endplate [51] (p. 15.120a). This type of RBE, called RBE 3 in Patran, defines the motion of a reference node (the center of gravity point in this case) as the weighted average of the motions of a set of nodes (the outboard nodes on the stabilizer skin) [50]. Thus, all degrees of freedom (DOF) (translations and rotations with respect to X, Y and Z axis) of the reference node are the average of the translations (in X, Y and Z direction) of the defined stabilizer nodes.

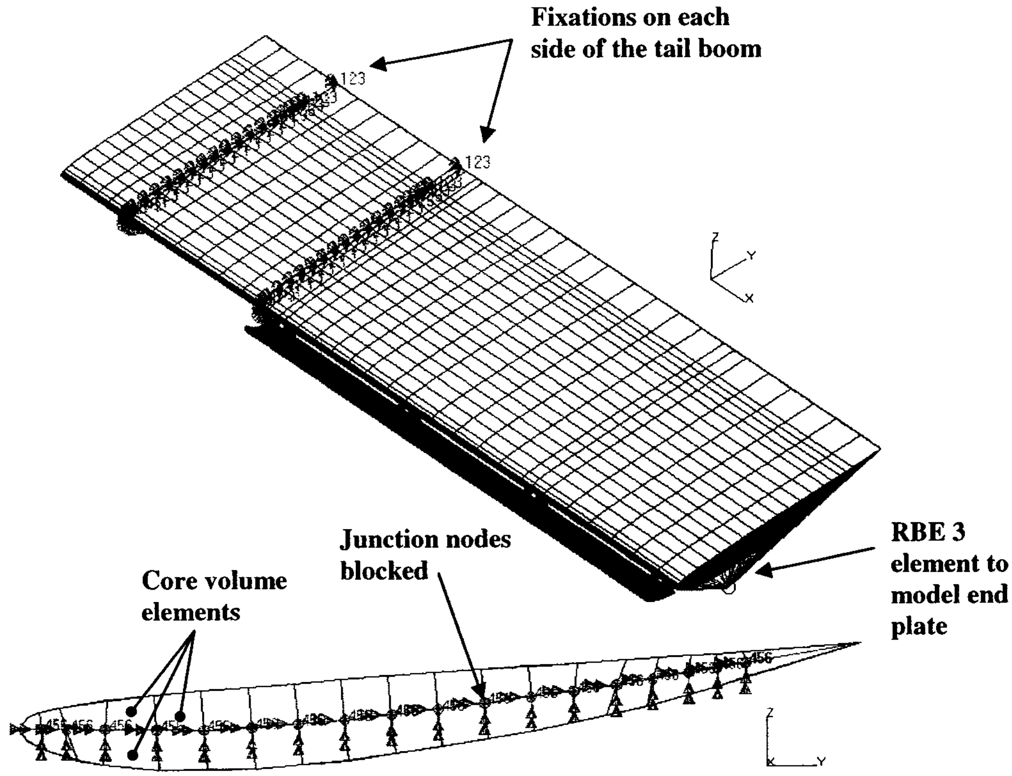

Figure 3.8: Boundary conditions applied on the stabilizer

3.5.3.2 Fixations of the slat on the stabilizer

As mentioned previously in Chapter 1, the slat is fixed to the stabilizer wing with screws and washers. To model this fixation, a combination of rigid body elements has been used. The shank of the screw and the potted insert inside the stabilizer is defined as a rigid body between 2 nodes [12] (p.12). This type of RBE is designated as RBE 2 (see Figure 3.9) in Patran and connects the displacements of a dependent node (in this case, an internal node between 2 volume core elements) with an independent node (junction node between the stabilizer skin and the middle of the top bracket hole). A RBE 3 has been used to model the head part of the screw (as illustrated in Figure 3.9). The reference attachment node, located at the middle of the top bracket hole, is dependent on the motion of the nodes at the screw contact points on the bracket [12] (p.13). The motion of the middle node is then represented as the weighted average of the motions and rotations of the bracket nodes in contact with the shank of the screw [50]. Thus, all degrees of freedom (translations and rotations with respect to X, Y and Z axis) of the reference node are the average of the translations and rotations (in X, Y and z direction) of the defined head bolt nodes. The difference between the RBE 2 and RBE 3 is subtle. RBE 2 elements define the selected degrees of freedom of a single dependent node with respect to only one independent node. RBE 3 defines the chosen degrees of freedom of a variable number of dependent nodes (one in this case) with respect to the average selected degrees of freedom of many dependent nodes.

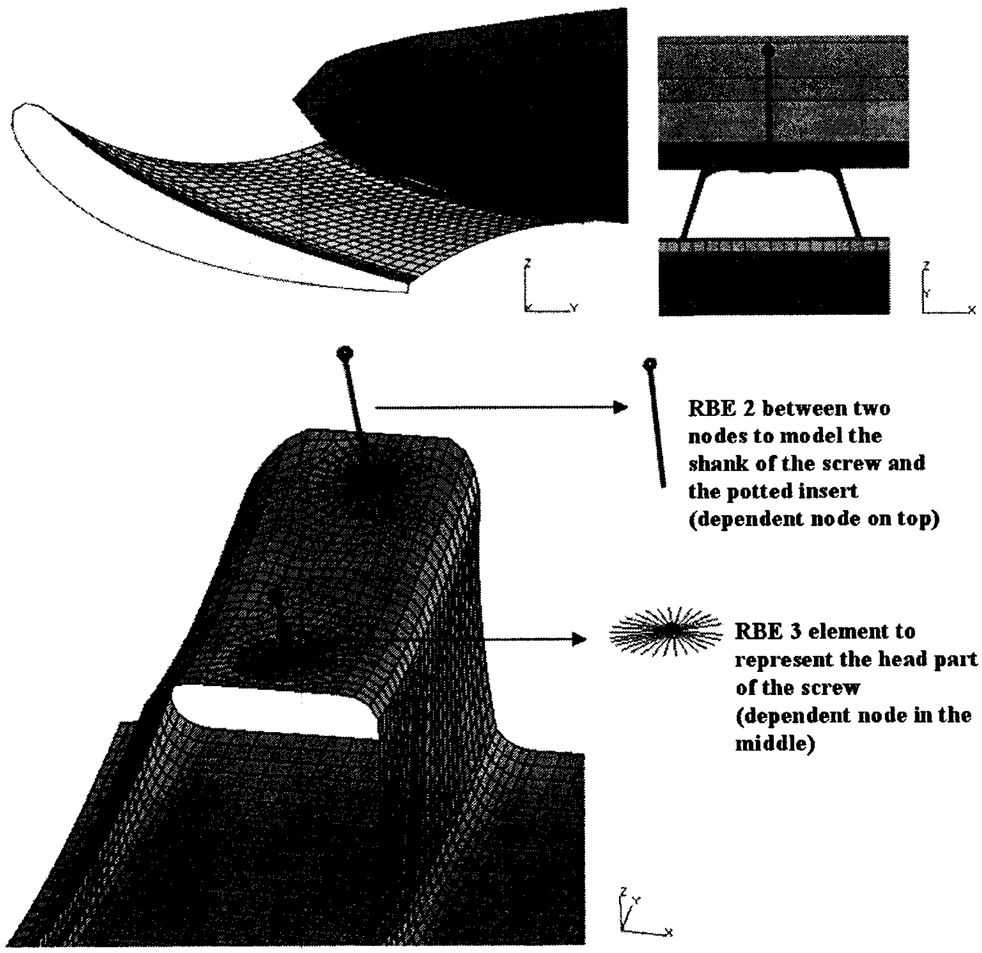

Figure 3.9: Different views (upper left corner: side view, upper right corner: front view) and details on the rigid body elements used to model the screw and bolt fixations between the slat and the stabilizer

3.5.4 Loading

Even if the models are not meant to generate actual magnitudes of stress or strain, it is still important to reproduce the loading conditions accurately enough to obtain valid comparative analyses with respect to the general behaviour of the part under flight conditions.

The load case used for the first design stage is based on Report 407-930-003 provided by Bell Helicopter [51]. In this report, the loads and moments acting on the stabilizer/end plate assembly are concentrated on a single point on the stabilizer (point A in Figure 3.10) and on the end plate (point B in Figure 3.10), forming an equivalent system. Point A corresponds to the middle of the exposed area of the stabilizer wing and point B matches the center of gravity of the end plate. To simplify the analysis, all loads are transposed to point B, which is easier to locate on the model. Thus, a force vector of <1152.09, 354.52, -2657.81> N (<259, 79.70, -597.5> lb) and a moment vector of <5.5, -39.28, 5.06> N·m (<1565.43, -11185.2, 1441.44> lb·in) are applied at the center of gravity of the end plate (detailed calculations in APPENDIX 1A).

A constant surface pressure of 3950.7 Pa (0.573 psi) is also applied on the slat [51] (p. 15.146).

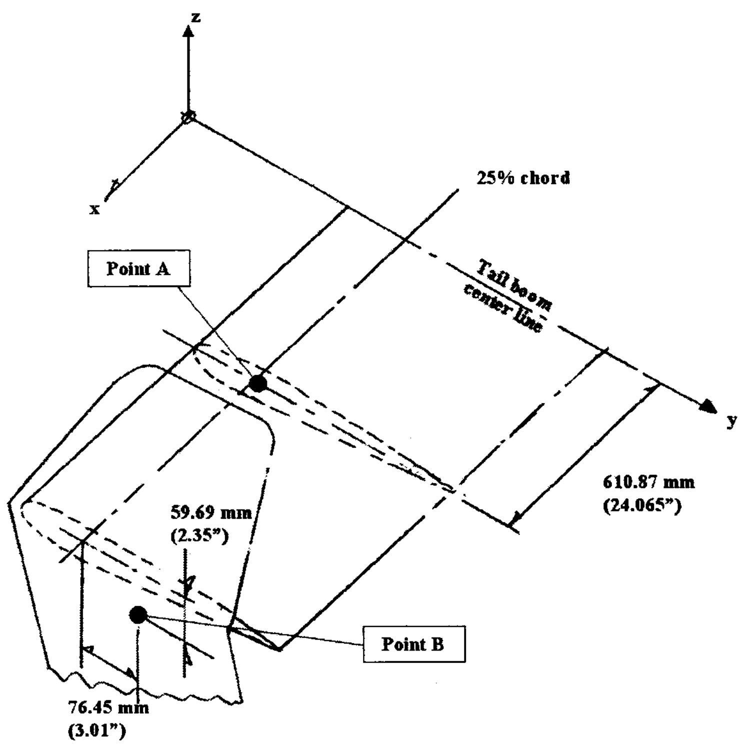

Figure 3.10: Location of the load application points of the equivalent system as described in report 407-930-003 [51]

An illustration of the forces applied at point B and the pressure applied on the slat is show in Figure 3.11.

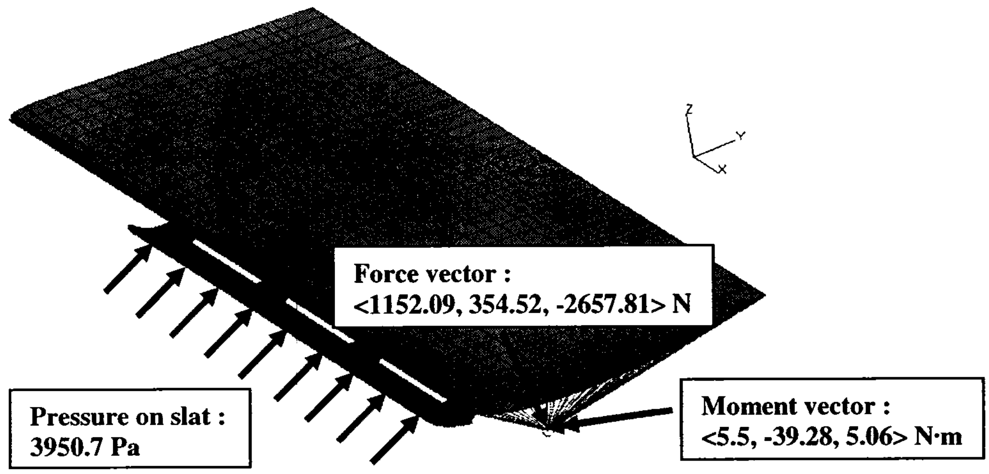

Figure 3.11: Load case applied on the model for the first design stage (see APPENDIX I for more details)

3.5.5 Analyses

The purpose of the analysis stage is developing an analytical tool as well as providing guidelines for eventual modifications on the leading edge slat. The objective is to gradually develop the best solution with the adequate tools.

3.5.5.1 Static analysis

The type of analysis selected for the first design stage is a simple steady-state static failure analysis. The static analysis is simple and time efficient, which makes it a good candidate for iterative analyses. Since the objective of this part of the project is to perform a comparative analysis with a certain number of different models, the static analysis is a better option. It is also known that the oscillatory strains are caused by two distinct modes only: slat bending and stabilizer torsion [12] (p.14).

Nevertheless, fatigue is a crucial aspect in this project since the slat is submitted to repetitive upward and downward deformations. This type of analysis is long and complex, and requires an extensive knowledge of the material properties under cyclic stress. Thus a fatigue analysis is beyond the scope of this current study.

3.5.5.2 Linear analysis

For this work, it is assumed that material properties remain essentially unchanged by loading (force, moment, temperature, etc.). In other words, the system can be simplified to a linear problem. Also, deformations of the slat are estimated to be small enough that equilibrium equations can be written using original geometry rather than deformed geometry [54]. Thus, large deformation theory need not be considered.

3.6 Second design stage

3.6.1 Elements

The models of the second design stage are also composed of Quad 4 shell elements. The size of the elements is similar to those used for the first design stage and is the same for all models (full and half brackets, 4 or 6 plies). As shown in Figure 3.12, isomesh elements are still used to mesh the airfoil surface, the sides of the brackets and the round edges. The top section of the brackets and the inside area of the holes are divided in paver elements. However, the size of the bracket hole has been reduced to correspond more accurately to the dimensions of the original model.

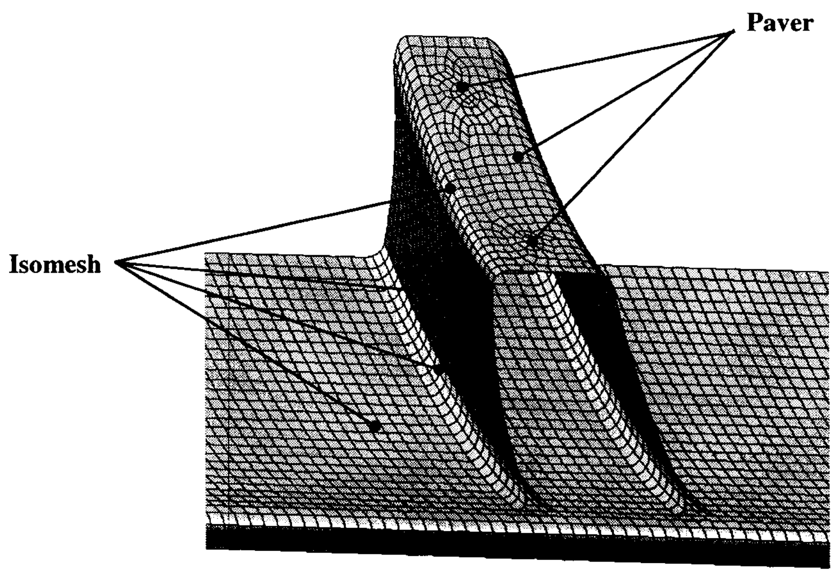

Figure 3.12: Mesh elements used in the different sections of the slat for the second design stage models

The lay-up of the models is done with Laminate Modeler. This time, properties of CYCOM 890 RTM / AS4-GP 6K-5HS woven carbon fabric are used

[41]. Properties at 24°C in dry condition with a Poisson's Ratio evaluated at 0.034 (from fabric T300/F934 in Patran Laminate Modeler support file [32, 50]) have been chosen. A 2D orthotropic material is created with these properties and used for the lay-up in Laminate Modeler.

Model 2A is similar to the model of the first design stage and has 4 layers everywhere of 0.42 mm (0.0165 in) thickness (see FIRST DESIGN STAGE section of Chapter 2 for more details). The sketch of the cross-section of model 2A is the same as the 1st model (see Figure 3.7).

Model 2B is a full bracket model as model 2A with 2 additional layers inside the brackets, which makes 4 plies on the airfoil and 6 plies on the brackets (see SECOND DESIGN STAGE section of Chapter 2 for more details). Figure 3.13 below shows the sketch of the cross-section of model 2B with the exploded view of the modeled lay-up.

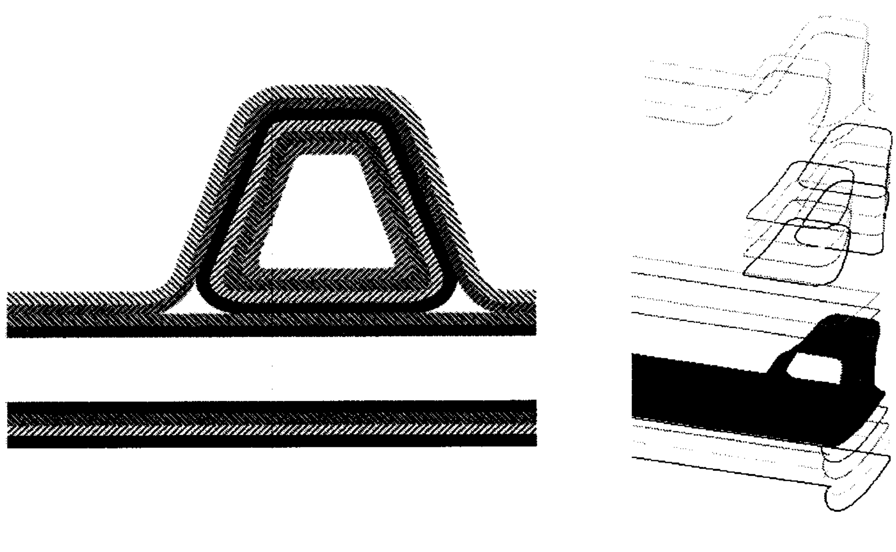

Figure 3.13: Sketch of the cross-section of the model 2B (left) compared with the laminate model in Patran Laminate Modeler (right)

Model 2C has a half bracket geometry with 4 plies on the simply bonded brackets and the airfoil (see SECOND DESIGN STAGE section of Chapter 2 for more details). Figure 3.14 below shows the sketch of the cross-section of model 2C with the exploded view of the modeled lay-up.

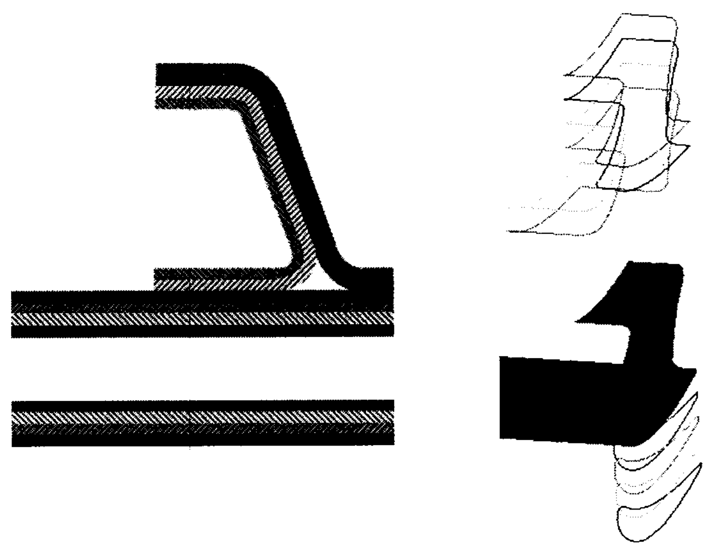

Figure 3.14: Sketch of the cross-section of the model 2C (left) compared with the laminate model in Patran Laminate Modeler (right)

3.6.2 Boundary conditions

Boundary conditions used for the models of the second design stage are the same as the ones used for the models of the first design stage unless otherwise specified. This section covers these specific modifications made on the stabilizer and slat models.

3.6.2.1 Stabilizer

The rigid body element (RBE 3) modeling the end plate is slightly modified. This RBE 3 is connecting the outboard nodes on the stabilizer skin to an outside node. In the first design stage, this outside note corresponded to the center of gravity of the endplate. This node is switched to the hanger test load application point [12] (p.12) since the load case of the second design stage is inspired by hanger test loads (discussed in the following loading section). This test node application point was used in previous FEA studies performed at Bell Helicopter during which the same load cases were applied and validated. This rigid body then corresponds to the interaction between the endplate attachment junction at the end of the stabilizer and the hanger test load application point (see Figure 3.15). The motion of the reference node (the load application point in this case) is the weighted average of the motions of the outboard nodes on the stabilizer skin [50]. Thus, all degrees of freedom (translations and rotations with respect to X, Y and Z axis) of the reference node are the average of the translations (in X, Y and Z direction) of the defined stabilizer nodes.

The coordinate system was also rotated -90° around the Z axis to match the one used for the hanger test (shown in Figure 3.15).

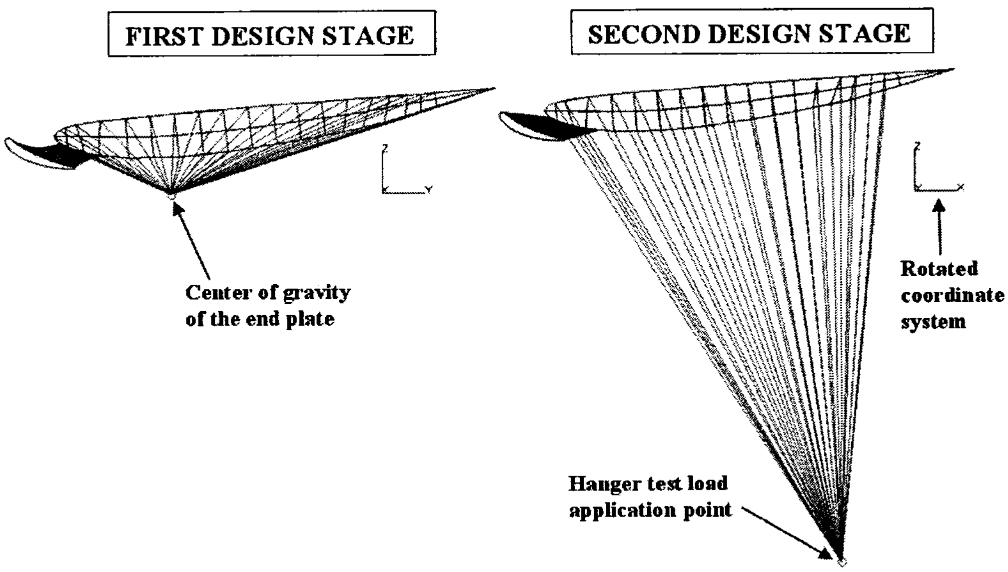

Figure 3.15: Modification of the location of the outside node of the RBE 3 modeling the end plate and the model coordinate system from the first design stage (left) to the second design stage (right)

3.6.2.2 Fixations of the slat on the stabilizer

As mentioned previously in the elements section, the size of the bracket holes is reduced to match the original model more accurately, leaving more space around the attachment hole. To model the slat/screw interaction, all rotations are blocked (456 blocked in Patran) at the nodes corresponding to the screw contact points on the bracket as illustrated in Figure 3.16 below.

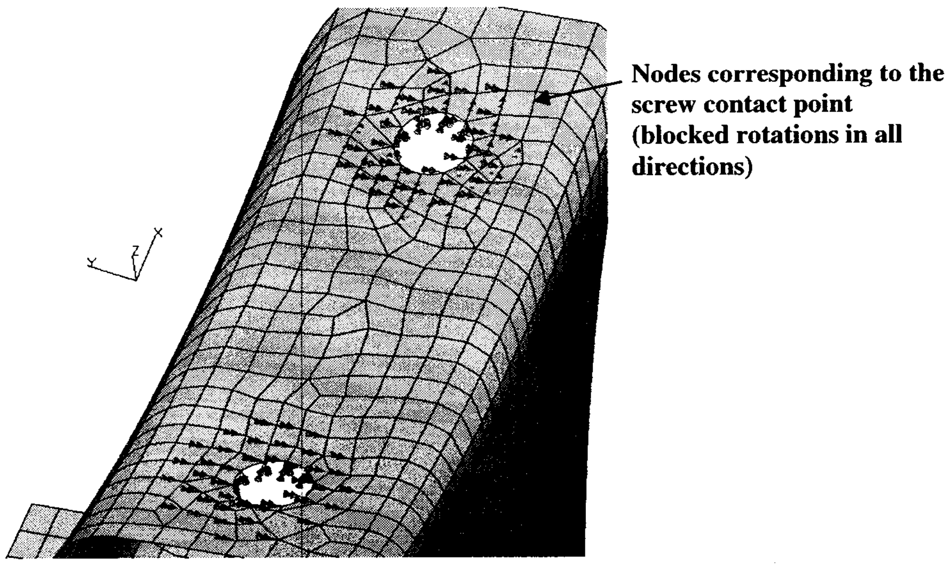

Figure 3.16: Boundary conditions modeling the screw contact points on the brackets

The same slat/screw interaction nodes are used as independent nodes of the RBE 3 rigid body modeling the head part of the screw (more details in the previous FIRST DESIGN STAGE section). This time, all degrees of freedom (translations and rotations with respect to X, Y and Z axis) of the reference node are the average of the displacements normal to the surface underneath the fastener head (translations in Z direction) and displacements normal to the fastener hole surface (translations in X and Y direction) [12] (p.13). The reference nodes located at the junction of the fastener hole and head have their translation average taken in all directions (X, Y and Z axis). The new definition of the RBE 3 modeling the head part of the screw is shown in Figure 3.16.

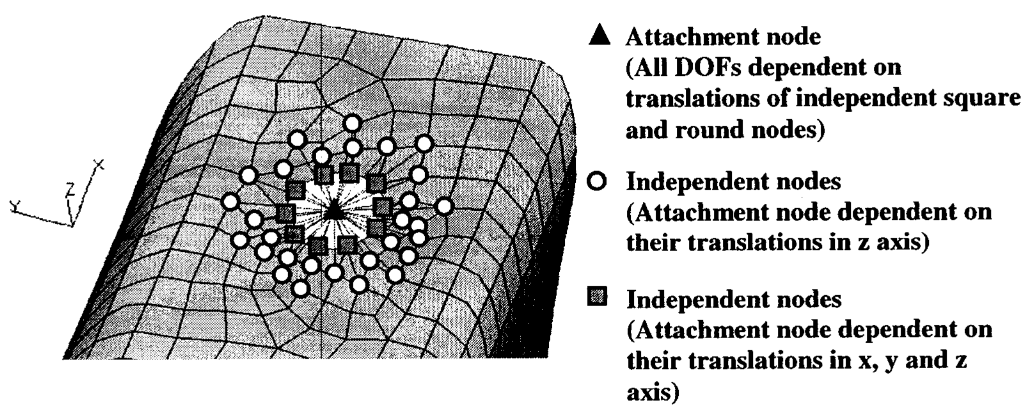

Figure 3.17: Definition of the rigid body nodes modeling the head part of the screw

3.6.3 Loading

The load used for the second design stage is based on the first case of the limit load conditions in R&D-CRIAQ1.15-002 report [12] (p. 4). A linearly distributed force of a total value of 2657.81 N (597.5 lb) is applied downwards on the stabilizer's exposed width. A uniform linear loading of 0.5 N/mm (2.87 lb/in) is acting downwards along the slat section. The force is applied along their respective center of gravity to prevent unwanted torsion (zero moment around the Y axis).

The stabilizer and slat loading are combined with a 177.93 N (40lb) aft load acting as the end plate and inflicting torsion on the stabilizer (see load case applied on all models of the second design stage in Figure 3.18).

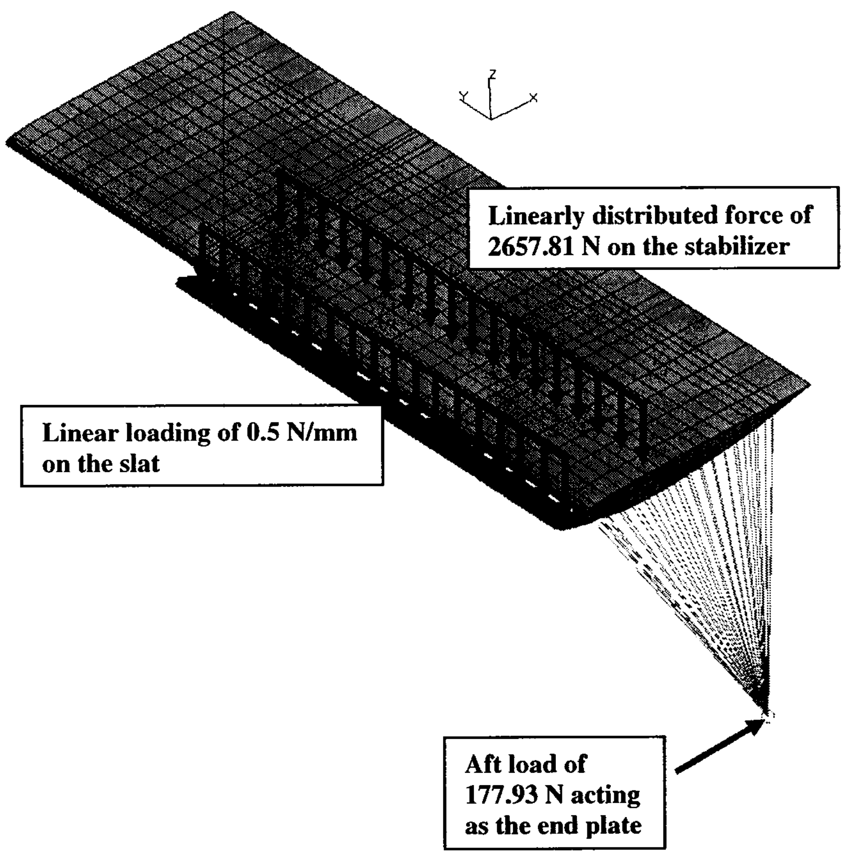

Figure 3.18: Load case applied on all models for the second design stage

3.6.4 Analyses

Static linear comparative analyses are performed on the original aluminium model and composite models 2A, 2B and 2C.

3.7 Third design stage

Under the advice of collaborators from Bell Helicopter, major modifications are made at this stage on several aspects of the models (elements, boundary conditions, loading and analyses). Thus, it increases the accuracy of the results obtained and the models behave in a way that approaches actual service conditions.

3.7.1 Elements

Models in the third design stage have a meshing adapted to the results obtained with the previous models (see sections 4.1.3 and 4.2.3 in Chapter 4 for further details). Since the stress concentration areas are always located on the brackets or its rounded edges, it is not necessary to keep a fine meshing on the airfoil area. This simplifies the model as well as saving simulation time. Moreover, this meshing matches better with the one used on the original aluminium model.

A new area is created to determine more accurately the nodes corresponding to the screw contact points. This area is also included on the original aluminium model. Meshed models used for all third design stage parts compared with the aluminium model are shown in Figure 3.19 below.

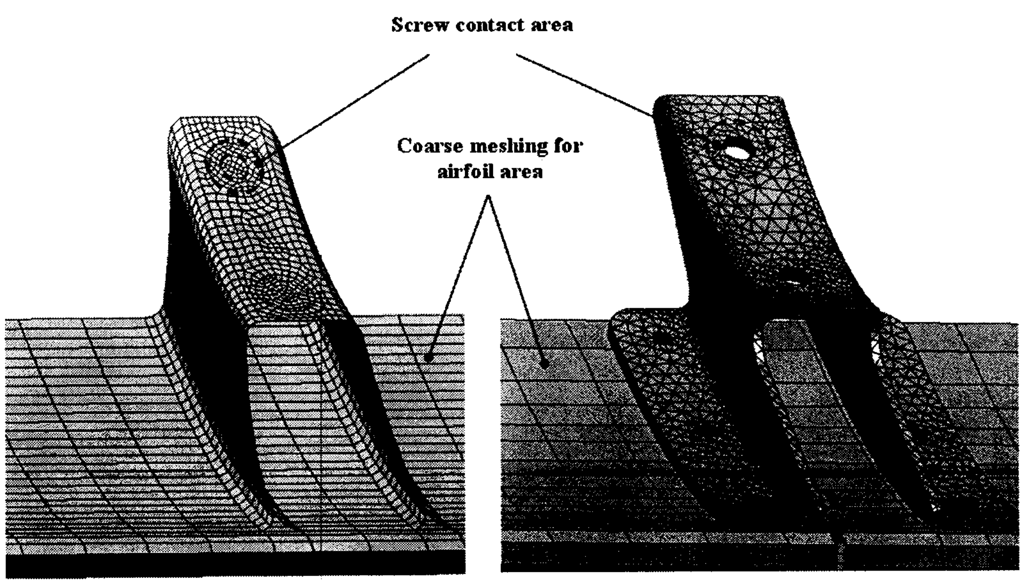

Figure 3.19: Meshed model of the third design stage models (left) and the aluminium part (right)

3.7.2 Draping and material properties

The lay-up of all models is done with the same material properties as the second design stage using Laminate Modeler.

Models 3A and 3B have a full bracket configuration with 4 layers everywhere and the same lay-up strategy as the first model and model 2A. The cross-section of models 3A-3B is the same as the 1st model and model 2A (sketched in Figure 3.7).

Although they have different bracket angle configurations and angles, models 3C-3G all have a half bracket geometry with 4 plies everywhere and the same lay-up approach as model 2C. The sketch of the cross-section of models 3C-3G is the same as model 2C (see Figure 3.14).

Model 3H also has half bracket geometry. Its middle brackets have a similar lay-up than models 3C-3G but its outer brackets are integrated with the airfoil. The sketch of the cross-section of the outer bracket of model 3H with the exploded view of the modeled lay-up is shown in Figure 3.20.

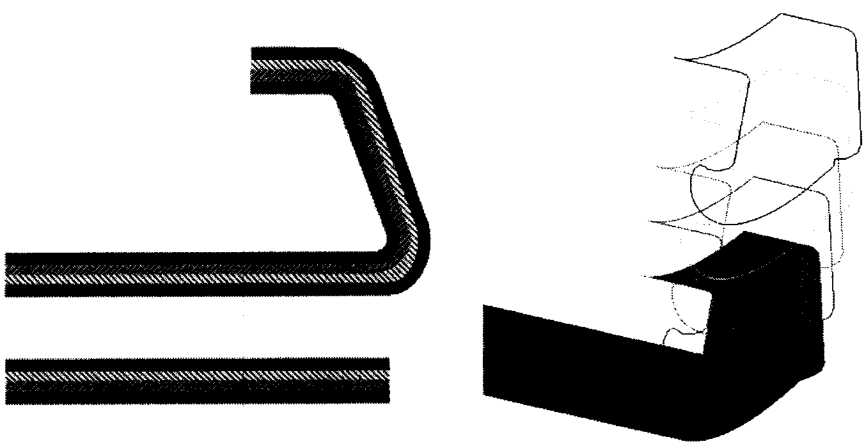

Figure 3.20: Sketch of the cross-section of the outer bracket of model 3H (left) with the laminate model in Patran Laminate Modeler (right)

Models 3I-3M have the same configuration as models 3C-3G with 2 additional plies on the brackets. The cross-section of these models counting 4 plies on the airfoil and 6 plies on the brackets is illustrated in Figure 3.21 with the exploded view of the modeled lay-up.

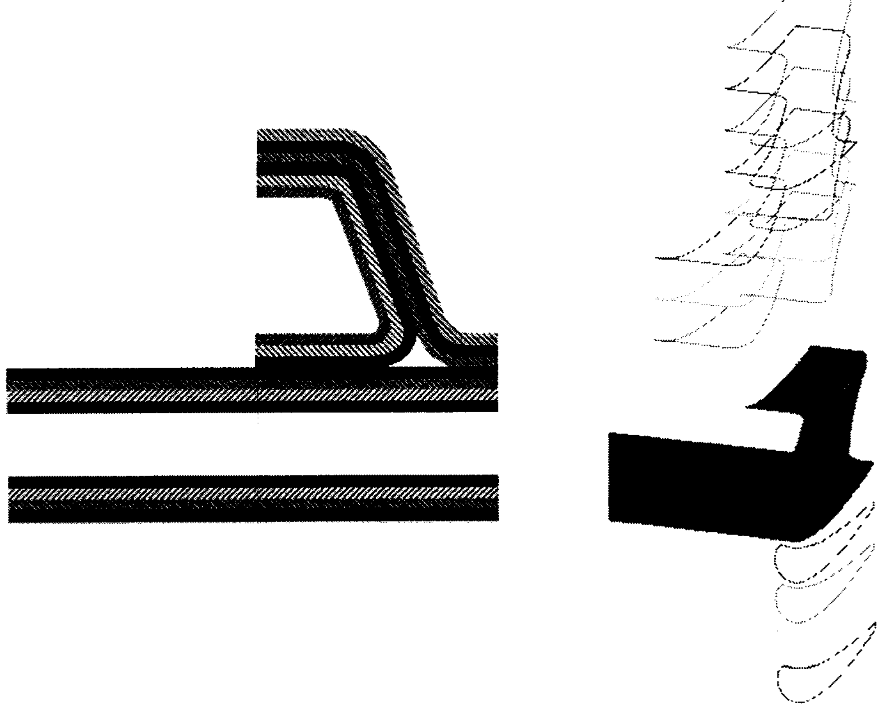

Figure 3.21: Sketch of the cross-section of models 3I-3M (left) with the laminate model in Patran Laminate Modeler (right)

Model 3N is similar to model 3H with 2 additional plies on the brackets. Its middle brackets have the same lay-up as models 3I-3M but its outer bracket cross-section is as illustrated in Figure 3.22. The exploded view of the modeled lay-up is shown on the right side of the figure.

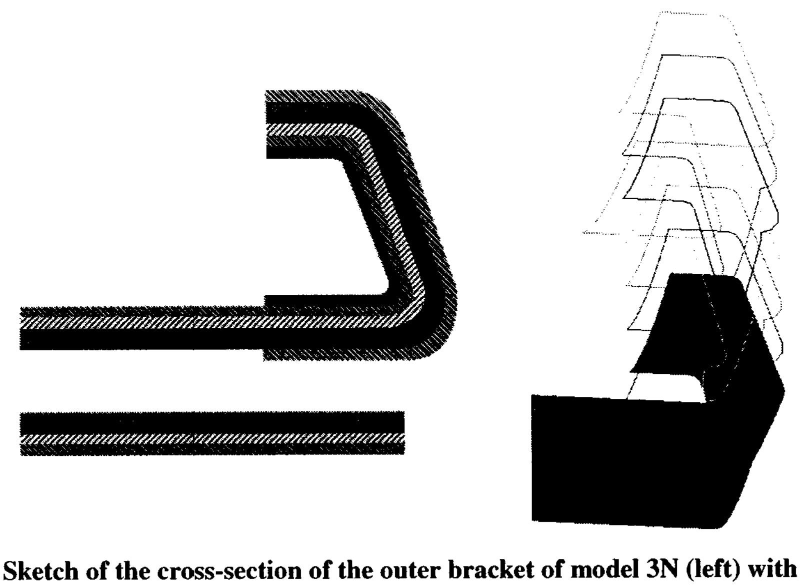

Figure 3.22: Sketch of the cross-section of the outer bracket of model 3N (left) with the laminate model in Patran Laminate Modeler (right)

The last model of the third design phase is model 3P with additional plies on the brackets only covering critical areas located on top of the brackets (return to Figure 1.6 for further justifications). The cross-section of this model is shown in Figure 3.23 for middle brackets and in Figure 3.24 for outer bracket with their respective exploded view of the modeled lay-up.

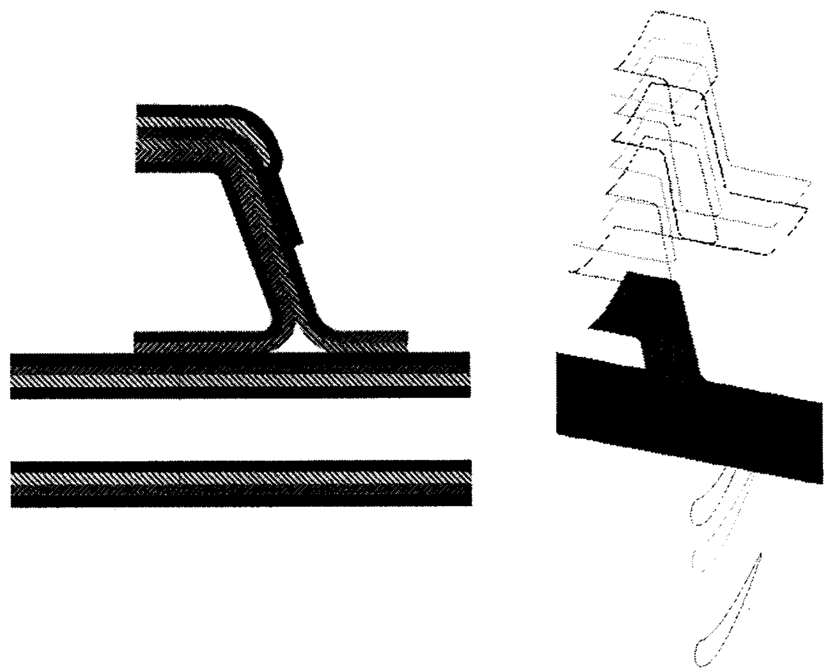

Figure 3.23: Sketch of the cross-section of the inside bracket of model 3P (left) with the laminate model in Patran Laminate Modeler (right)

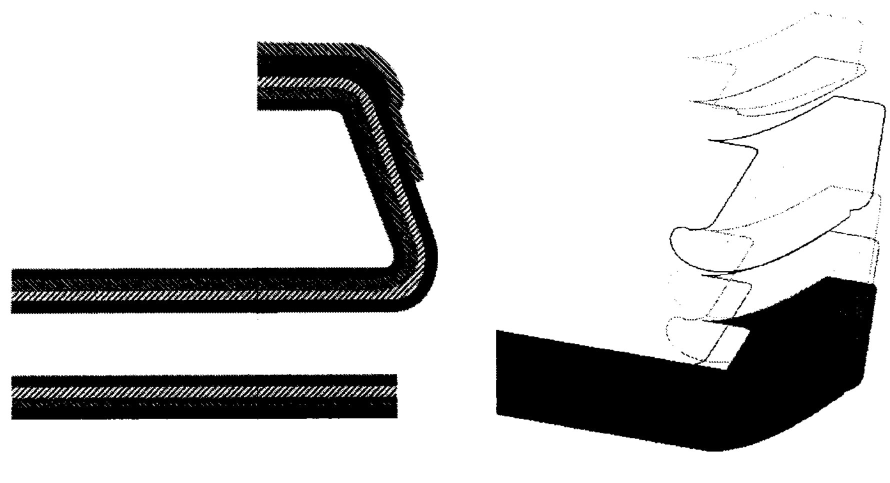

Figure 3.24: Sketch of the cross-section of the outer bracket of model 3P (left) with the laminate model in Patran Laminate Modeler (right)

3.7.3 Boundary conditions

3.7.3.1 Stabilizer

The first modifications on the boundary conditions of the third design stage concern the fixation of the stabilizer to the tail boom. The rigid type of fixation described in the BOUNDARY CONDITIONS section of the first design stage does not adequately reproduce the real tail boom attachment conditions. The real attachments are not as rigid as those of the model (see top of Figure 3.25 for the stabilizer's overall deformation when all junction node have blocked translations). The stiffness of the tail boom is low compared to the stabilizer's stiffness. The stabilizer, being a one piece wing going through the tail boom, should have a deformed shape that looks more like the bottom of Figure 3.25 [55].

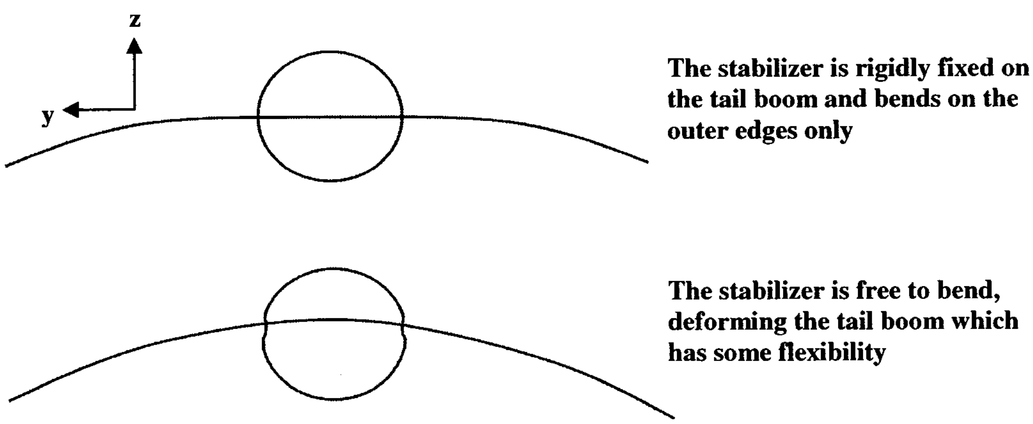

Figure 3.25: Overall deformation of the stabilizer modeled with translations fixed on all directions (top) and deformed shape when the stabilizer is free to bend (bottom)

So, in reality, a small deformation in the Y-direction is present and the model should reflect this by releasing the degree-of-freedom in that direction. It is not necessary to model the tail boom stiffness in the Y-direction because its stiffness is negligible compared to the stabilizer's. A visual justification of the degree of freedom in the Y-direction at the stabilizer/tail boom junction line is shown in Figure 3.26.

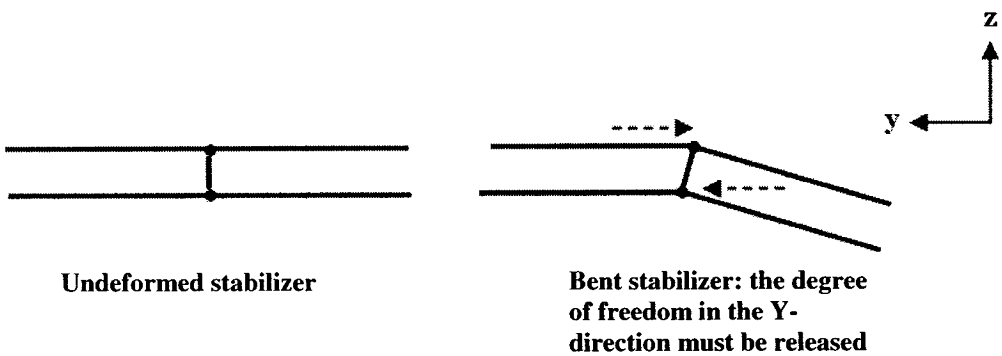

Figure 3.26: Illustration of the nodal displacement when the stabilizer model is bending and justification for releasing the degree-of-freedom in the Y-direction

However, to prevent the model from behaving as a rigid body, it is important to fully constrain it by keeping one node blocked in all directions on each loop corresponding to the junction line of the tail boom and stabilizer (see Figure 3.27).

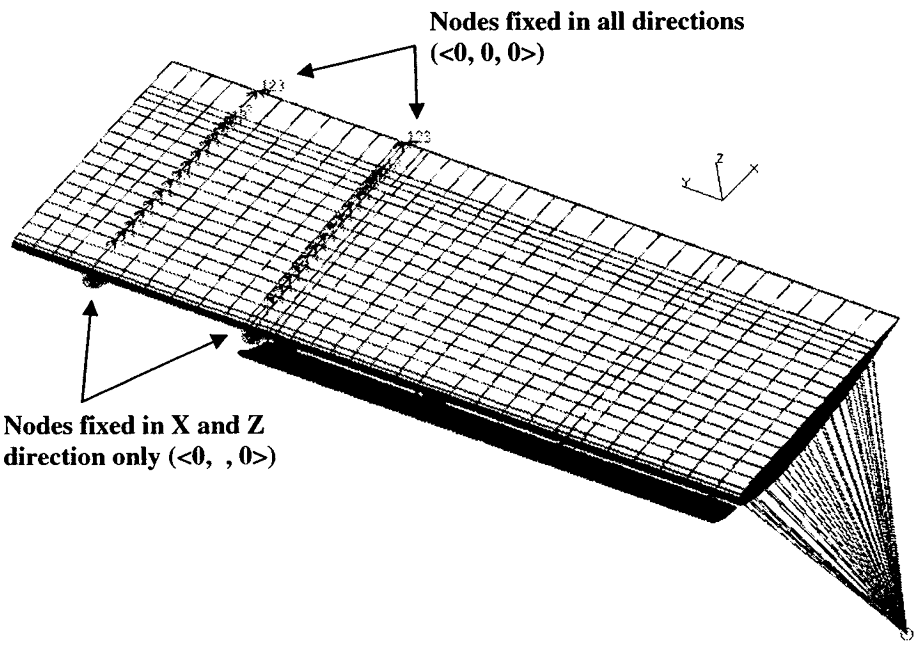

Figure 3.27: Boundary conditions applied on the stabilizer for the third design stage

3.7.3.2 Fixations of the slat on the stabilizer

As mentioned previously in the elements section, the nodes corresponding to the screw contact points on the brackets are more accurately defined by a new area. Figure 3.28 shows these nodes on which all rotations are blocked (456 blocked in Patran) as previously defined in the second design stage (left) and their improved configuration in the third design stage (right).

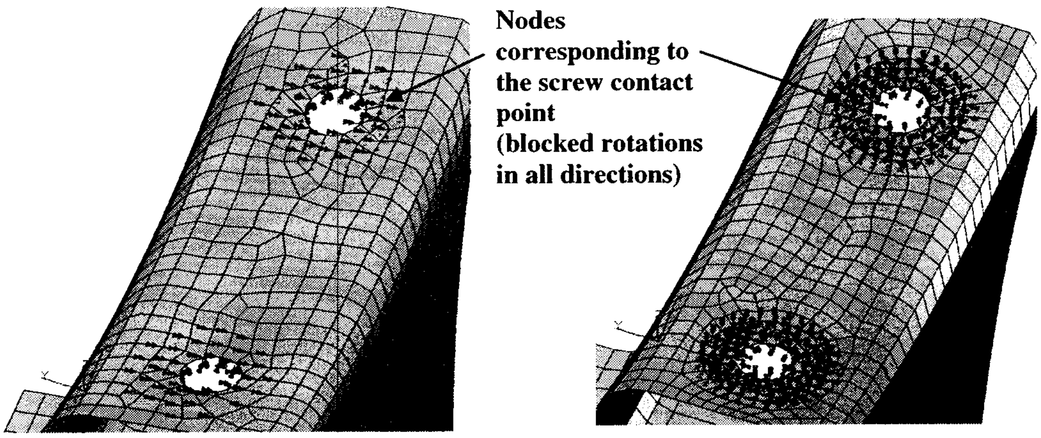

Figure 3.28: Blocked nodes as defined in the second design stage (left) and in the third design stage (right)

3.7.4 Loading

The load case modifications are based on previous FEA models provided by collaborators at Bell [49, 55]. These documents suggested using load application nodes distributed over the top area of the stabilizer and slat. This load distribution over full area is constant along the length and has a triangular distribution along the width with the maximum value corresponding to the center of gravity (approximated at the aerodynamic center of the wing: ¼ chord). A sketch of this triangular load distribution over the area is shown in Figure 3.29.

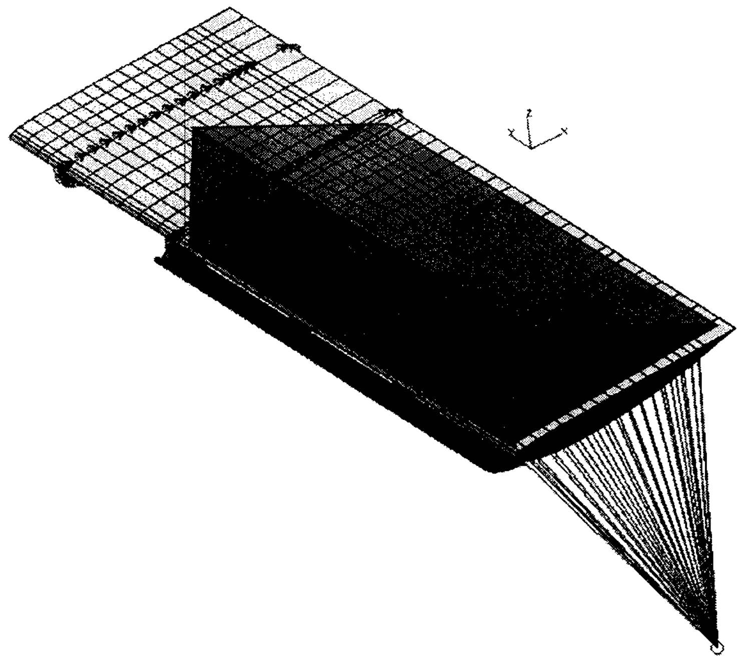

Figure 3.29: Sketch of the triangular load distribution over stabilizer and slat areas (downward loading case)

The total value of the force applied on the stabilizer is still 2657.81 N (597.5 lb). It is distributed over the exposed area of 20 (length) x 14 (width) nodes and can be oriented upwards or downwards. The side view of the triangular distribution on the stabilizer is shown in Figure 3.30 (detailed calculations in APPENDIX 1B).

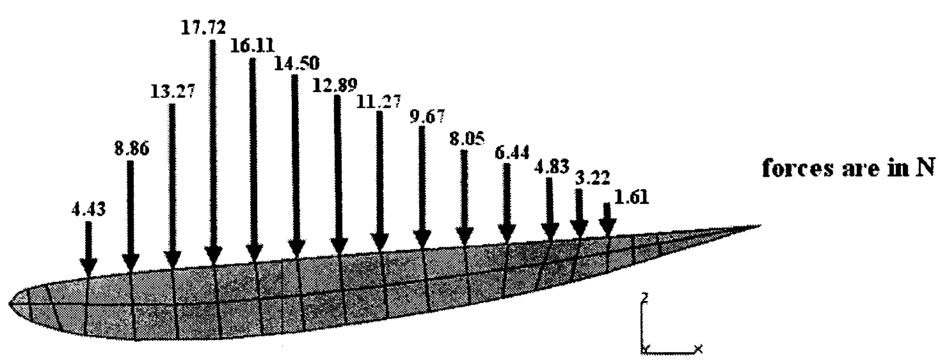

Figure 3.30: Side view of the triangular distribution on the stabilizer (downward loading case)

The same uniform linear loading of 0.5 N/mm (2.87 lb/in) is acting on the slat. It is distributed over an area of 36 (length) x 8 (width) nodes and can be oriented upwards or downwards. The triangular distribution is shown in Figure 3.31 (detailed calculations in APPENDIX 1C).

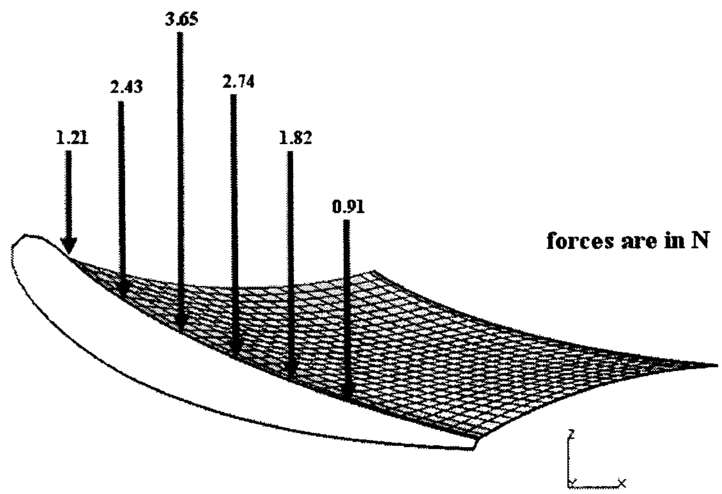

Figure 3.31: Side view of the triangular distribution on the slat (downward loading case)

The 177.93 N (40lb) aft load acting as the end plate and inflicting torsion on the stabilizer is applied again on the hanger test node.

All applied loads are multiplied by a load factor of 1.5 that acts as a form of safety factor. This overdesigned the model accounts for imperfections in materials, flaws in assembly, material degradation and uncertainty in load estimates [56].

For this model iteration, 4 load cases considered to be limit [12] (p. 4) and simulating a wider set of flight conditions are applied on the assembly. These load cases are the following:

<u>Load case 1</u>: Stabilizer down + Slat down + aft load

<u>Load case 2</u>: Stabilizer up + Slat down + aft load

<u>Load case 3</u>: Stabilizer down + Slat up + aft load

<u>Load case 4</u>: Stabilizer up + Slat up + aft load

3.7.5 <u>Analyses</u>

As for models from the previous design stage, the original model as well as models 3A-3P, is subjected to static linear comparative analyses.

3.8 Fourth design stage

Modifications of the fourth design stage are again greatly influenced by the expertise and advice of collaborators from Bell Helicopter. New ply drop draping, more accurate material properties, improved boundary conditions and additional load cases take place at this final design stage.

3.8.1 *Elements*

The elements of the fourth design stage models are similar to those of the third design stage. However, new areas are created to determine the limits of the ply drops described in the FOURTH DESIGN STAGE section of Chapter 2. Figure 3.32 shows meshed models used for all parts of the third design stage compared with those of the fourth design stage.

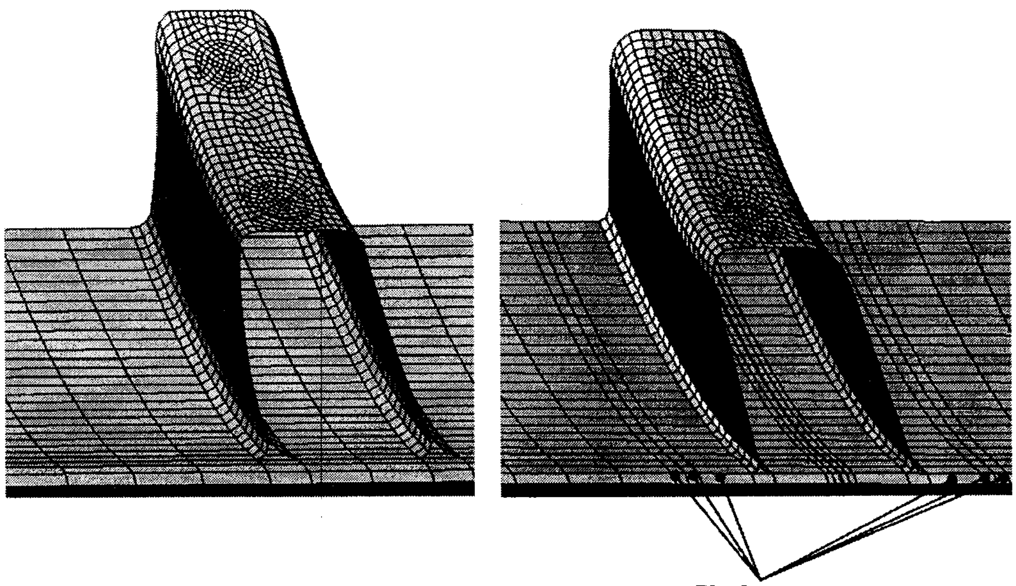

Figure 3.32: Meshed model used for the third (left) and fourth (right) design stage parts

3.8.2 *Draping and material properties*

The material properties used on the composite models are changed to high temperature / wet properties of 890 RTM / AS4-GP 6K-5HS (120 °C wet). These properties are more realistic considering the operating temperature of 100°C (212 °F) [12] (p. 4). The wet aspect considers the worst possible flight conditions. The coefficient of thermal expansion of 1.2E-05 / °C (6.67E-06 / °F) is taken from the graphite/epoxy model (fabric T300/F934) from Patran Laminate Modeler support file [32, 50]. Again, a 2D orthotropic material is created with these properties and used for the lay-up in Laminate Modeler.

More modifications are brought to material properties to take barely visible impact damage (BVID) into account. These small damages are produced by low velocity impact resulting from dropped tools, runway stones or other causes. Even though they may not be found during heavy maintenance general visual inspections, they can significantly reduce the compressive strength. This degrading effect is due to the formation of internal delaminations which extend beyond the immediate contact area made by the impactor. The delaminated plies in the damage zone buckle under compressive load because of the pronounced stiffness loss. However, BVID has little effect on residual tensile strength [57]. It has been proven that BVID reduce the compression strength by 50% [58] and the shear strength is lowered to 85% of its original value [55]. Since the slat must be able to support residual strength loads without failure until the damage is found and repaired [59], the properties assigned to the part simulate the worst BVID case: 50% of the original compression strength (Compression stress limit 11 = 50% of 588 MPa = 294 MPa, Compression stress limit 22 = 50% of 555 MPa = 277.5 MPa) and 85% of the shear strength (Shear stress limit = 85% of 68 MPa = 57.8 MPa).

Models 4A-4D have a full bracket configuration with 4 plies on the airfoil and 6 plies on the brackets, with a ply drop on the airfoil bonding area. Figure 3.33 shows the cross-section of the middle brackets simply bonded on the airfoil (left) and Figure 3.34 shows outer brackets integrated with the airfoil (right).

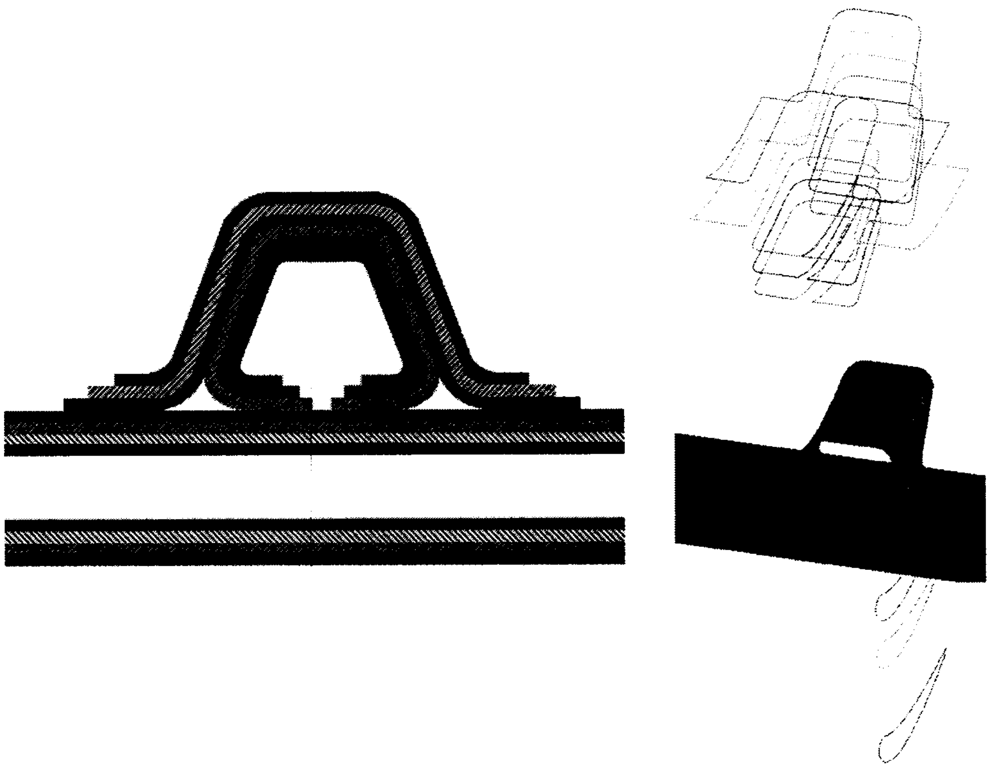

Figure 3.33: Sketch of the cross-section of the middle brackets of models 4A-4D (left) with the corresponding laminate model in Patran Laminate Modeler (right)

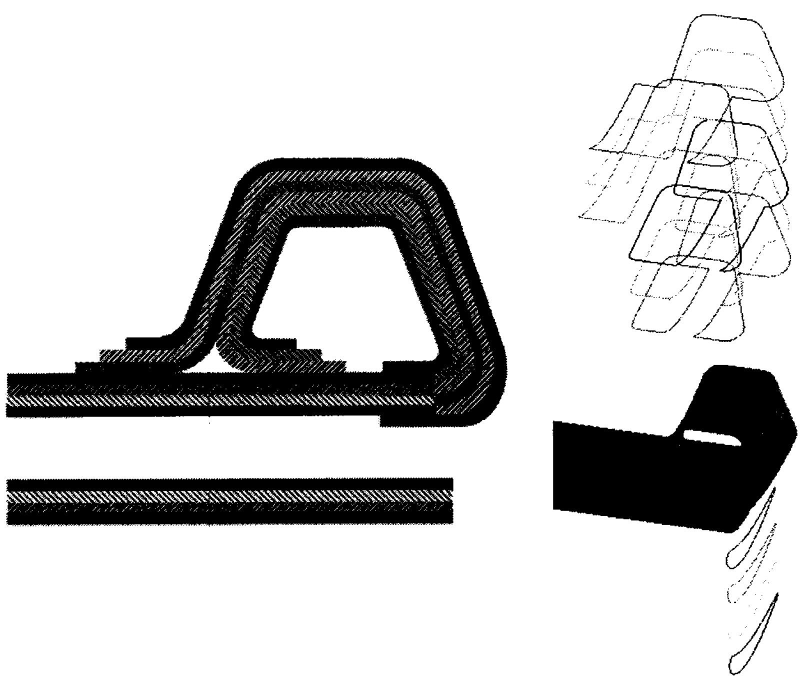

Figure 3.34: Sketch of the cross-section of the outer brackets of models 4A-4D (left) with the corresponding laminate model in Patran Laminate Modeler (right)

Models 4E-4H have a half bracket configuration, with their brackets opened towards the outside. Like previous models from the fourth design stage, they count 4 plies on the airfoil and 6 plies on the brackets, with a ply drop on the airfoil bonding area. The cross-section of all brackets is the same as the middle brackets of models 4I-4L (see Figure 3.35 below)

Models 4I-4L also have a half bracket configuration, with their brackets opened towards the inside with 4 plies on the airfoil and 6 plies on the brackets and a ply drop on the airfoil bonding area. Figure 3.35 shows the cross-section of the middle brackets simply bonded on the airfoil (left). The cross-section of the outer brackets integrated with the airfoil is the same as model 3N (shown in Figure 3.22).

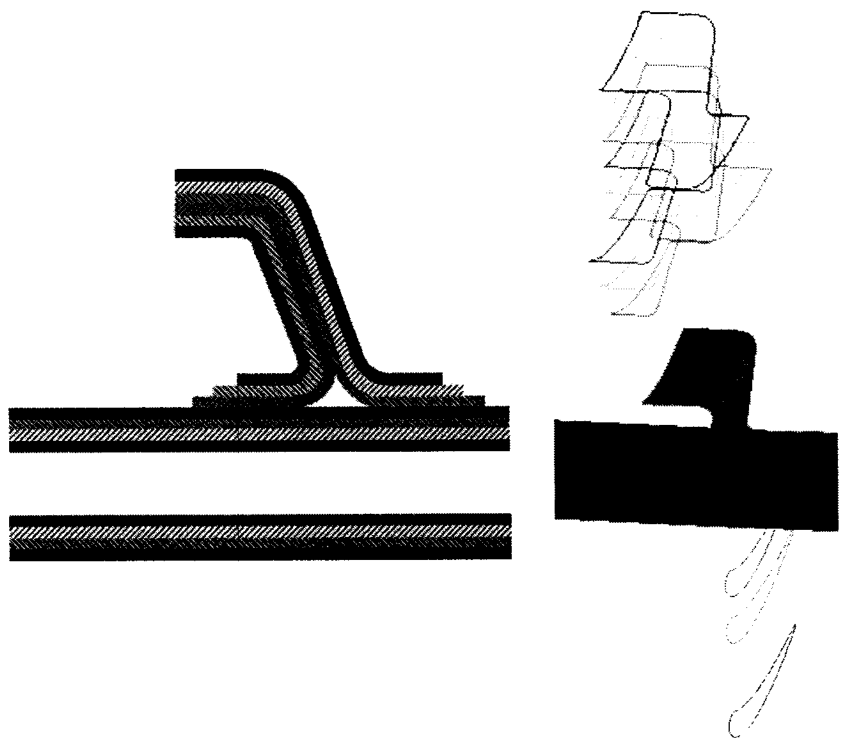

Figure 3.35: Cross-section of the middle brackets of models 4I-4L (left) with the laminate in Patran Laminate Modeler (right)

Since the original model is composed of 3D elements and has a different meshing and geometry, it is difficult to compare it efficiently with the composite models, with respect to material performance. This is important to be able to detect and interpret the similarities and differences in stress concentration areas as well as thermal expansion behaviour. Models 4M-4Y are then created directly from finite element models of models 4A-4L, respectively. These additional models have the same meshing, boundary conditions and loading parameters with different assigned material properties. The models are assumed to be one-piece without any modeled screws or internal attachments.

Material properties of aluminium 6061-T6 with a thickness of 1.52 mm (0.06 in) are assigned to the airfoil surface. The same thickness value is assigned to the airfoil surface of the original model provided by Bell [49]. The brackets have properties of aluminium 2024-T3511 with a thickness of 1.78 mm (0.07 in). This value corresponds to the average of all thicknesses shown in the bracket drawing [45] (sheet 4). The junction surfaces between the brackets and the airfoil have a thickness of 3.3 mm (0.13 in) which corresponds to both components' thicknesses. Since it is not possible to assign two different material properties to the same surface, the material assigned for this region is the one with the lower strength: aluminium 6061-T6. By assuming this junction not as strong as the real area, it provides an additional safety factor on the structure. Figure 3.36 shows the assigned material properties and thicknesses of aluminium models 4M-4Y.

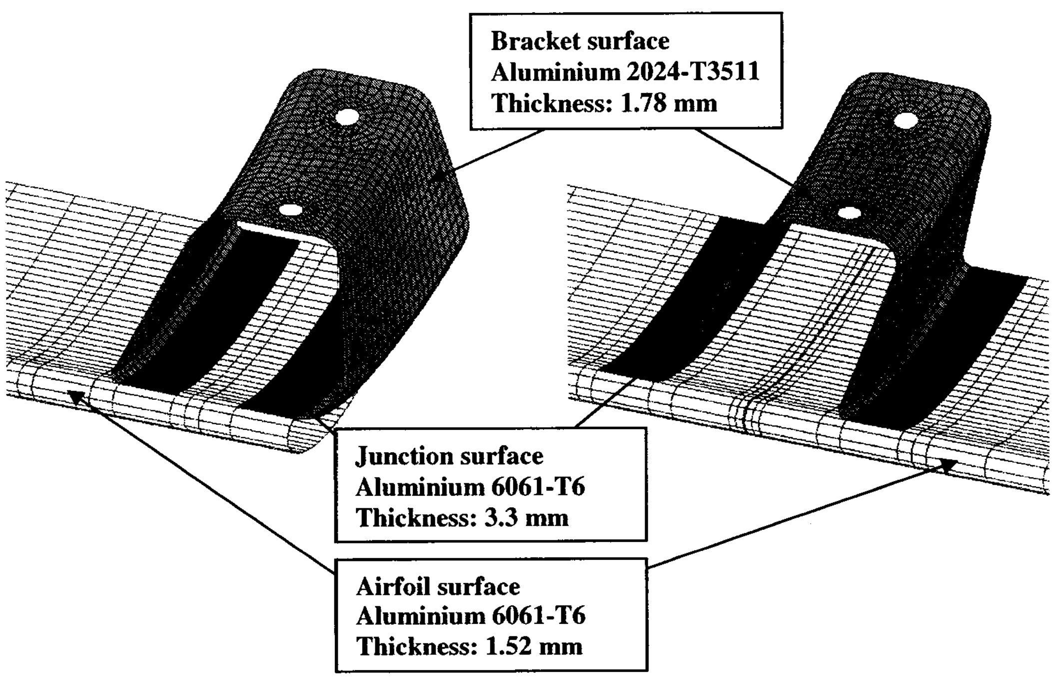

Figure 3.36: Material properties and thicknesses assigned to models 4M-4Y (left: outer bracket section, right: middle bracket section)

3.8.3 Boundary conditions

3.8.3.1 Stabilizer

A small correction is made on the fixation of the stabilizer on the tail boom. Since the stiffness of the tail boom does not prevent the stabilizer from deforming freely, the one piece wing should have constraints that are as minimal as possible. Only one node in both loops corresponding to the junction line of the tail boom and stabilizer should be blocked in all directions as shown in Figure 3.37 below.

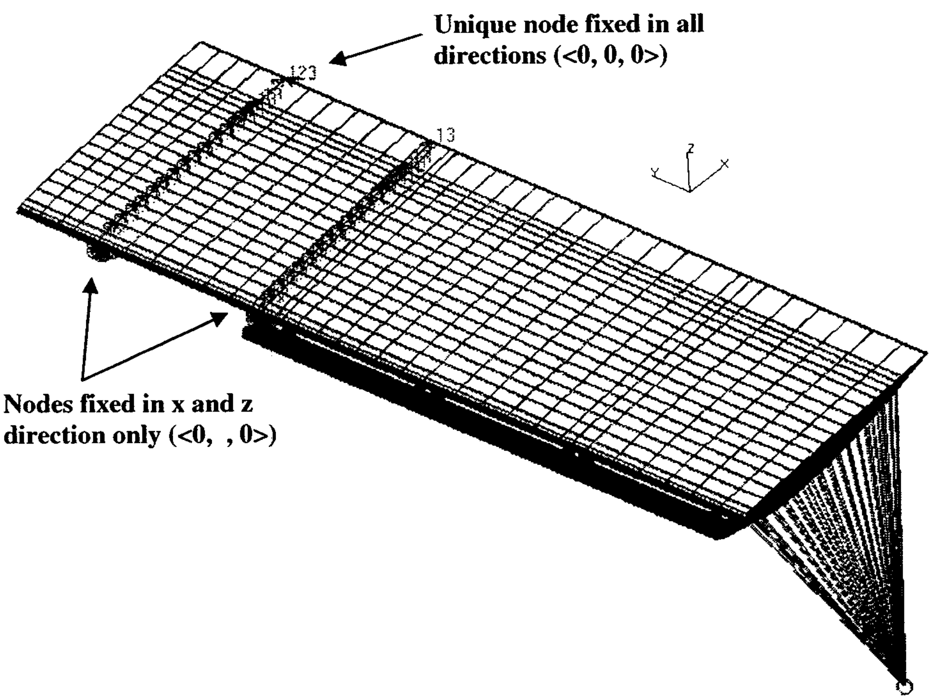

Figure 3.37: Boundary conditions applied on the stabilizer for the fourth design stage

3.8.3.2 Fixations of the slat on the stabilizer

Modifications are brought to the definition of the rigid body elements modeling the screw fixations of the slat on the stabilizer. As described in the FIRST DESIGN STAGE section of this chapter, different types of RBE connect specific nodes with determined displacement constraints. For the previous design stages, these displacements were associated to the global coordinate system. This analysis coordinate frame is adequate for RBE 2s modeling the screw shafts since they are already aligned with the Z axis of the global coordinate system. However, it is more adequate to associate each RBE 3 modeling the head part of the screw with a local analysis coordinate system which is aligned with the surface (see Figure 3.38). The degrees of freedom of the associated nodes are then represented by displacements normal to the surface underneath the fastener head. Local coordinate systems are used to properly align the degrees-of-freedom of nodes used with the RBE 3s with the fastener axis [12] (p.13).

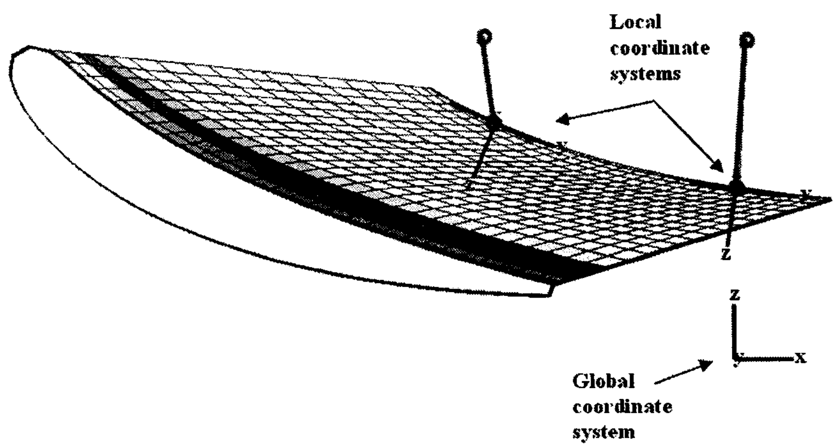

Figure 3.38: Orientation of local coordinate systems used for RBE 3s with respect to global coordinate system

The same local coordinate systems are used for the definition of the blocked rotation (456 blocked in Patran) corresponding to the screw contact points on the brackets (shown in Figure 3.28).

To model the screw fasteners with more accuracy, a bush element is added between RBE 2 (rigid body between 2 nodes) and the RBE 3 elements (motion of the middle node is the weighted average of the motions of the screw contact points). The bush element is, in fact, a 2D bar element to which fastener properties has been assigned. It is created between RBE 2's dependent node (junction node between the stabilizer skin and the middle of the top bracket hole) and RBE 3's dependent node (middle of the top bracket hole) as shown in Figure 3.39. A stiffness of 17.51 N/mm (100 lb/in) around the Z axis is specified to model fastener rotation (twist along fasteners' axis) [12] (p.13). The local coordinate systems are used for the definition of the bush element.

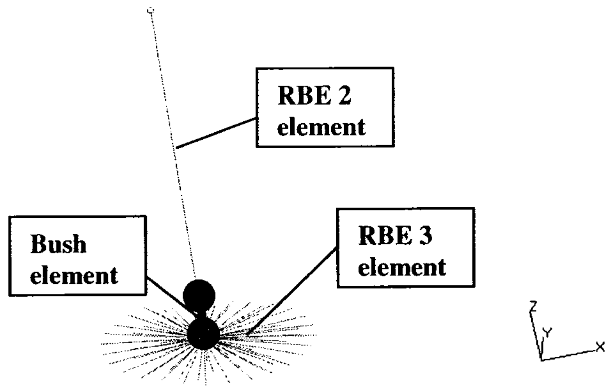

Figure 3.39: Location of the bush element between RBE 2 and RBE3 elements

3.8.4 Loading

The high operating temperature of the slat could potentially have a major influence on its performance. As mentioned in the BENEFITS AND DRAWBACKS OF COMPOSITES section of Chapter 2, temperature induced deformations are an important aspect to investigate, especially when the composite part is to be statically combined with metal parts. The deformations have the potential to create additional stresses on the part, especially on the outboard brackets. To study this aspect, a thermal load of 121 °C (250 °F) [12] (p. 4) is created and applied on all nodes.

To account for thermal effects, 5 additional load cases are created, for a total of 9 different load cases simulating an even wider set of flight conditions. The thermal load has been added to all current load cases. Load cases 5-8 have different force values applied to the parts. In load cases 5-8, the total value of the force applied on the stabilizer is 1334.47 N (300 lb) and a linear loading of 0.53 N/mm (3 lb/in) is acting on the slat. A 88.96 N (20 lb) aft load is applied on the hanger test node, acting as the end plate and inflicting torsion on the stabilizer [55]. Although these loads are lower than load cases 1-4, it is not clear whether the additional effect of the thermal load will be additive or not. Thus the lower load, combined with thermal, could be worse than the higher load cases.z Load case 9 is composed of a thermal load only.

The 9 different load cases applied to the assembly are as follows:

Load case 1: Stabilizer down + Slat down + aft load + thermal
Load case 2: Stabilizer up + Slat down + aft load + thermal
Load case 3: Stabilizer down + Slat up + aft load + thermal
Load case 4: Stabilizer up + Slat up + aft load + thermal

Original
Slat : 0.5 N/mm
Stabilizer : 2657.81 N
Aft load: 177.93 N

Load case 5: Stabilizer down + Slat down + aft load + thermal
Load case 6: Stabilizer up + Slat down + aft load + thermal
Load case 7: Stabilizer down + Slat up + aft load + thermal
Load case 8: Stabilizer up + Slat up + aft load + thermal

Additional
Slat : 0.53 N/mm
Stabilizer : 1334.47 N
Aft load: 88.96 N

Load case 9: Thermal load only

Some modifications are also brought to the triangularly distributed loading applied on the stabilizer and slat. The triangular distribution defined at the third design stage results in a torsion moment to the assembly. To eliminate this unwanted additional load on both parts, the new triangular distribution has to have a zero moment around the Y axis at ¼ chord (corresponding to the approximated center of gravity of each airfoil). The distribution area on each part (stabilizer and slat) is modified in order to obtain a torsion-free load distribution.

For load cases 1-4, the total value of the force applied on the stabilizer is still 2657.81 N (597.5 lb). It is distributed over the exposed area of 20 (length) x 16 (width) nodes and can be oriented upwards or downwards. The side view of the triangular distribution on the stabilizer is shown in Figure 3.40 (detailed calculations in APPENDIX 1D).

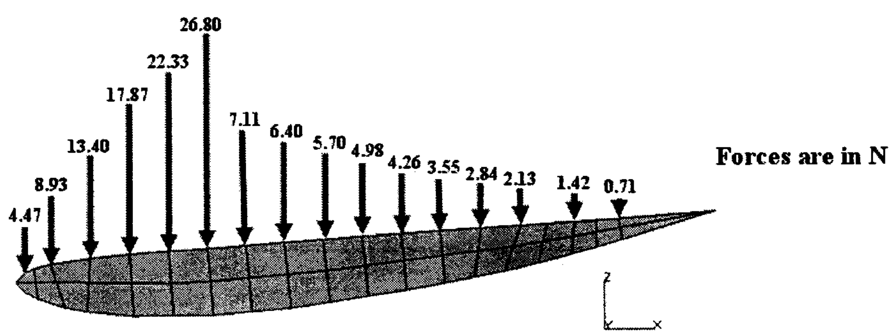

Figure 3.40: Side view of the triangular distribution on the stabilizer for load cases 1-4 (downward loading case)

For load cases 1-4, a uniform linear loading of 0.5 N/mm (2.87 lb/in) is acting on the slat. It is distributed over a wider area of 35 (length) x 11 (width) nodes and can be oriented upwards or downwards. The side view of the triangular distribution is shown in Figure 3.41 (detailed calculations in APPENDIX 1E).

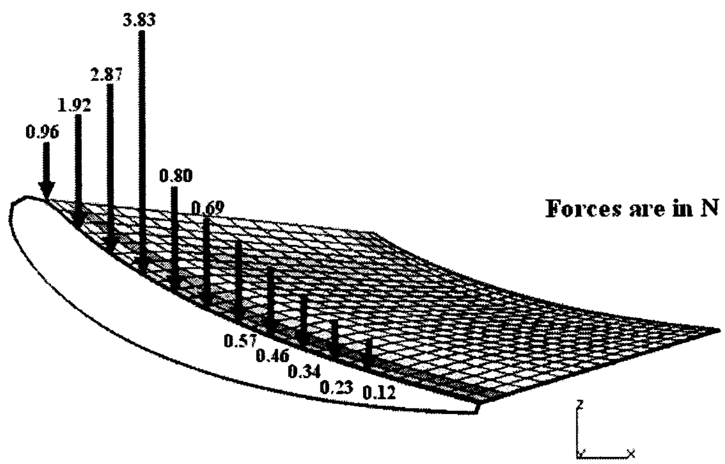

Figure 3.41: Side view of the triangular distribution on the slat for load cases 1-4 (downward loading case)

For load cases 5-8, the total value of the force applied on the stabilizer is almost half the one used for the precedent cases: 1334.47 N (300 lb). It is distributed over the same exposed area described for load cases 1-4 of 20 (length) x 16 (width) nodes and can be oriented upwards or downwards. The side view of the triangular distribution on the stabilizer is shown in Figure 3.42 (detailed calculations in APPENDIX 1F).

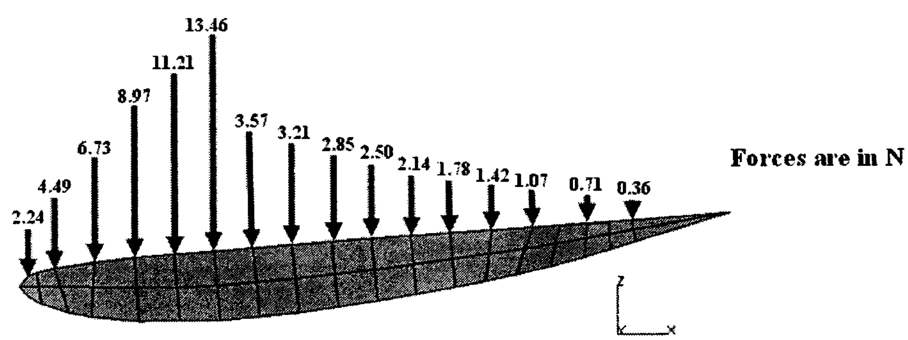

Figure 3.42: Side view of the triangular distribution on the stabilizer for load cases 5-8 (downward loading case)

For load cases 5-8, a slightly higher uniform linear loading of 0.53 N/mm (3 lb/in) is acting on the slat. This value is almost the same as the one used for previous load cases but is modified to meet the hanger test requirement load case

[12] (p. 9). It is distributed over an area of 35 (length) x 11 (width) nodes and can be oriented upwards or downwards. The side view of the triangular distribution is shown in Figure 3.43 (detailed calculations in APPENDIX 1G).

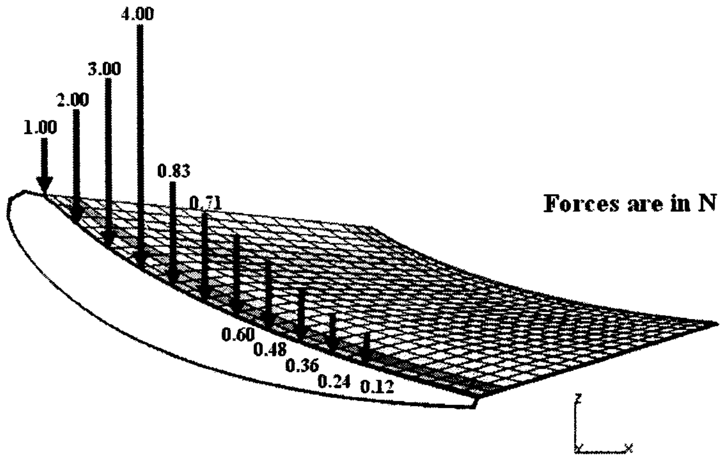

Figure 3.43: Side view of the triangular distribution on the slat for load cases 5-8 (downward loading case)

3.8.5 Analyses

The original aluminium model, composite models (models 4A-4L) and aluminium shell models (models 4M-4Y) are all subjected to static linear comparative analyses.

3.9 Comments on finite element models

The overall objective of the finite element model section was to describe the decision process through the different aspects involved in the development of FEA models. For the 4 design stages, a number of perspectives were analyzed individually, modified and improved through the modeling sequence. Hence, elements, draping and material properties, boundary conditions, loading and analysis were all gradually changed in function of justified criteria. This evolution of the models is a lengthy process but is essential in order to obtain comparative analyses as accurate as possible with respect to the real behaviour of the parts in service.

The following section contains the results obtained with each of the models described. It constitutes an essential part of the project since the final design choice is greatly influenced by the results collected in this comparative analysis.

4. COMPARATIVE ANALYSIS RESULTS

This section deals with results generated by models from all design stages. It constitutes an important step in the comparative design process since the behaviour of each model is studied and interpreted. Areas with stress concentration and overall deformations of the part are shown and compared. As mentioned previously in the introduction of Chapter 3, these simulations are not meant to generate actual magnitudes corresponding to those of the part in service, but act as a reference for design evolution. Indeed, decisions and justifications concerning the design are closely dependent on analysis findings.

For all design stages, failure criteria used are described and explained. Justifications concerning changes in models as well as advantages and disadvantages of each model are also discussed.

Before showing and interpreting the results, it is convenient to assign each bracket a number in order to localize it without having to display the whole part every time. Figure 4.1 shows the front view of the slat with the identified brackets.

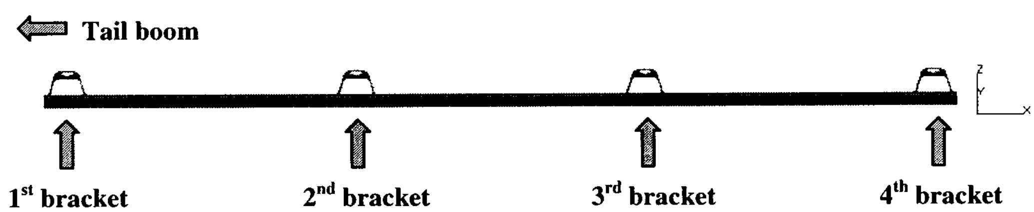

Figure 4.1: Front view of the left hand side leading edge slat with the identified brackets

4.1 First design stage

4.1.1 Overall deformations

One way to make sure the behaviour of the composite assembly model is comparable with the actual assembly in service is to compare its deformations with the model of the current aluminium part. This model, inspired from a finite element study performed by Bell Helicopter is considered to be reliable enough to serve as a reference.

Figure 4.2 shows the overall deformations of the aluminium and composite assemblies under the first design stage load case. Downward deflection of the assembly and torsion of the stabilizer are similar. This deformation scheme is mainly influenced by the force and moment applied at the center of gravity of the end plate. The maximum resultant displacement value is 9.32 mm (0.367 in) for the original model and 9.88 mm (0.389 in) for the composite assembly which is comparable. The composite model is then estimated to have a similar behaviour than the real wing assembly thus, expected to have similar aerodynamic behaviour.

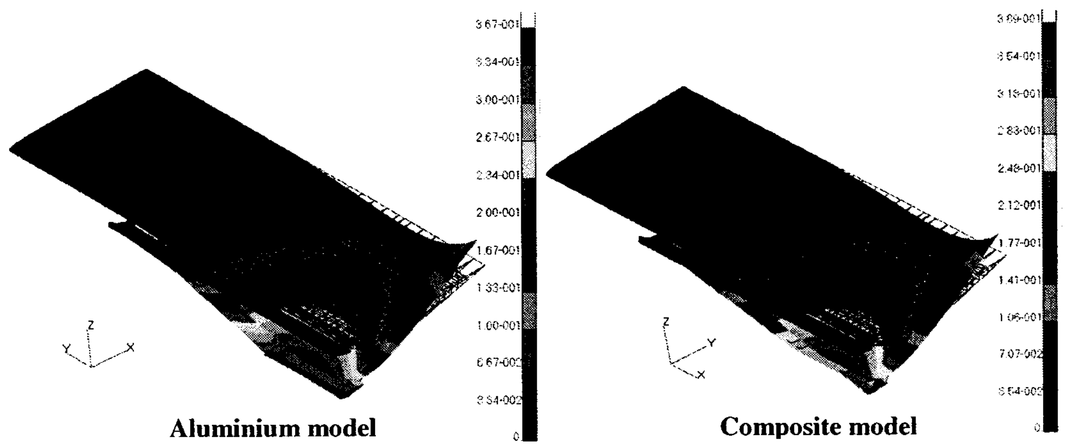

Figure 4.2: Overall deformations of the aluminium slat assembly (left) and the composite slat assembly (right)

As illustrated in Figure 4.3, the overall deformation of the slat under loading is oriented downwards (negative Z-direction) and towards the back of the helicopter (positive Y-direction). The maximum deflection is 9.80 mm (0.386 in) at the tip of the slat. The location of the maximum translational displacement was expected to be there since the stabilizer is fixed on the tail boom as a cantilever beam.

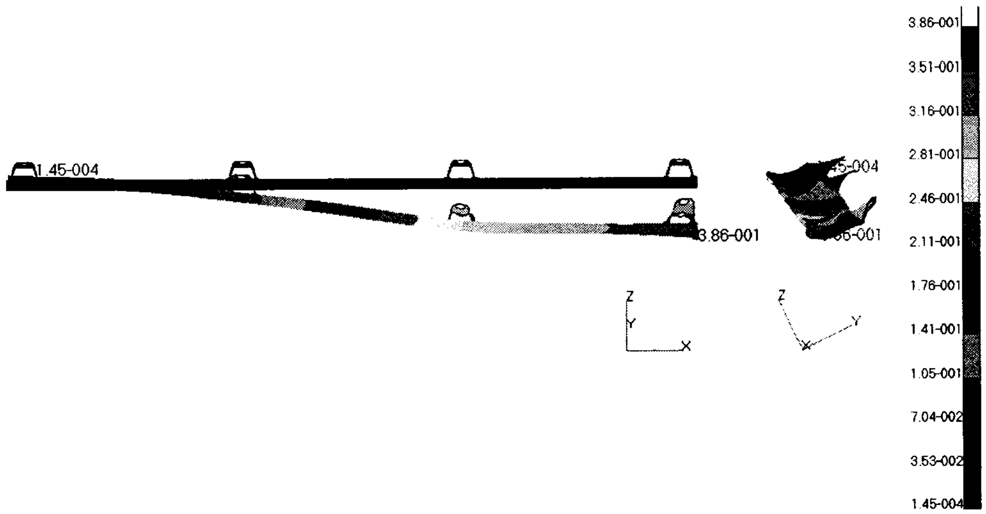

Figure 4.3: Overall deformation of the composite slat for the first design stage (values are in inches)

4.1.2 Stress failure criteria

Von Mises stress criterion is used for the isotropic aluminium model. The generalized form of the Von Mises stress criterion is the following [50]:

$$\frac{1}{2}(\sigma_x-\sigma_y)^2+\frac{1}{2}(\sigma_x-\sigma_z)^2+\frac{1}{2}(\sigma_y-\sigma_z)^2+3\tau_{xy}^2+3\tau_{yz}^2+3\tau_{zx}^2\le\sigma_{yield}^2 \quad (1)$$

The margin of safety is then calculated as:

$$MS=\frac{\textit{Limit tensile stress}}{\textit{Maximum Von Mises stress}}-1 \quad (2)$$

Hill criterion is the stress failure criterion selected for the composite model of the first design stage. Hill's theory was one of the first attempts to develop a single formula to account for the different strengths in the various principal directions [50]. Hill is a widely used criterion for anisotropic materials such as composites where the failure index is defined as:

$$F_{xx}\sigma_x{}^2+F_{YY}\sigma_y{}^2+2F_{xy}\sigma_x\sigma_y+F_{ss}\tau_{xy}{}^2=FI \quad (3)$$

And where:

$$F_{xx}=\frac{1}{X^2}\text{ if }\sigma_x\ge 0 \quad (4)$$

$$=\frac{1}{X'^2}\text{ if }\sigma_x<0 \quad (5)$$

$$F_{yy} = \frac{1}{Y^2} \text{ if } \sigma_y \geq 0 \tag{6}$$

$$= \frac{1}{Y'^2} \text{ if } \sigma_y < 0 \tag{7}$$

$$F_{xy} = \frac{-1}{2X^2} \text{ if } \sigma_x \sigma_y \geq 0 \tag{8}$$

$$= \frac{-1}{2X'^2} \text{ if } \sigma_x \sigma_y < 0 \tag{9}$$

$$F_{ss} = \frac{1}{S_{xy}^{\ 2}} \tag{10}$$

Let X = Longitudinal tensile strength (along the X axis)

X' = Longitudinal compressive strength (along the X axis)

Y = Transverse tensile strength (along the Y axis)

Y' = Transverse compressive strength (along the Y axis)

S_{xy} = Shear strength in the XY plane

Because this failure theory is quadratic, the strength ratio (ϕ) which is the ratio that the load must be factored to fail is expressed as:

$$\phi = \frac{1}{\sqrt{FI}} \tag{11}$$

The margin of safety criterion is expressed as following:

$$MS = \phi - 1 \tag{12}$$

If the value of MS > 0 ($FI < 1$) no failure occurs, correspondingly if MS ≤ 0 ($FI \geq 1$) there is failure. For every ply, the lowest of the margins of safety for fibre and matrix is calculated and displayed.

4.1.3 <u>Stress results</u>

4.1.3.1 Composite model

The worst failure index found with the Hill criterion is located around the back fixation hole of the 4th bracket (see Figure 4.4) where it reaches the value of 4.10, which corresponds to a negative margin of safety of -0.756. This negative margin of safety indicates a failure in the part.

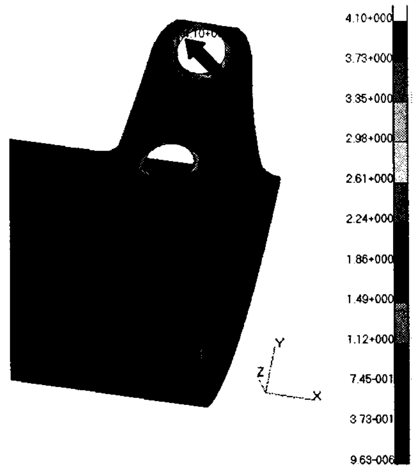

Figure 4.4: Location of the worst failure index (Hill criterion) on the 4th bracket

Areas with margins of safety lower than 3 are illustrated in Figure 4.5 below. They are located around the holes, at the bracket radii, on the front side of the brackets and at the front of the airfoil. These locations correspond to the critical areas of the original aluminium part in service with the exception of the airfoil section and the side of the brackets (see Figure 1.6).

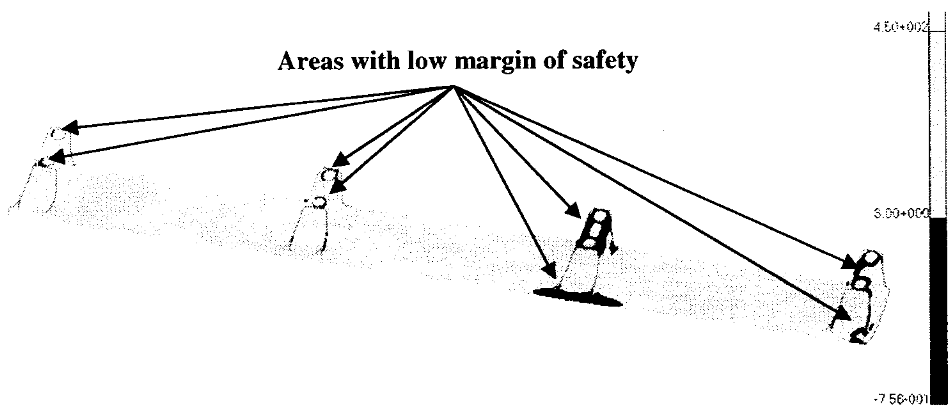

Figure 4.5: Critical areas on the first model

4.1.3.2 Original model

The maximum stress is 244.07 MPa (35.4 ksi) on the back corner of the 4th bracket of the aluminium model as shown in Figure 4.6 below. This corresponds to a margin of safety of 0.55 for a limit tensile stress value of 389.967 MPa (55 ksi) (from AL2024-T3511 properties [33]). This positive margin of safety indicates no failure in the part.

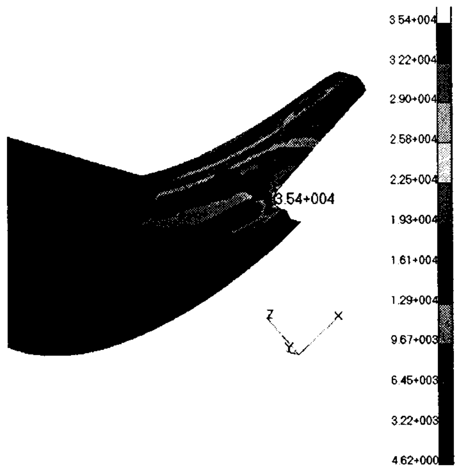

Figure 4.6: Location of the maximum Von Mises stress on the 4th bracket for the first design stage

4.1.4 Comments on results of the first design stage

The first design stage analyses show that the composite model and the original aluminium model have similar deflection behaviours under comparable loading conditions (described in FIRST DESIGN STAGE section of Chapter 3). This validates the behaviour of the composite assembly.

Most areas with low margins of safety on the composite model correspond to the critical areas of the part in service. Margin of safety values obtained for the first composite model cannot be compared with those obtained with the original model but will be used as a comparative reference for the following design stages.

4.2 Second design stage

4.2.1 Overall deformations

Figure A2.1 of APPENDIX II shows the overall deformations of the aluminium and all composite assemblies under the second design stage load case. The deformation scheme of the assembly is similar for all models. The maximum resultant displacement values are the following for all models:

Aluminium model: 22.43 mm (0.883 in)

Model 2A: 23.44 mm (0.923 in)

Model 2B: 22.99 mm (0.905 in)

Model 2C: 29.93 mm (0.942 in)

Once again, composite models have a similar behaviour than the aluminium model and are then estimated to be fairly reliable. The deflections are slightly larger than that of the first design stage. This can be explained by the fact that linearly distributed forces are oriented both downwards (compared with the upwards pressure applied on the slat for the first design stage) and are acting on a more important portion of the part area.

The overall deformation of the slat under loading is oriented downwards (negative Z-direction) and towards the back of the helicopter (positive X-direction). As shown in Figure 4.7, the respective maximum deflection at the tip of the slat for each model is:

Model 2A: 23.16 mm (0.912 in)

Model 2B: 22.50 mm (0.886 in)

Model 2C: 23.62 mm (0.930 in)

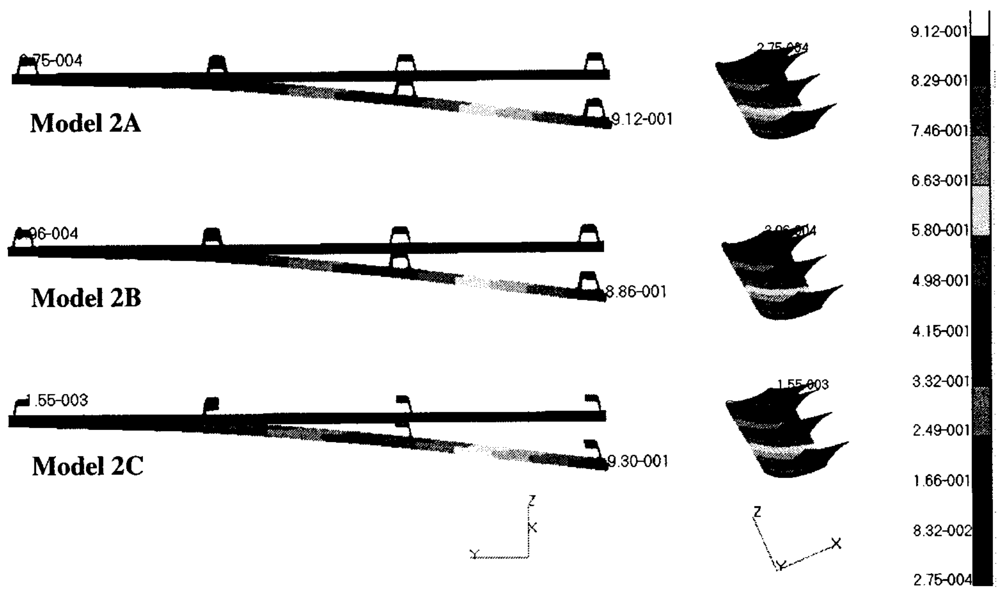

Figure 4.7: Deflection of the slat for all composite models for the second design stage

Model 2A has a more important deflection than model 2B, thus is a more flexible design. This difference in compliance can be explained by the 2 additional plies inside the brackets of model 2B that are adding stiffness to the part.

Model 2C and model 2A have the same number of plies (4 everywhere) but, as expected, the half bracket model shows a better flexibility.

These models show that the difference in flexibility is almost twice more important for variation of bracket geometry (full to half bracket configuration) than for added number of plies (4-ply bracket to 6-ply bracket).

4.2.2 Stress failure criterion

A simple maximum stress criterion is used this time for composite models of the second design stage. This criterion is simpler than the Hill criterion and allows an equivalent comparative analysis for anisotropic materials. Here, the maximum stress criterion is calculated by comparing the allowable load with the actual strength for each component. Its failure index is calculated as follows [50]:

$$FI = \max\left(\frac{\sigma_x}{X}, \frac{-\sigma_x}{X'}, \frac{\sigma_y}{Y}, \frac{-\sigma_y}{Y'}, \frac{abs(\tau_{xy})}{S_{xy}}, \frac{abs(\tau_{yz})}{S_{yz}}, \frac{abs(\tau_{xz})}{S_{xz}}\right) \quad (13)$$

Let X = Longitudinal tensile strength (along the X axis)

X' = Longitudinal compressive strength (along the X axis)

Y = Transverse tensile strength (along the Y axis)

Y' = Transverse compressive strength (along the Y axis)

S_{xy} = Shear strength in the XY plane

S_{yz} = Shear strength in the YZ plane

S_{xz} = Shear strength in the XZ plane

In this case, the strength ratio (ϕ) which is the ratio about the load must be factored to fail is expressed simply as:

$$\phi = \frac{1}{FI} \quad (14)$$

The margin of safety criterion is expressed as Equation 12.

4.2.3 Stress results

4.2.3.1 Composite model

The worst failure index using the maximum stress criterion is located in the same area for both models 2A and 2B: around the front fixation hole of the 4th bracket (see Figure 4.8). It reaches the value of 0.395 for model 2A and 0.363 for model 2B, which corresponds to respective positive margins of safety of 1.53 and 1.75 and indicates no failure in the part.

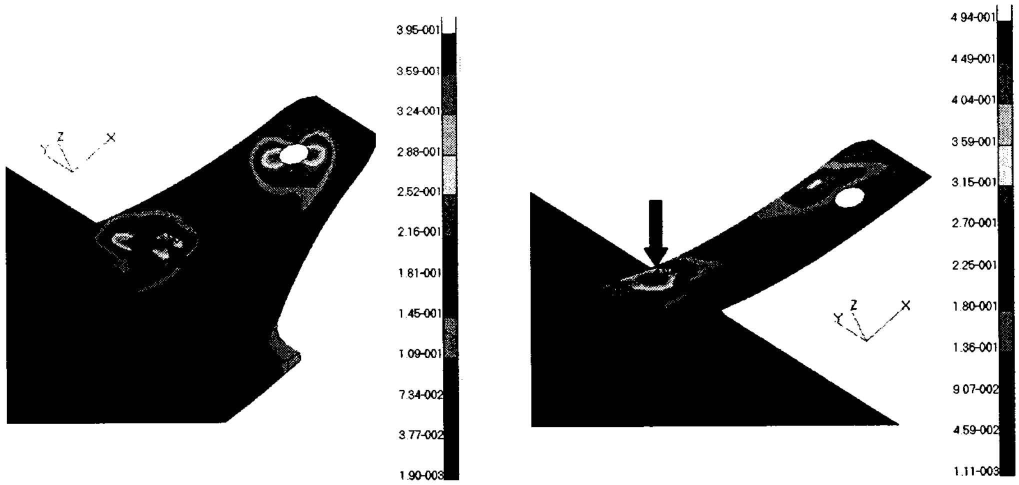

Figure 4.8: Location of the worst failure index (maximum stress criterion) for models 2A and 2B (left) and model 2C (right)

The location of the worst failure index for model 2 C is at the front corner of the 2nd bracket (see Figure 4.8) where it reaches the value 0.494 which corresponds to a positive margin of safety of 1.02 and suggests no failure in the part.

Areas with margins of safety lower than 3 are illustrated in Figure 4.9 for all configurations of the second design stage. These areas are smaller than for the first design stage and correspond more accurately to the critical areas of the original aluminium part in service (see Figure 1.6).

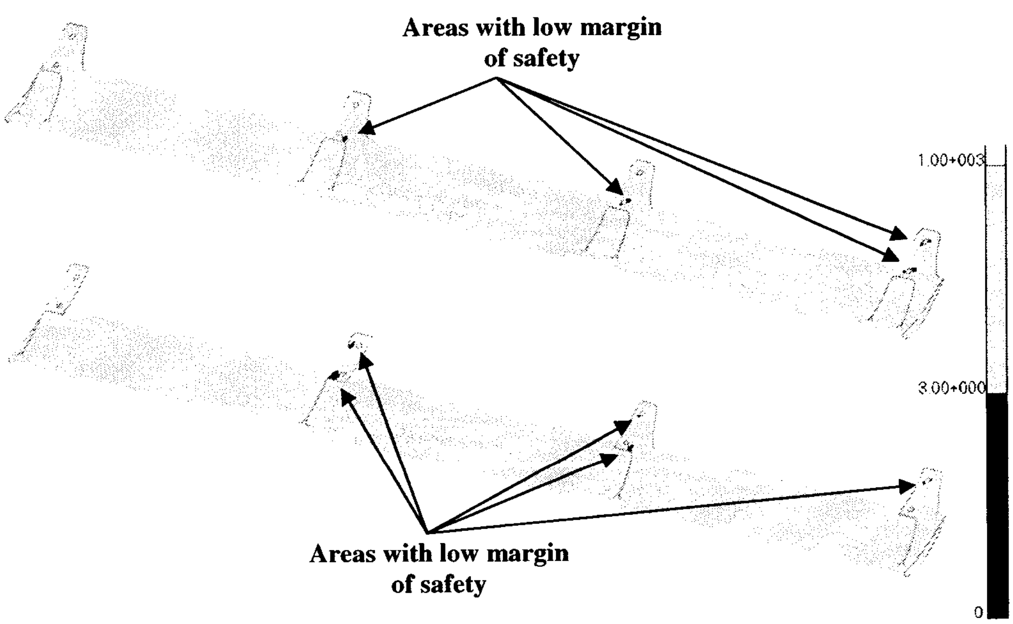

Figure 4.9: Critical areas on models of the second design stage

4.2.3.2 Original model

The maximum stress is 224.77 MPa (32.6 ksi) on the back corner of the 2nd bracket of the aluminium model as shown in Figure 4.10 below. This new location indicates an improvement in the accuracy of the applied load. In fact, the second bracket is submitted to the maximum load concentration on the part in service [12] (p. 6). This corresponds to a margin of safety of 0.69 using the same limit stress value as for the first design stage. This positive margin of safety indicates no failure in the part and is more important than the value obtained for the first design stage.

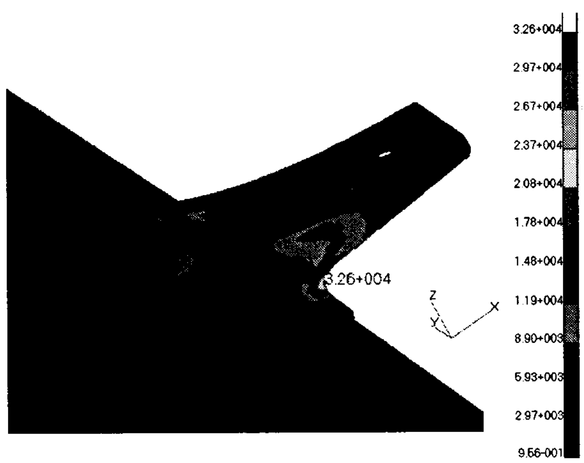

Figure 4.10: Location of the maximum Von Mises stress on the 2nd bracket for the second design stage

4.2.4 Comments on results of the second design stage

As for the first design stage, analyses of the second design stage show that the composite and original aluminium models have similar deflection schemes under comparable loading conditions, thus validating the behaviour of the composite assembly.

Stress analyses of the second design stage reveal that none of the composite models is failing. By comparing failure index results, it can be observed that model 2B has a lower maximum failure index than model 2A. That is to be expected since model 2B had additional plies inside the brackets that are strengthening the part.

Model 2C has a highest worst failure index attributable to its half bracket configuration (weaker structural geometry) and its more important deformations (more flexible model).

The strongest model of the second design stage is model 2B with full brackets with additional plies on the brackets.

The failure of the previous composite model of the first design stage can be explained by the properties used for the laminate. The graphite/epoxy fabric model (fabric T300/F934) from Patran Laminate Modeler support file [32, 50] has lower stress limits than dry RTM / AS4-GP 6K-5HS at 24°C.

The location of stress concentrations on the original aluminium model shows evidence of an improvement on the accuracy of the applied loading representing flight conditions.

4.3 Third design stage

4.3.1 Overall deformations

As previously explained in this chapter, the overall deformations of the aluminium assembly are used as a reference to confirm the validity of the composite assemblies. For the third design stage, there are 4 deformation configurations to compare (for each of the four load cases) for each model.

The first load case has the most important deflection downwards caused by the two distributed loads oriented downwards. The second load case has a moderate deflection upward (caused by the upward distributed load along the stabilizer) with a slight twist caused by the downward distributed load acting on the slat. The third load case has a moderate deflection downward (caused by the downward distributed load on the stabilizer) with a slight twist caused by the distributed load acting on the slat in the opposite direction. Finally, the fourth load case has an important deflection upward caused by the two distributed loads oriented upwards.

Deformation schemes are the same for all models and maximum deformation values are comparable, confirming the reliability of the models. Figure 4.11 shows the overall deformation of the aluminium assembly for each load case that can be used as a reference for all composite model deformations.

The values of the maximum resultant displacements for all models are shown in Table A2.1 of APPENDIX II.

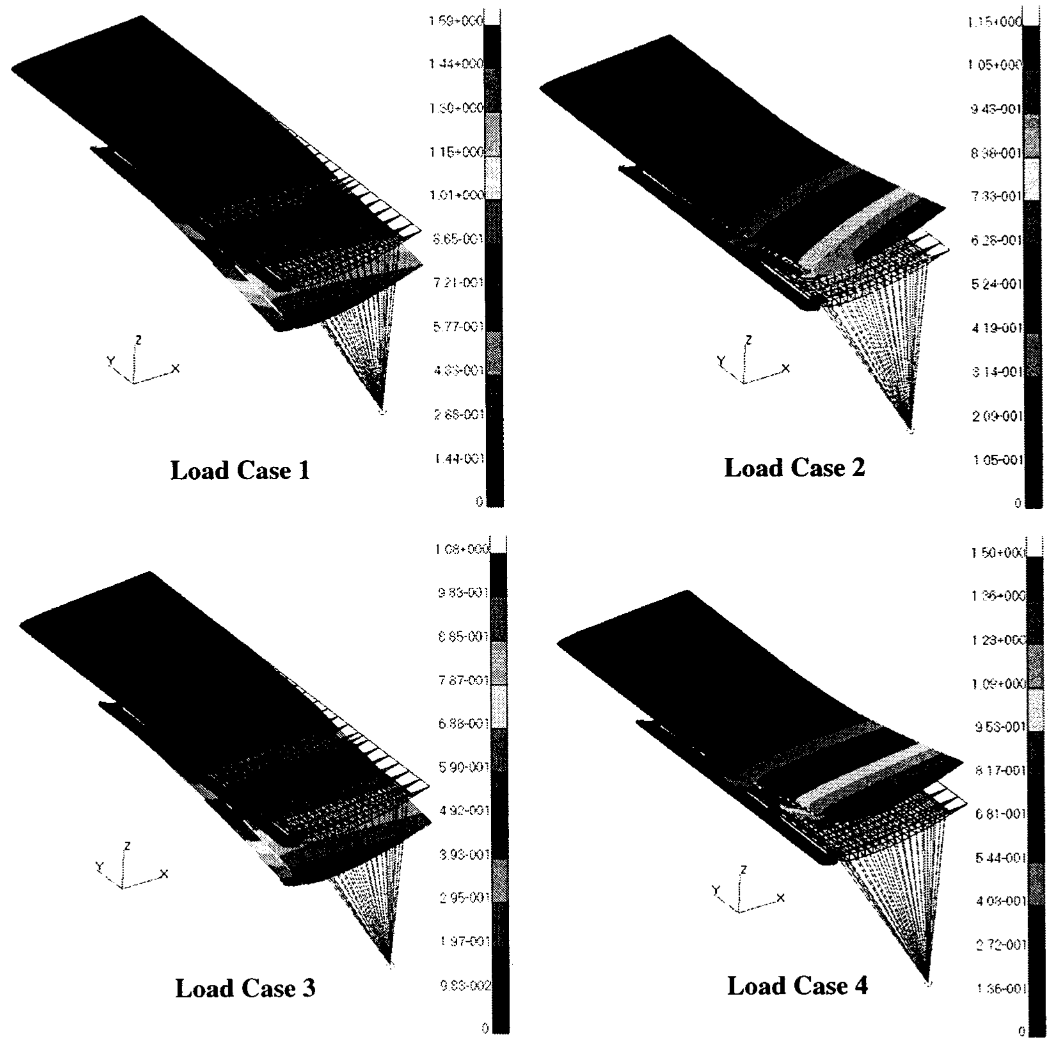

Figure 4.11: Overall deformations of the aluminium assembly for each load case (values are in inches)

The values of the deflections are more important for the third design stage than for the previous ones. The load factor of 1.5 multiplying the applied loads has an important influence on these results.

The overall deformation of the slat is similar for all models. Deflection scheme for each load case is shown in Figure 4.12 below (model 3A case). For load cases 1 and 3, the slat is bending downwards (negative Z-direction) and towards the back of the helicopter (positive X-direction). For load cases 2 and 4, the slat is bending upwards (positive Z-direction) and towards the front of the helicopter (negative X-direction). For all models, the maximum deflection values are reached under load case 1. The respective values of the maximum deflection at the tip of the slat for each model under the 4 load cases are shown in Table A2.2 of APPENDIX II.

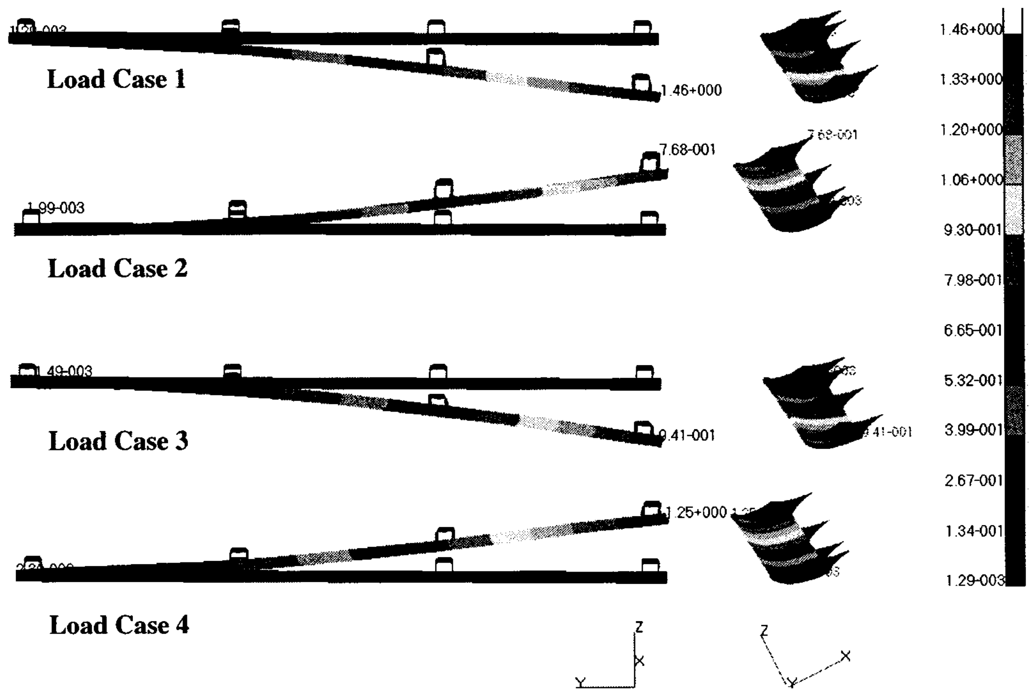

Figure 4.12: Deflection of the Model 3A slat for the 4 load cases of the third design stage

In general, full bracket models 3A and 3B have the smallest deflection values. This can be explained by the full bracket configuration that adds stiffness to the slat structure.

Models 3C-3E (with brackets opened towards the outside) have slightly higher deformation values (more flexible) than models 3I-3K that have two additional plies on the brackets. Likewise, models 3F-3H (with brackets opened towards the inside) have slightly higher deflection values (more flexible) than models 3L-3N with two additional plies on the brackets.

Model 3N and 3P, thus having a different lay-up strategy, have the same deflection values for all load cases.

Bracket angle seems to have no considerable impact on the flexibility of the slat. Half bracket configuration (opened towards the inside or the outside) does not show any noticeable influence when it comes to compliance.

Of all models, the original model has the highest deflection values for all load cases. This can be explained by the 3-part airfoil that permits a higher flexibility for large deflections.

These models show that, for larger deflections, flexibility is slightly decreased when plies are added on the brackets. The critical aspect that affects flexibility under heavier load cases causing considerable deformations is the multiple section airfoil allowing larger deformations for the original aluminium model.

4.3.2 Failure criterion

This time, the Tsai-Wu failure criterion is used as a criterion for composite parts. It is one of the simplest and widely used quadratic failure criteria for anisotropic materials. Tsai-Wu is the generalization of the Von Mises criteria in 2D without terms containing linear and first-degree shear stress [31]. This is due to the condition that the strength should be unaffected by the direction or sign of the shear stress component (if shear stress is reversed, the strength should remain the same). The quadratic Tsai-Wu criterion for laminate materials is expressed as:

$$F_{xx}\sigma_x^{\ 2} + 2F_{xy}\sigma_x\sigma_y + F_{yy}\sigma_y^{\ 2} + F_{ss}\tau_{xy}^{\ 2} + F_x\sigma_x + F_y\sigma_y = 1 \tag{15}$$

Where the coefficients can be calculated as:

$$F_{xx} = \frac{1}{XX'} \tag{16}$$

$$F_x = \frac{1}{X} - \frac{1}{X'} \tag{17}$$

$$F_{yy} = \frac{1}{YY'} \tag{18}$$

$$F_y = \frac{1}{Y} - \frac{1}{Y'} \tag{19}$$

$$F_{ss} = \frac{1}{S_{xy}^{\ 2}} \tag{20}$$

Let $X =$ Longitudinal tensile strength (along the X axis)

$X' =$ Longitudinal compressive strength (along the X axis)

$Y =$ Transverse tensile strength (along the Y axis)

$Y' =$ Transverse compressive strength (along the Y axis)

S_{xy} = Shear strength in the XY plane

$$F_{xy} = F_{xy}^{*}\sqrt{F_{xx}F_{yy}} \tag{21}$$

The interaction term F_{xy}^{*} relates the two normal stress components (failure modes due to loading along both the X and Y material directions). For this case, it was assumed that the failure criterion is a generalization of the Von Mises criterion by assigning a value for F_{XY}^{*} that works in most cases:

$$F_{xy}^{*} = -\frac{1}{2}$$

The margin of safety is related to the increase in load when failure occurs. Since Tsai-Wu is a quadratic criterion, the linear parameters and the quadratic parameters are grouped and multiplied by a strength ratio (ϕ). This strength ratio is the ratio by which the load must be factored to reach failure.

The Tsai-Wu quadratic criterion then becomes:

$$\phi^2(F_{xx}\sigma_x{}^2 + F_{yy}\sigma_y{}^2 + 2F_{xy}\sigma_x\sigma_y + F_{ss}\sigma_s{}^2) + \phi(F_x\sigma_x + F_y\sigma_y) - 1 = 0 \tag{22}$$

In Patran Laminate Modeler, the Tsai-Wu criterion for in-plane loads (modeling fibre failure) has been supplemented by a maximum load theory for out-of-plane shear loads (modeling matrix failure) [50].

$$FI = \max\left(\frac{abs(\tau_{yz})}{S_{yz}}, \frac{abs(\tau_{xz})}{S_{xz}}\right) \tag{23}$$

In this case, the strength ratio is calculated with Equation 14.

For all cases, the margin of safety criterion is expressed as Equation 12.

4.3.3 <u>Stress results</u>

4.3.3.1 Composite model

In general, load case 1 is the worst case for all models: it generates the highest failure index values on the slat. The critical areas are around the back attachment hole for full bracket models and the corner of the brackets for half bracket models (see Figure 4.13 below). All maximum failure indices for all models under the 4 load cases with their respective location are shown in Table A2.3 to Table A2.7 of APPENDIX II.

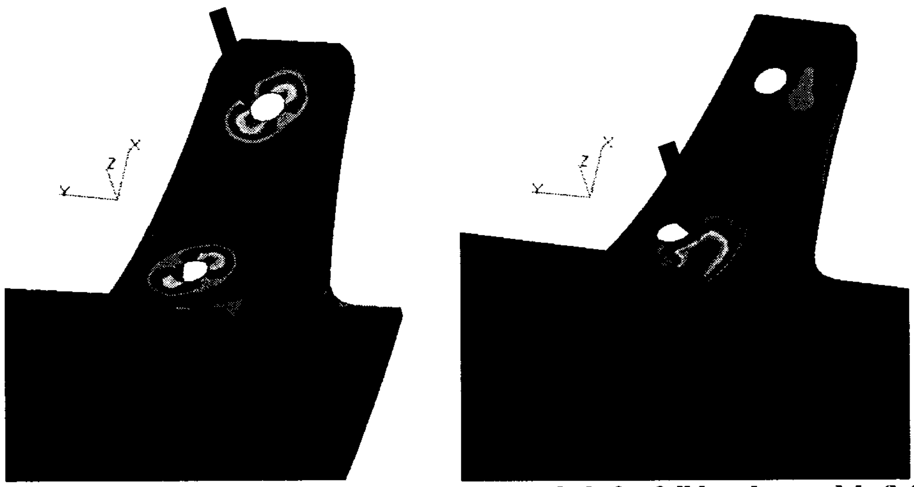

Figure 4.13: Critical area around the back attachment hole for full bracket models (left) and at the bracket corner for half bracket models (right)

The model with the lowest failure index for all load cases is model 3N with half brackets opened towards the inside at an angle of 70 degrees with 6 plies on the brackets and 4 plies on the airfoil.

There is no significant difference between the failure indices obtained with full bracket models (models 3A-3B) and half bracket ones (models 3C-3P). However, failure indices obtained with half brackets opened towards the outside (models 3C-3E and 3I-3K) are slightly higher than those obtained with half brackets opened towards the inside (models 3F-3H and 3L-3P). Furthermore, models with additional plies on the brackets (models 3I-3P) have lower failure indices than those with 4 plies everywhere (models 3C-3H).

Full bracket models (models 3A-3B) and models with half brackets opened towards the inside with additional plies (models 3L-3P) have a diminishing failure index when the bracket angle is decreased. No particular trend has been observed for the other models.

Model 3P with a gradual lay-up only covering the area with a higher potential for stress concentration does not generate lower failure index than model 3N without the gradual lay-up.

Areas with margins of safety lower than 3 are illustrated in Figure 4.14 for all configurations of the third design stage (full bracket, half bracket opened towards the outside and half bracket opened towards the inside). These locations correspond once again to the critical areas of the original aluminium part in service (see Figure 1.6) with an additional area at the front part of the airfoil in front of the second bracket.

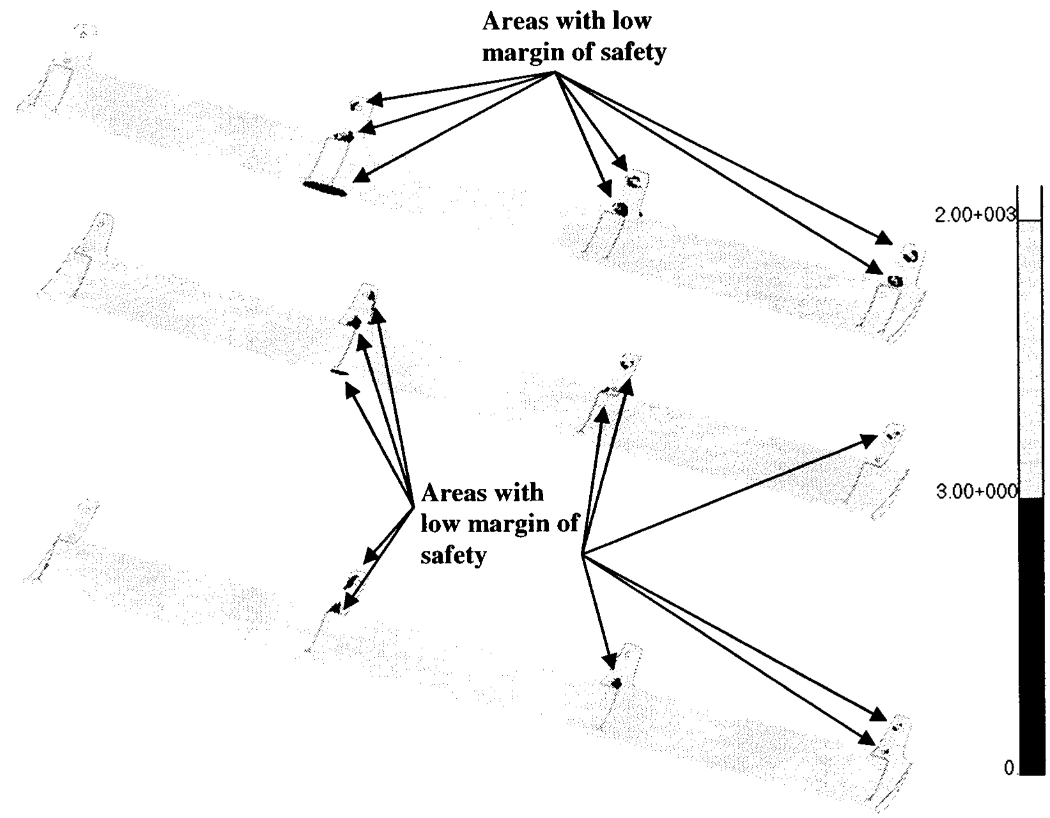

Figure 4.14: Critical areas on all configurations of the third design stage

4.3.3.2 Original model

The maximum Von Mises stress is 367.49 MPa (53.3 ksi) on the aluminium model under the 1st load case. The stress concentration is at the same location as for the second design stage (back corner of the 2nd bracket) as shown in Figure 4.10 of second design stage section. Other maximum Von Mises stress value for the original model under the 4 load cases with their respective location are shown in Table A2.8 of APPENDIX II.

This corresponds again to the same location of the maximum load concentration on the part in service [12] (p. 6) with a margin of safety of 0.03. This small margin of safety, thus indicating no failure in the part, suggests critical conditions that can be attributable to the applied load factor of 1.5.

4.3.4 Comments on results of the third design stage

As for the second stage, stress analyses of the third design stage reveal that none of the composite models is failing. It can be observed that failure indices are generally higher for models of the third design stage than for those of the previous design stage. The load factor of 1.5 multiplying the forces acting on the stabilizer and slat is the main cause of this increase.

Comparative analyses of the third design stage showed that there is no significant difference between stress behaviour of full bracket models and half bracket ones. However, models with half brackets opened towards the inside generally yield before those with half brackets opened towards the outside. This difference gets more evident with additional plies on the brackets. Gradual lay-up only covering the area with a higher potential for stress concentration does not show any improvement in the maximum failure index on the brackets.

With comparable stress behaviour than full bracket configurations, models with half brackets opened towards the inside are the preferred choice according to material savings, ease of processing and flexibility. Since their failure index diminishes when the bracket angle is decreased, the model with half bracket opened towards the inside and a small bracket angle is the best option. Furthermore, considering that additional plies diminish the failure index and that there is no improvement with a gradual lay-up configuration, the best option is model 3N (with brackets opened towards the inside, additional plies on the brackets and bracket angle of 70 degrees).

4.4 Fourth design stage

4.4.1 Overall deformations

4.4.1.1 Load cases 1-8

For the fourth design stage, there are 9 deformation configurations to compare (for each of the 9 load cases) for each load case. Once again, the overall deformations of the original aluminium assembly are used as a reference to confirm the validity of composite and one-piece aluminium surface assemblies. However, since all models have different thermal expansion behaviours, load case 9 is not used as a reference. The overall deformations of the original assembly were shown in Figure 4.11 for load cases 1-4 (see third design stage section) and in Figure 4.15 below for load case 5-8.

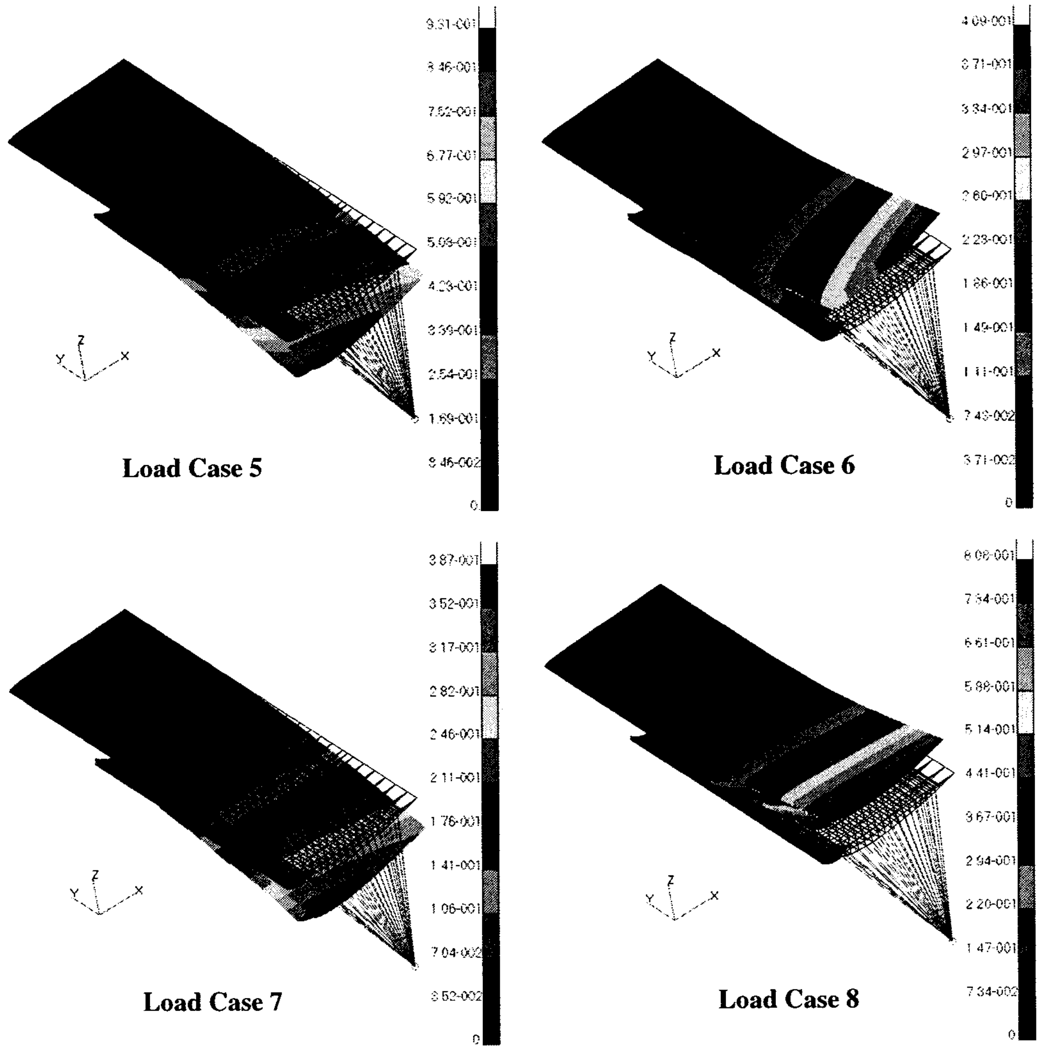

Figure 4.15: Overall deformations of the aluminium assembly for load case 5-8 (values are in inches)

Overall deformations under additional load cases 5-8 are similar to load cases 1-4 but with smaller maximum deformation values. Deformation schemes under load cases 1-8 are the same for all models and maximum deformation values are comparable, confirming the reliability of the models. The values of the maximum resultant displacements for all models are shown in Table A2.9 of APPENDIX II.

The overall deformation of the slat is similar for all models. Deflection schemes for load cases 1-4 are the same as the ones shown in Figure 4.12 (third design stage section) and deformation for load cases 5-8 are illustrated in Figure 4.16 below. Once again, deformation schemes of load cases 5-8 are similar to those of load cases 1-4 with smaller maximum deformation values.

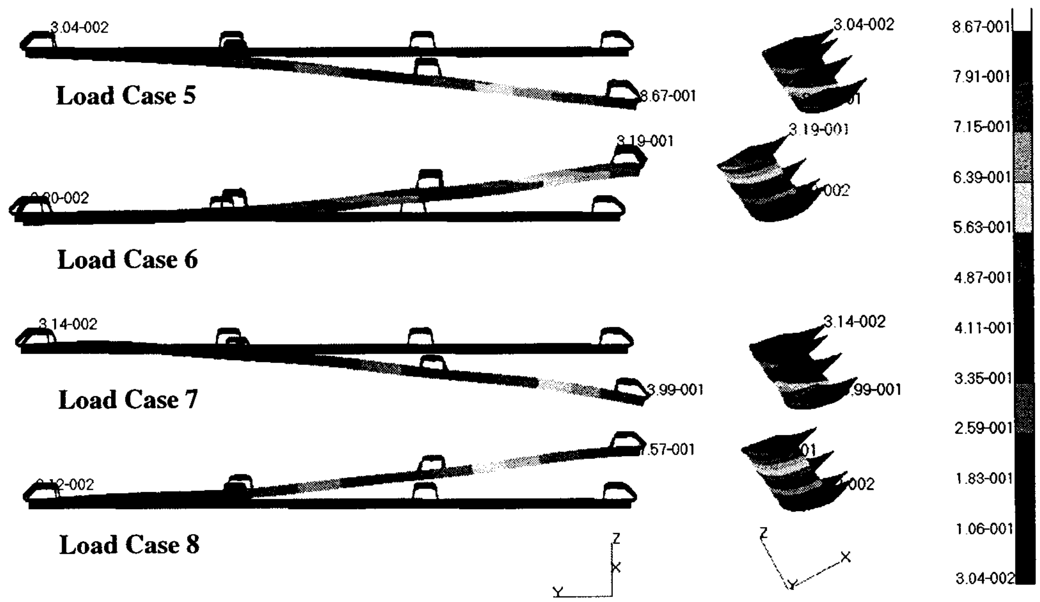

Figure 4.16: Deflection of the Model 4A slat for the load cases 5-8 of the fourth design stage

The respective values of the maximum deflection at the tip of the slat for each model under load cases 1-8 are shown in Table A2.10 of APPENDIX II.

As mentioned earlier, the range of deflections is smaller for load cases 5-8 than for load cases 1-4 for all models. Composite models (models 4A-4L) have a higher maximum deflection value than aluminium surface models (models 4M-4Y). In other words, composite models are more flexible than aluminium models.

Half bracket models (models 4E-4L) are more flexible than full bracket ones (models 4A-4D). There seems to be no significant difference between the half bracket models with different bracket configurations (opened towards the outside (models 4E-4H) or towards the inside (models 4I-4K)).

Bracket angle seems to have no considerable impact on the flexibility of the slat.

Model 4H with half brackets opened towards the outside with an angle of 60^{o} is slightly more flexible than most models, as shown on the graph of the maximum deflection values at the tip of the slat for all composite models for each load case shown in Figure A2.2 of APPENDIX II.

4.4.1.2 Thermal load case

The difference or thermal expansion between the slat and the stabilizer is greater for the composite assemblies (models 4A-4L) than for the original aluminium model assembly and the aluminium surface models assemblies (models 4M-4Y). This can be explained by the difference of coefficient of thermal expansion of aluminium and 890 RTM / AS4-GP 6K-5HS. Figure 4.17 shows the thermal deformation schemes of the following assemblies: original aluminium model, aluminium surface model with full brackets at 90^{o} (model 4M) and the composite model with full brackets at 90^{o} (model 4A). Deformations of the remaining models with different bracket angle and configurations (composite models 4B-4L and aluminium surface models 4N-4Y) are respectively similar to deformations of the composite and aluminium models shown below.

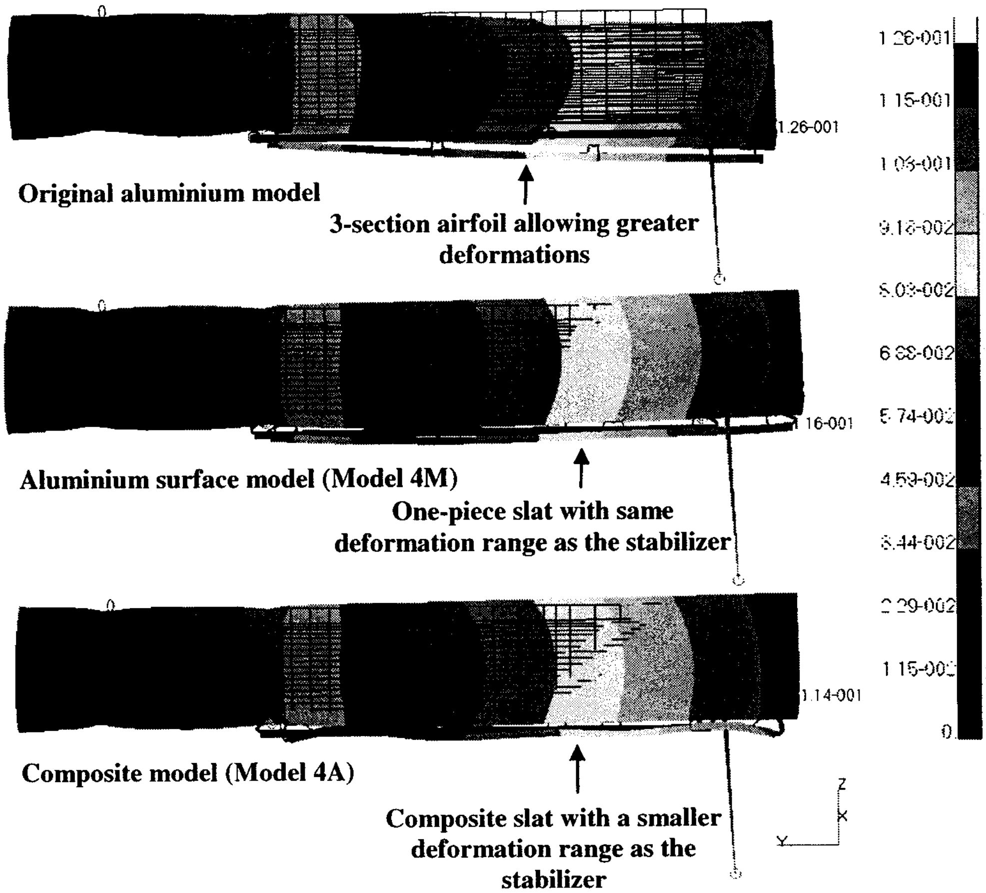

Figure 4.17: Thermal deformation schemes of the following assemblies: Original aluminium model (top), aluminium surface model 4M (middle) and composite model 4A (bottom).

Values of the overall maximum deflection of all assemblies under the thermal load case (Load case 9) are shown in Table A2.9 of APPENDIX II. These deflections are considerably smaller than those under load cases 1-8, thus not critical.

All values of the maximum deflections at the tip of the slat for each model under load case 9 (thermal) are shown in Table A2.10 of APPENDIX II. Composite models (models 4A-4L) have a smaller maximum deformation value than aluminium surface models (models 4M-4Y).

Models of the fourth design stage show that there is no significant difference between the compliance of all models. The values of their maximum deflections are very comparable (see graph of Figure A2.2 in APPENDIX II). The thermal load case is not causing outstanding deformations.

4.4.2 *Failure criterion*

As for the third design stage, Tsai-Wu failure criterion is used as a criterion for composite parts (see FAILURE CRITERION part of THIRD DESIGN STAGE section for details).

4.4.3 *Stress results*

4.4.3.1 Composite and aluminium surface models

Load case 1 generates the highest failure index values on the slat for models 4A-4D as well as 4I-4L, and load case 4 is the worst case for models 4E-4H. Critical areas are located around the attachment holes (for load cases 1-8) or at the bottom radius (for some cases of occurrences of load case 9) of the brackets as shown in Figure 4.18 below. All maximum failure indices for the 12 composite models under the 9 load cases with their respective location are shown in Table A2.11 to Table A2.13 of APPENDIX II.

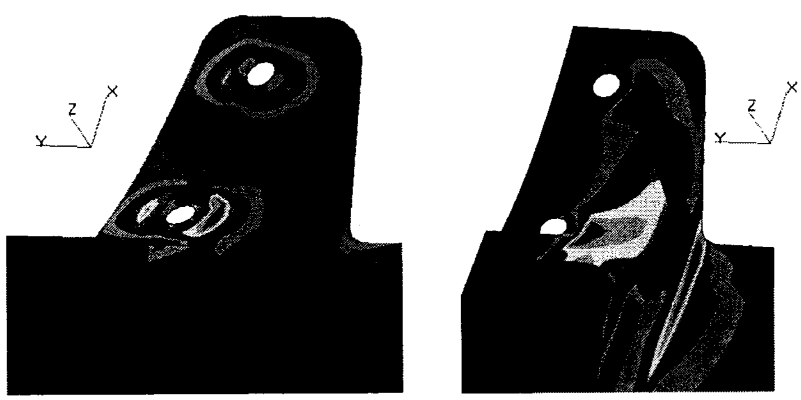

Figure 4.18: Typical critical areas around an attachment hole (left) and at the bottom radius (right)

The aluminium surface models also have their critical areas located around the attachment holes and the bottom radius of the brackets. Maximum Von Mises stress values for all these models are shown in Table A2.15 of APPENDIX II. To allow a comparison between models with respect to material performance, margin of safety values are calculated for all models (4A-4Y) (shown in Table A2.16 of APPENDIX II). Margins of safety allow a clearer representation of the capability over the requirements of the slat: all negative values indicate failure in the part. Comparative graphs of the minimum margin of safety of all composite models

(Figure A2.3) and aluminium surface models (Figure A2.4) are displayed in APPENDIX II.

All models of the fourth design stage obtain a negative margin of safety under at least one load case. This indicates that all models are failing under the suggested load cases. These results can be explained by the difference in load distribution that increases deflection values. The barely visible impact damage (BVID) decreasing compression strength (50% of original limit) and shear strength (85% of original limit) is also a factor contributing to the decrease of the margin of safety of composite models.

Composite models with half brackets opened toward the inside (models 4I-4L) are the configurations with the smallest average among the load cases in the critical zone (2.75 for full brackets, 4 for half brackets opened towards the outside and 2 for half brackets opened towards the inside). They also have the smallest average of negative margin of safety value (-0.174 for full brackets, -0.166 for half brackets opened towards the outside and -0.0467 for half brackets opened towards the inside). See Table A2.16 and Figure A2.3 of APPENDIX II for more details.

Model 4K (with half brackets opened towards the inside at an angle of 70 degrees) is the model with the least number of load cases in the critical zone (negative margin of safety): only load case 1 is giving a negative margin of safety of -0.0601. This value is also the smallest average of negative margin of safety of all models.

Areas with margins of safety lower than 3 are illustrated in Figure 4.19 for all configurations of the fourth design stage (full bracket, half bracket opened towards the outside and half bracket opened towards the inside). The critical areas are bigger than those of the third stage but are located around the same areas. These locations correspond once again to the critical areas of the original aluminium part in service (see Figure 1.6) with additional areas on the front part of the airfoil and on the side of the brackets.

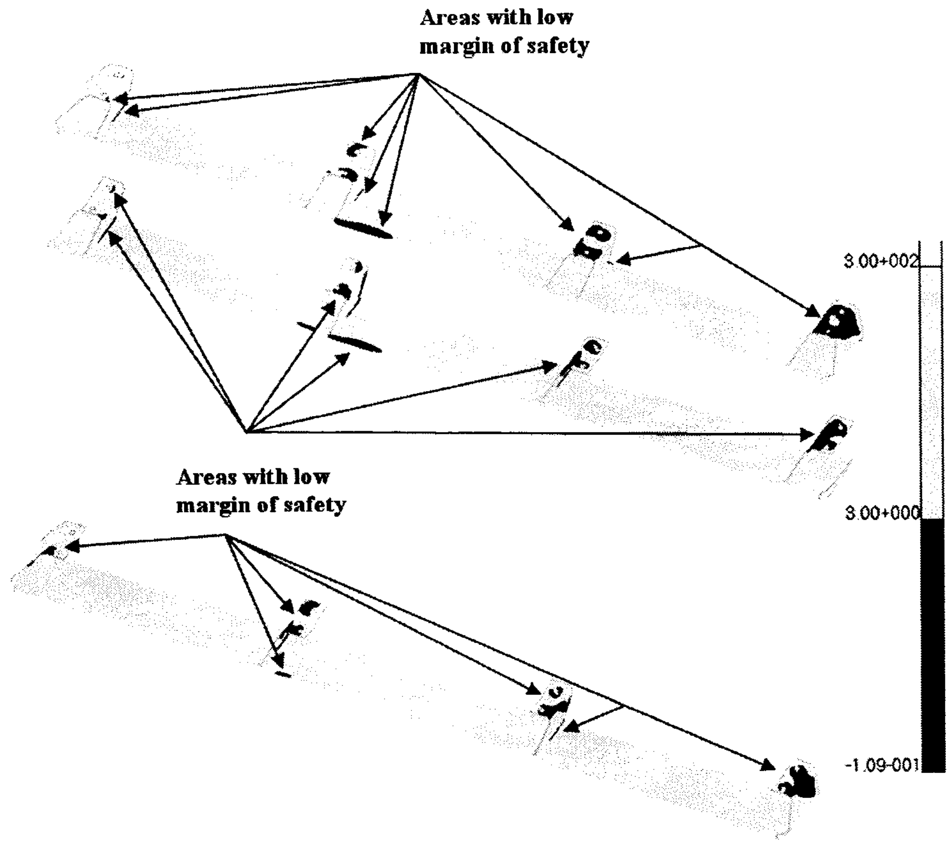

Figure 4.19: Critical areas on all configurations of the fourth design stage

4.4.3.2 Original model

The maximum Von Mises stress is 397.83 MPa (57.7 ksi) on the aluminium model under the 1st load case. Once again, the maximum stress is at the same location as for the second design stage (back corner of the 2nd bracket) as shown in Figure 4.10 of second design stage section. Other maximum Von Mises stress value for the original model under the 9 load cases with their respective location are shown in Table A2.14 of APPENDIX II.

This corresponds again to the same location of the maximum load concentration on the part in service [12] (p. 6) with a negative margin of safety of -0.0468. This indicates failure in the part. However, the original model is getting a negative margin of safety under load case 1 only. This can be attributable once again to the different load distribution and confirms the validity of the results obtained with the composite models.

4.4.4 Comments on results of the fourth design stage

Stress analyses of the fourth design stage reveal that applied simulation cases are very severe and correspond to heavier loading than real flight conditions. Failure of the original aluminium model under the first load case and critical results of composite models confirm this fact. However, these conditions do not affect comparative analysis findings.

The thermal load case (load case 9) is the one generating the highest minimum margin of safety value for all models. This indicates, along with the deflection results that the thermal loading is not critical.

Aluminium surface models have a high average of load cases in the critical zone (6.5 for full brackets, 7.25 for half brackets opened towards the outside and 6.5 for half brackets opened towards the inside). Table A2.16 and Figure A2.4 show the margin of safety values for models 4M-4Y). This indicates that all models fail (obtaining a negative margin of safety) under the suggested load cases. These results show that aluminium models are not as strong as composite models for the same geometry. It justifies the choice of using a CYCOM 890 RTM / AS4-GP 6K-5HS composite over aluminium for the slat.

Comparative analyses of the fourth design stage show that half bracket models opened towards the inside obtain less critical results (least number of load cases in the critical zone) and lower average of negative margin of safety values than the other configurations. According to material savings, ease of processing and flexibility, they are the best option.

The analyses performed show that the safest composite configuration is model 4K with half brackets opened towards the inside with an angle of 70 degrees. This conclusion agrees with the findings of the third design stage, which states that the best option is model 3N (with brackets opened towards the inside, additional plies on the brackets and bracket angle of 70 degrees).

4.5 Comparative analysis process discussion

The comparative analysis section showed the results obtained throughout the design process, motivating the evolution of the models. Each design stage was generating findings allowing further developments of the models. Table 1 to Table 4 below highlight the main findings of all design stages.

Table 1: Summary of the main findings for the first design stage

FIRST DESIGN STAGE			
Number of models and Configuration	**Bracket angle**	**Number of plies**	**Lay-up and Material**
1 x 	85	Airfoil: 4 – Brackets: 4	Alternation of ±45 and 0/90 T300/F934
Deflections	Overall deformation of composite and aluminium assemblies are comparable – Shows that the composite model is reliable		
Stress Failure Criteria	<u>Aluminium:</u> Von Mises – Isotropic failure criteria (same for all stages) <u>Composite:</u> Hill – Widely used criterion for anisotropic materials		
Stress Analysis - Composite model	Areas with low Margin of Safety correspond to the critical areas of the part in service – Reliable model		
Stress Analysis - Original model	Worst Margin of Safety : 0.55 on the 4th bracket, does not correspond to load concentration of the part in service – Applied loading not accurate		

Table 2: Summary of the main findings for the second design stage

SECOND DESIGN STAGE			
Number of models and Configuration	**Bracket angle**	**Number of plies**	**Lay-up and Material**
1 x  1 x  1 x 	85 85 85	Airfoil: 4 – Brackets: 4 Airfoil: 4 – Brackets: 6 Airfoil: 4 – Brackets: 4	±45 Dry RTM/AS4-GP 6K-5HS at 24°C
Deflections	• Model with additional plies on the brackets is the least flexible • Half bracket models is the most flexible		
Stress Failure Criterion	<u>Composite:</u> Maximum stress – Simpler than Hill and equivalent for comparative analysis of anisotropic materials		
Stress Analysis - Composite model	• Model with additional plies on the brackets is the strongest • Half bracket model is the weakest		
Stress Analysis - Original model	Worst Margin of Safety : 0.69 on the 2nd bracket, corresponds to load concentration of the part in service – Applied loading more accurate		

Table 3: Summary of the main findings for the third and fourth design stages

THIRD DESIGN STAGE			
Number of models and Configuration	**Bracket angle**	**Number of plies**	**Lay-up and Material**
2 x	90, 85	Airfoil: 4 – Brackets: 4	±45 Dry RTM/AS4-GP 6K-5HS at 24°C
3 x	90, 85, 60	Airfoil: 4 – Brackets: 4	
3 x	90, 85, 60	Airfoil: 4 – Brackets: 4	
3 x	90, 85, 70	Airfoil: 4 – Brackets: 6	
3 x	90, 85, 70	Airfoil: 4 – Brackets: 6	
1 x	70 (gradual lay-up)	Airfoil: 4 – Brackets: 6	
Deflections	• Models with additional plies on the brackets are the least flexible • Half bracket models are the most flexible • Bracket angle have no considerable impact on flexibility • Half bracket configuration does not noticeably influence compliance		
Stress Failure Criterion	Composite: Tsai-Wu – Simple and more widely used for composite materials (same for fourth design stage)		
Stress Analysis - Composite model	• Models with additional plies on the brackets are the strongest • The strongest half bracket configuration is opened towards the inside • Gradual lay-up does not have a noticeable influence on the strength • Half bracket model opened towards the inside with an angle of 70 degrees is the strongest model		
Stress Analysis - Original model	Worst Margin of Safety : 0.03 on the 2nd bracket – Applied loading is more critical (attributable to the load factor of 1.5)		

Table 4: Summary of the main findings for the fourth design stage

FOURTH DESIGN STAGE			
Number of models and Configuration	**Bracket angle**	**Number of plies**	**Lay-up and Material**
4 x 4 x 4 x	90, 80, 70, 60 90, 80, 70, 60 90, 80, 70, 60	Airfoil: 4 – Brackets: 6 Airfoil: 4 – Brackets: 6 Airfoil: 4 – Brackets: 6	±45 0/90 brackets outer plies Wet RTM/AS4-GP 6K-5HS at 120°C
4 x 4 x 4 x	90, 80, 70, 60 90, 80, 70, 60 90, 80, 70, 60	N/A	AL 6061-T6 (airfoil) AL 2024-T3511 (brackets)
Deflections	• Half bracket models are the most flexible • Bracket angle have no considerable impact on flexibility • Half bracket configuration does not noticeably influence compliance • Composite models are more flexible than aluminium models • Difference in thermal expansion is greater for composite assembly but not causing outstanding deformations		
Stress Analysis - Composite model	• Half brackets opened towards the inside is the strongest configuration • Half bracket model opened towards the inside with an angle of 70 degrees is the strongest model • Thermal loading is not critical (high margin of safety values obtained) • Aluminium models are not as strong as composites for same geometries		
Stress Analysis - Original model	Worst Margin of Safety : -0.0468 on the 2nd bracket – Applied loading is heavier than flight conditions (attributable to load distribution)		

The first design stage validated the behaviour of the composite assembly model, followed by the second design stage showing that additional plies on the brackets are improving the strength of the slat. The third design stage demonstrated that models with half brackets opened towards the inside with a bigger angle tend to perform better than other configurations. Finally, the fourth design stage confirmed all previous findings by showing that the best option is the composite model with brackets opened towards the inside with additional plies on the brackets and bracket angle of 70 degrees.

This section is a constitutive part of the work done on the project and serves as an analytical reference for the following FUTURE WORK and CONCLUSIONS sections.

5. FUTURE WORK

This project focuses on preliminary findings and serves as a basis for future optimization work. There are clearly many aspects left to be covered in the scope of this project. This is a list of recommendations for future work to be undertaken:

- Validation of models through more accurate load distribution, boundary conditions and modeling of the composite part in order to obtain models with behaviour as similar as possible to the real parts under flight conditions.
- Implementation of mechanical tests on samples to obtain more complete and precise material data.
- Once accurate stress concentration values are obtained, an interlaminar stress analysis is recommended, as mentioned in the FINITE ELEMENT MODEL OVERVIEW chapter. This will study the possibility of delamination in upper corners of brackets or other sections with high potential for interlaminar load concentration.
- A more exhaustive strain and shear analysis is suggested in order to predict the strengths and weaknesses of the processed final part.
- Development of models in order to reproduce the weaknesses of the processed composite part (process-induced residual stresses, resin rich areas, dry spots, etc.)
- An optimization study focusing on a more efficient lay-up orientation, ply drop respecting the standards, and lay-up strategy (adding 0 degree plies on the trailing edge of the slat airfoil to add stability to the structure) would contribute to a better performing part.
- Additional analyses such as dynamic, buckling and failure modes.
- Some more modifications on the geometry can be made and tested with FEA, depending on manufacturing issues following prototype manufacturing.
- Testing carried out with real helicopter parts

6. CONCLUSIONS

The scope of this project was the re-design of an existing metallic part into a one-part composite model which will be processed using resin transfer moulding (RTM). An iterative approach is taken in order to find the optimum design of the leading edge slat through evolution and improvement of comparative models.

Different key criteria of the part design such as ply lay-up, bracket geometry, angle and configuration were tested using FEA technology with the objective of selecting the optimal composite part that minimizes stress concentrations. The influence of the modification of model-related parameters was also observed.

Preliminary comparative studies show that the configuration with half brackets opened towards the inside with an angle of 70 degrees (angle between the top of the airfoil and the side of the bracket) is the best option according to minimum stress concentration and flexibility. This choice is confirmed by other factors such as material savings and ease of processing.

The main contribution of this introductory comparative finite element study serves as a basis for further developments in the use of RTM technology in re-designing metallic aeronautic components. This work constitutes the preliminary steps of the overall collaborative project involving multiple aspects of analysis and optimization.

As a general contribution to knowledge, this research participated to the improvement and optimization of future re-design processes using RTM technology implemented in the helicopter/aerospace sector.

REFERENCES

1. Mason, K.F., *Composites take off ... in some civil helicopters.* High Performance Composites, March 2005. **13**(2): p. p 38-41.

2. Backman, B.F., *Composite structures, design, safety, and innovation.* 2005, Amsterdam ; Boston, Mass. :: Elsevier.

3. Lessard, *Optimized Design of Composite Parts by RTM*, in *NRC/NSERC Research Partnership Program.* 2004. p. p 7-16.

4. *Bell Flies Low-Cost Composite Stabilizer* AHS International - The Vertical Flight Society 2005 [cited; Available from: http://www.vtol.org/news/issues505.html.

5. Anon, *Composite stabilizer reduces cost and weight on helicopter.* Advanced Materials and Processes, 2005. **163**(8): p. 23.

6. Armstrong, D.L., et al., *Development of a low-cost integrated RTM horizontal stabilizer that flies on Bell Helicopter's MAPL.* SAMPE Journal, 2006. **42**(3): p. 54-62.

7. Baker, D.J. and A.J. Gustafson, *COMPOSITE FLIGHT SERVICE EVALUATION PROGRAM FOR HELICOPTERS.* Journal of the American Helicopter Society, 1981. **26**(4): p. 70-74.

8. Hutchins, J.G. *Operational durability of thermoplastic composites in primary aircraft structure.* 1996. Washington, DC, USA: American Helicopter Soc, Alexandria, VA, USA.

9. Anderson, T.C. and R.C. Holzwarth. *Design and manufacture of Low-Cost Composite - Bonded Wing.* 1998. Long Beach, CA, USA: AIAA, Reston, VA, USA.

10. Rousseau, C., A. Dobyns, and P. Minguet, *Past, present and future composite structures applications in rotorcraft.* American Society of Mechanical Engineers, Aerospace Division (Publication) AD, 1999. **58**: p. 167-168.

11. Carlson, D. and B.J. Benda, *Fabrication of the BA609 wing skin.* Annual Forum Proceedings - American Helicopter Society, 1999. **1**: p. 777-782.

12. Minderhoud, P., et al., *R&D-CRIAQ1.15-002* in *CRIAQ R&D 1.15 "Optimum Design of Composite Parts by RTM"*. 2006, Bell Helicopter Textron Canada Limited: Mirabel. p. 26.

13. Minderhoud, P., *R&D-CRIAQ1.15-003*, in *CRIAQ R&D 1.15 "Optimum Design of Composite Parts by RTM"*. August 2006, Bell Helicopter: Mirabel. p. 5.

14. Baker, D.J., *FLIGHT SERVICE EVALUATION OF COMPOSITE COMPONENTS ON BELL 206L AND SIKORSKY S-76 HELICOPTERS.* Journal of the American Helicopter Society, 1984. **29**(2): p. 3-11.

15. Mardoian, G.H. and M.B. Ezzo, *Flight service evaluation of composite helicopter components.* Journal of the American Helicopter Society, 1994. **39**(1): p. 31-40.

16. Brahney, J.H., *Composites: Helicopters leading the way.* Aerospace Engineering (Warrendale, Pennsylvania), 1989. **9**(5): p. 19-26.

17. Garbo, S.P. and K.M. Rosen, *Composites usage on the RAH-66 Comanche.* Vertiflite, 1992. **38**(2): p. 8-13.

18. Fallon, W.P., JR and S.P. Garbo. *Material Usage and Selection on the RAH-66 Comanche.* in *Materials Challenge: Diversification and the Future.* 8-11 May 1995. Anaheim, California, USA.

19. Sanders, G. and W. Townsend. *The design, fabrication, ground test and flight test of an outboard composite Stabilator for the H-60 helicopter.* 2004. Baltimore, MD, United States: American Helicopter Society, Alexandria, United States.

20. Riesel, P., et al. *Development of a folding composite stabilator for the sikorsky H-60 helicopter.* 2005. Grapevine, TX, United States: American Helicopter Society, Alexandria, United States.

21. Caramaschi and Putelli. *DESIGN AND MANUFACTURING OF COMPOSITE HORIZONTAL STABILIZER FOR THE AGUSTA A 109 HELICOPTER.* 1982. Stresa, Italy: SAMPE European Chapter, Lyon, Fr.

22. Tingen, K. and T. Bond. *H-1 composite elevator.* 2006. Phoenix, AZ, United States: American Helicopter Society, Alexandria, VA 22314-2538, United States.

23. Vitlip, M.L., A.D. Stemple, and T.R. Lee. *Design and manufacture of an advanced thermoplastic horizontal stabilator for the AH-64A*. 1991. Phoenix, AZ, USA: Publ by American Helicopter Soc, Alexandria, VA, USA.

24. Jouin, P., T. Lee, and R. Vitlip. *Manufacture of a primary flight structure using thermoplastics*. 1991. San Diego, CA, USA: Publ by SAMPE, Covina, CA, USA.

25. Bell Helicopter Textron Web Page 2006 [cited; Available from: http://www.bellhelicopter.textron.com/.

26. Prouty, R.W., *Helicopter performance, stability, and control*. 1990, Malabar, Fla. :: R.E. Krieger Pub. Co.

27. *Performance Enhancing Controls*. Aviation Intranet 2006 [cited; Available from: http://selair.selkirk.bc.ca/aerodynamics1/controls/Page5.html.

28. *Alert Service Bulletin, No. 407-02-52*, in *Bell Helicopter Textron*. March 20, 2002. p. p 2-20.

29. U.S. Department of Transportation, F.A.A., *Aviation Maintenance Alerts, AC No. 43-16A*, . July 1998. p. p15-16.

30. Strong, A.B. and C.A. Ploskonka, *Fundamentals of composites manufacturing : materials, methods, and applications*. 1989, Dearborn, Mich. :: Society of Manufacturing Engineers, Publications Development Dept., Reference Publications Division.

31. Lessard, L., *Mechanics of Composite Materials Course Notes*, in *MECH 530*. 2004, Department of Mechanical Engineering, McGill University. p. 285.

32. MSC, *Patran*. 2005 r2.

33. United, S. and Knovel, *Metallic materials and elements for aerospace vehicle structures*. Military handbook ; MIL-HDBK-5H. 2003, Norwich, N.Y. :: Knovel.

34. Raja, M.H., *Experimental optimization of process parameters to obtain class A surface finish in resin transfer molding process*, in *McGill theses*. 2005.

35. Roy, M.M., *Design and fabrication of a lightweight robotic manipulator*, in *McGill theses*. 1997.

36. Octeau, M.-A., *Composite bicycle fork design for vacuum assisted resin transfer moulding*, in *McGill theses*. 2001.

37. Thouin, M., *Design of a carbon fiber bicycle stem using an internal bladder and resin transfer molding*, in *McGill theses*. 2004.

38. Lizotte, P.L., *Stress analysis and fabrication of composite monocoque bicycle frames*, in *McGill theses*. 1996.

39. Potter, K. and Knovel, *Resin transfer moulding*. 1997, London ; New York :: Chapman & Hall.

40. Potter, K.D., *Early history of the resin transfer moulding process for aerospace applications*. Composites - Part A: Applied Science and Manufacturing, 1999. **30**(5): p. 619-621.

41. *Cycom 890 RTM Technical Datasheet*, in *Cytec Engineered Materials*. 2006.

42. Khoun, L. and P. Hubert, *Preliminary Resin Selection – Revision 2*, in *CRIAQ R&D 1.15 "Optimum Design of Composite Parts by RTM"*. 2006, McGill University: Montréal. p. 14.

43. Khoun, L. and P. Hubert, *Fibre selection*, in *CRIAQ R&D 1.15 "Optimum Design of Composite Parts by RTM"*. 2006, McGill University: Montréal.

44. *Drawing 40-304*, in *Bell 407 Helicopter Drawings*: Mirabel.

45. *Drawing 407-023-001*, in *Bell 407 Helicopter Drawings*: Mirabel.

46. *Hexcel Fabrics Carbon Data Sheets - AS4GP 6K 5H satin (AGP370-5H) Properties*. [cited; Available from: http://www.hexcel.com/Products/Downloads/Fabrics+Data+Sheets.htm?map=P3&t=Carbon+Data+Sheets.

47. Lalonde, S., *Investigation into the static and fatigue behaviour of a helicopter main rotor yoke made of composite materials*. McGill theses. 2000.

48. MSC, *Nastran*. 2005.

49. Textron, B.H., *CDTR #CDO4745*.

50. *MSC Software Patran documentation*. 2005 r2.

51. Yang, J. and P. McConnel, *Report 407-930-003*. 1996.

52. PTC, *Pro/ENGINEER Wildfire 3.0*. 2006.

53. *Drawing 407-023-801 Rev K SH 3*, in *Bell 407 Helicopter Drawings*: Mirabel.

54. Cook, R.D. and R.D. Cook, *Concepts and applications of finite element analysis*. 2002, New York :: Wiley.

55. Minderhoud, P. and S. Bernier, *Email and meetings with collaborators from Bell Helicopter*. 2006.

56. Wikipedia. *http://en.wikipedia.org/wiki/Factor_of_safety*. 2006 [cited; Available from: http://en.wikipedia.org/wiki/Factor_of_safety.

57. Poon, C., T. Benak, and R. Gould, *Assessment of impact damage in toughened resin composites*. Theoretical and Applied Fracture Mechanics, 1990. **13**(2): p. 81-97.

58. McGowan, D.M. and D.R. Ambur, *Damage-Tolerance Characteristics of Composite Fuselage Sandwich Structures With Thick Facesheets*, in *NASA Technical Memorandum 110303*. February 1997, Langley Research Center: Hampton, Virginia.

59. Fawcett, A.J. and G.D. Oakes. *Boeing Composite Airframe Damage Tolerance and Service Experience*. Boeing Commercial Airplanes 787 Program 2006 [cited; Available from: http://www.niar.wichita.edu/chicagoworkshop/Chicago%20Damage%20Tolerance%20Workshop%20-%20July%2019-21,%202006/Wednesday%20-%20Session%201%20Presentations/Boeing%20Transport%20Experience%20with%20Composite%20Damage%20Tolerance%20&%20Maintenance%20-%20Fawcett%20&%20Oakes.pdf.

APPENDIX I

A.1 Load case calculations

A. *Calculations of the load case of the first design stage*

→ From Report 407-930-003 (p.15.120a):

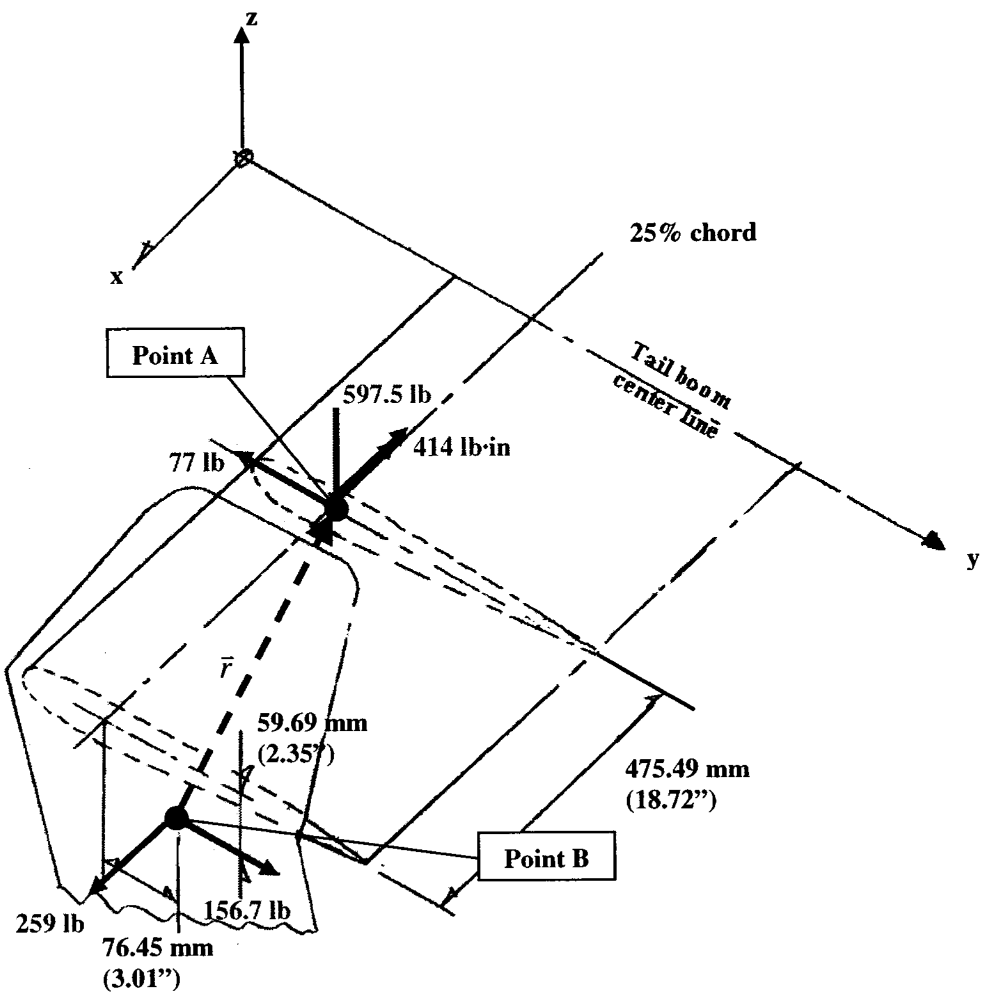

Figure A1.1: Location of points A and B for load case calculation of the first design stage

Point A: F < 0, -77, -597.5> lb

M < -414, 0, 0> lb·in

Point B: F <259, 156.7, 0> lb

$\vec{r}$ = (-18.72 $\vec{i}$ - 3.01 $\vec{j}$ + 2.35 $\vec{k}$)

→ From Report 407-930-003 (p.15.121), to calculate the distance alongXaxis between point A and point b:
$\left[\frac{(41.98-5.568)+(43.56-5.095)}{2}\right]/2 = 18.72"$ (A is in the middle of the exposed area)

<u>A→ B:</u> $\sum \vec{F}$: 259 $\vec{i}$ + (156.7-77) $\vec{j}$ -597.5 $\vec{k}$

F <259, 79.7, 597.5> lb

$\sum \vec{M} : \vec{r} \times \vec{F}_A + M_A$

$$\begin{vmatrix} \vec{i} & \vec{j} & \vec{k} \\ -18.72 & -3.01 & 2.35 \\ 0 & -77 & -597.5 \end{vmatrix} -414\vec{i}$$

[(-3.01)(-597.5)-2.35(-77)] $\vec{i}$ - [(-18.72)(-597.5)-0] $\vec{j}$
+ [(-18.72)(-77)-0] $\vec{k}$ - 414 $\vec{i}$

M <1565.43, -11185.2, 1441.44> lb·in

Pressure on slat (from p.15.146 of Report 407-930-003):

$\boxed{\text{q = 82.39 psf = } \mathbf{0.572\ psi}}$

B. *Calculations of the stabilizer's triangular load distribution for the third design stage*

20 (length) x 16 (width) = 320 nodes

597.5 lb (total force)

Total load along the width: 597.5 lb / 20 nodes = **29.875 lb**

29.875 = bh/2 (area of a triangle) = 15h/2

→ h = 3.983 lb (maximum value of the triangular) – at node #5 corresponding to stabilizer's center of gravity

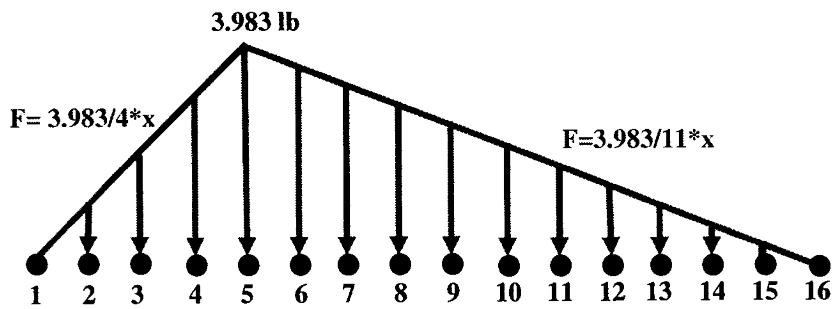

Figure A1.2: Side view of the load distribution on the stabilizer for the third design stage

<u>Node 1</u>: 3.983/4*0 = 0 lb
<u>Node 2</u>: 3.983/4*1 = 0.996 lb (4.43 N)
<u>Node 3</u>: 3.983/4*2 = 1.992 lb (8.86 N)
<u>Node 4</u>: 3.983/4*3 = 2.987 lb (13.72 N)
<u>Node 5</u>: 3.983/4*4 = 3.983/11*11= 3.983 lb (17.72 N)
<u>Node 6</u>: 3.983/11*10 = 3.621 lb (16.11 N)
<u>Node 7</u>: 3.983/11*9 = 3.259 lb (14.50 N)
<u>Node 8</u>: 3.983/11*8 = 2.897 lb (12.89 N)
<u>Node 9</u>: 3.983/11*7 = 2.535 lb (11.27 N)
<u>Node 10</u>: 3.983/11*6 = 2.173 lb (9.67 N)
<u>Node 11</u>: 3.983/11*5 = 1.81 lb (8.05 N)
<u>Node 12</u>: 3.983/11*4 = 1.448 lb (6.44 N)
<u>Node 13</u>: 3.983/11*3 = 1.086 lb (4.83 N)
<u>Node 14</u>: 3.983/11*2 = 0.724 lb (3.22 N)
<u>Node 15</u>: 3.983/11*1 = 0.362 lb (1.61 N)
<u>Node 16</u>: 3.983/11*0 = 0 lb

$\sum F_{nodes}$ = **29.873 lb**
(total load along width)

Total force = 29.873 lb x 20 (nodes along length) = 597.5 lb

C. *Calculations of the slat's triangular load distribution for the third design stage*

36 (length) x 8 (width) = 288 nodes

On the slat, chosen application nodes are spaced out with a distance of 1 in

2.87 lb / in = 2.87 lb / node

Total load along the width: 2.87 lb

2.87 = bh/2 (area of a triangle) = 7h/2

→ h = 0.82 lb (maximum value of the triangular distribution) – at node #4 corresponding to slat's center of gravity)

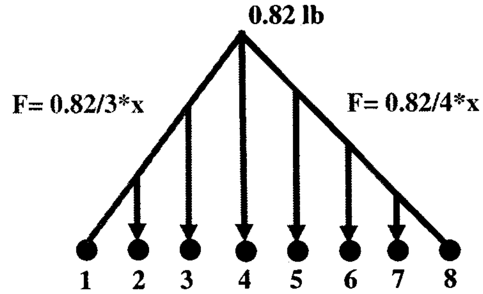

Figure A1.3: Side view of the load distribution on the slat for the third design stage

Node 1: 0.82/3*0 = 0 lb
Node 2: 0.82/3*1 = 0.273 lb (1.21 N)
Node 3: 0.82/3*2 = 0.547 lb (2.43 N)
Node 4: 0.82/3*3 = 0.82/4*4 = 0.82 lb (3.65 N)
Node 5: 0.82/4*3 = 0.615 lb (2.74 N)
Node 6: 0.82/4*2 = 0.41 lb (1.82 N)
Node 7: 0.82/4*1 = 0.205 lb (0.91 N)
Node 8: 0.82/4*0 = 0 lb

$\sum F_{nodes}$ = **2.87 lb**
(total load along width)

Distributed force = 2.87 lb / node = 2.87 lb / in

D. *<u>Calculations of the stabilizer's triangular load distribution for load cases 1-4</u>*

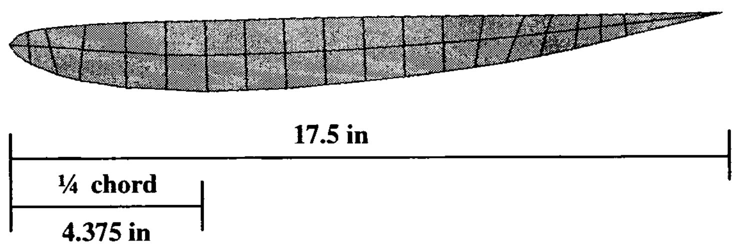

Figure A1.4: Location of the aerodynamic center of gravity on the stabilizer

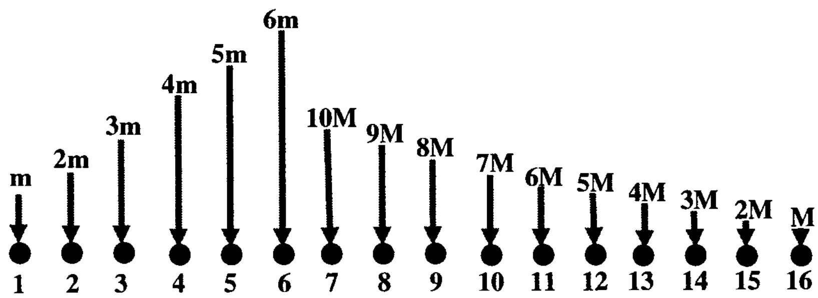

Figure A1.5: Side view of the load distribution on the stabilizer for load cases 1-4 of the fourth design stage

Total load along the width: 597.5 lb / 20 nodes = **29.875 lb**

$m + 2m + 3m + 4m + 5m + 6m + 10M + 9M + 8M + 7M + 6M + 5M + 4M + 3M$

$+ 2M + M = 29.875$

$21m + 55M = 29.875$

$$\rightarrow m = \frac{1}{21}(29.875 - 55M)$$

Moment = 0 at ¼ chord (node 6):

Σ M: $5(m) + 4(2m) + 3(3m) + 2(4m) + 1(5m) - 10(M) - 9(2M) - 8(3M) - 7(4M) - 6(5M) - 5(6M) - 4(7M) - 3(8M) - 2(9M) - 1(10M) = 0$

$35m - 220M = 0$

$$35\left(\frac{1}{21}(29.875 - 55M)\right) - 220M = 0$$

$$\boxed{M = 0.160 \text{ lb}}$$

$$m = \frac{1}{21}[29.875 - 55(0.160)]$$

$$\boxed{m = 1.004 \text{ lb}}$$

Node 1: 1.004 lb (4.47 N)
Node 2: 1.004*2 = 2.008 lb (8.93 N)
Node 3: 1.004*3 = 3.012 lb (13.40 N)
Node 4: 1.004*4 = 4.016 lb (17.87 N)
Node 5: 1.004*5 = 5.021 lb (22.33 N)
Node 6: 1.004*6 = 6.025 lb (26.80 N)
Node 7: 0.160*10 = 1.600 lb (7.11 N)
Node 8: 0.160*9 = 1.438 lb (6.40 N)
Node 9: 0.160*8 = 1.278 lb (5.70 N)
Node 10: 0.160*7 = 1.119 lb (4.98 N)
Node 11: 0.160*6 = 0.959 lb (4.26 N)
Node 12: 0.160*5 = 0.799 lb (3.55 N)
Node 13: 0.160*4 = 0.639 lb (2.84 N)
Node 14: 0.160*3 = 0.479 lb (2.13 N)
Node 15: 0.160*2 = 0.320 lb (1.42 N)
Node 16: 0.160 lb = 0.160 lb (0.71 N)

$\sum F_{nodes}$ **= 29.875 lb**
(total load along width)

E. <u>*Calculations of the slat's triangular load distribution for load cases 1-4*</u>

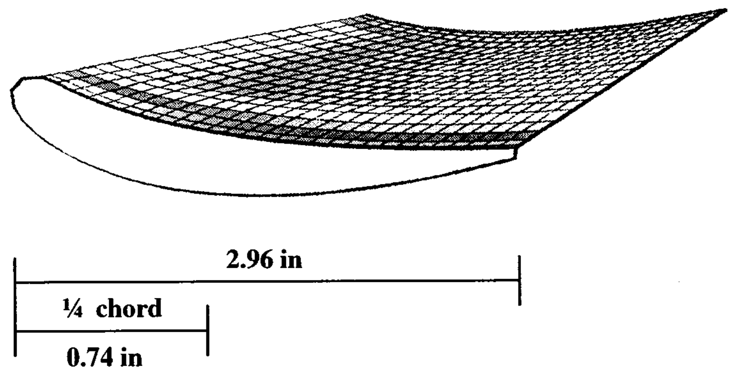

Figure A1.6: Location of the aerodynamic center of gravity on the slat

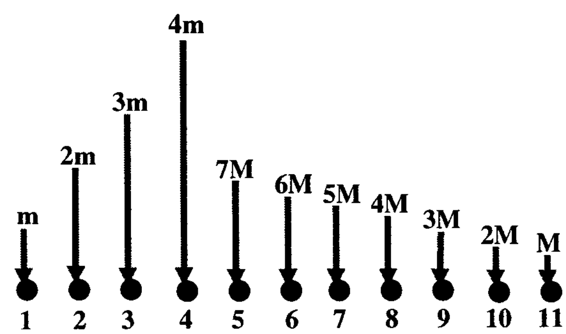

Figure A1.7: Side view of the load distribution on the slat for load cases 1-4 of the fourth design stage

On the slat, chosen application nodes are spaced out with a distance of 1 in

2.87 lb / in = 2.87 lb / node

Total load along the width: 2.87 lb

$m + 2m + 3m + 4m + 7M + 6M + 5M + 4M + 3M + 2M + M = 2.87$

$10m + 28M = 29.875$

$\rightarrow m = 0.287 - 2.8M$

Moment = 0 at ¼ chord (node 4):

Σ M: 3(m) + 2(2m) + 1(3m) – 7(M) – 6(2M) – 5(3M) – 4(4M) – 3(5M) – 2(6M) - 1(7M) = 0

10m – 84M = 0

10(0.287 – 2.8M) – 84M = 0

$\boxed{M = 0.026 \text{ lb}}$

m = 0.287 – 2.8(0.026)

$\boxed{m = 0.215 \text{ lb}}$

Node 1: 0.215 lb (0.96 N)
Node 2: 0.215*2 = 0.431 lb (1.92 N)
Node 3: 0.215*3 = 0.646 lb (2.87 N)
Node 4: 0.215*4 = 0.861 lb (3.83 N)
Node 5: 0.026*7 = 0.179 lb (0.80 N)
Node 6: 0.026*6 = 0.154 lb (0.69 N)
Node 7: 0.026*5 = 0.128 lb (0.57 N)
Node 8: 0.026*4 = 0.103 lb (0.46 N)
Node 9: 0.026*3 = 0.077 lb (0.34 N)
Node 10: 0.026*2 = 0.051 lb (0.23 N)
Node 11: 0.026 lb (0.12 N)

$\sum F_{nodes}$ **= 2.87 lb**
(total load along width)

F. *Calculations of the stabilizer's triangular load distribution for load cases 5-8*

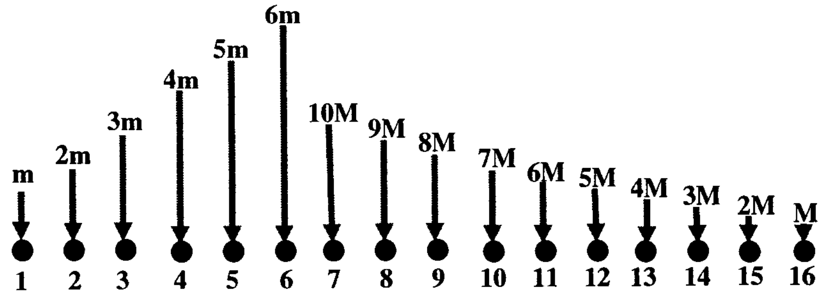

Figure A1.8: Side view of the load distribution on the stabilizer for load cases 5-8 of the fourth design stage

Total load along the width: 300 lb / 20 nodes = **15 lb**

$$m + 2m + 3m + 4m + 5m + 6m + 10M + 9M + 8M + 7M + 6M + 5M + 4M + 3M$$

$$+ 2M + M = 15$$

$$21m + 55M = 15$$

$$\rightarrow m = \frac{1}{21}(15 - 55M)$$

Moment = 0 at ¼ chord (node 6):

ΣM: $5(m) + 4(2m) + 3(3m) + 2(4m) + 1(5m) - 10(M) - 9(2M) - 8(3M) - 7(4M)$
$- 6(5M) - 5(6M) - 4(7M) - 3(8M) - 2(9M) - 1(10M) = 0$

$$35m - 220M = 0$$

$$35\left(\frac{1}{21}(15 - 55M)\right) - 220M = 0$$

$$\boxed{M = 0.0802 \text{ lb}}$$

$$m = \frac{1}{21}[15 - 55(0.0802)]$$

$$\boxed{m = 0.5042 \text{ lb}}$$

Node 1: 0.5042 lb (2.24 N)
Node 2: 0.5042*2 = 2.008 lb (4.49 N)
Node 3: 0.5042*3 = 3.012 lb (6.73 N)
Node 4: 0.5042*4 = 4.016 lb (8.97 N)
Node 5: 0.5042*5 = 5.021 lb (11.21 N)
Node 6: 0.5042*6 = 6.025 lb (13.46 N)
Node 7: 0.0802*10 = 1.600 lb (3.57 N)
Node 8: 0.0802*9 = 1.438 lb (3.21 N)
Node 9: 0.0802*8 = 1.278 lb (2.85 N)
Node 10: 0.0802*7 = 1.119 lb (2.50 N)
Node 11: 0.0802*6 = 0.959 lb (2.14 N)
Node 12: 0.0802*5 = 0.799 lb (1.78 N)
Node 13: 0.0802*4 = 0.639 lb (1.42 N)
Node 14: 0.0802*3 = 0.479 lb (1.07 N)
Node 15: 0.0802*2 = 0.320 lb (0.71 N)
Node 16: 0.0802 lb = 0.160 lb (0.36 N)

$\sum F_{nodes}$ **= 15 lb**
(total load along width)

G. *Calculations of the slat's triangular load distribution for load cases 5-8*

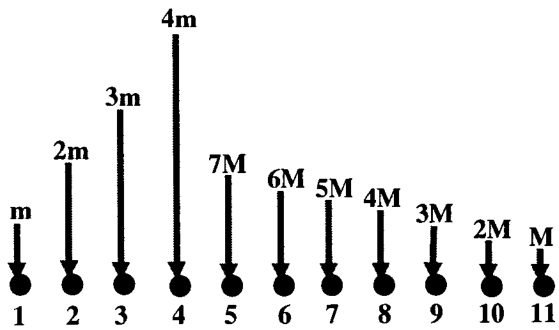

Figure A1.9: Side view of the load distribution on the slat for load cases 5-8 of the fourth design stage

On the slat, chosen application nodes are spaced out with a distance of 1 in

3 lb / in = 3 lb / node

Total load along the width: 3 lb

$m + 2m + 3m + 4m + 7M + 6M + 5M + 4M + 3M + 2M + M = 3$

$10m + 28M = 3$

$\rightarrow m = 0.3 - 2.8M$

Moment = 0 at ¼ chord (node 4):

ΣM: $3(m) + 2(2m) + 1(3m) - 7(M) - 6(2M) - 5(3M) - 4(4M) - 3(5M) - 2(6M) - 1(7M) = 0$

$10m - 84M = 0$

$10(0.3 - 2.8M) - 84M = 0$

$\boxed{M = 0.027 \text{ lb}}$

$m = 0.3 - 2.8(0.027)$

$\boxed{m = 0.225 \text{ lb}}$

Node 1: 0.225 lb (1.00 N)
Node 2: 0.225*2 = 0.45 lb (2.00 N)
Node 3: 0.225*3 = 0.675 lb (3.00 N)
Node 4: 0.225*4 = 0.9 lb (4.00 N)
Node 5: 0.027*7 = 0.1875 lb (0.83 N)
Node 6: 0.027*6 = 0.1607 lb (0.71 N)
Node 7: 0.027*5 = 0.1339 lb (0.60 N)
Node 8: 0.027*4 = 0.1071 lb (0.48 N)
Node 9: 0.027*3 = 0.0804 lb (0.36 N)
Node 10: 0.027*2 = 0.0536 lb (0.24 N)
Node 11: 0.0268 lb (0.12 N)

$\sum F_{nodes}$ **= 3 lb**
(total load along width)

APPENDIX II

A.2 Finite element analysis results

A. <u>*Overall deformation results for the 2^{nd} design stage*</u>

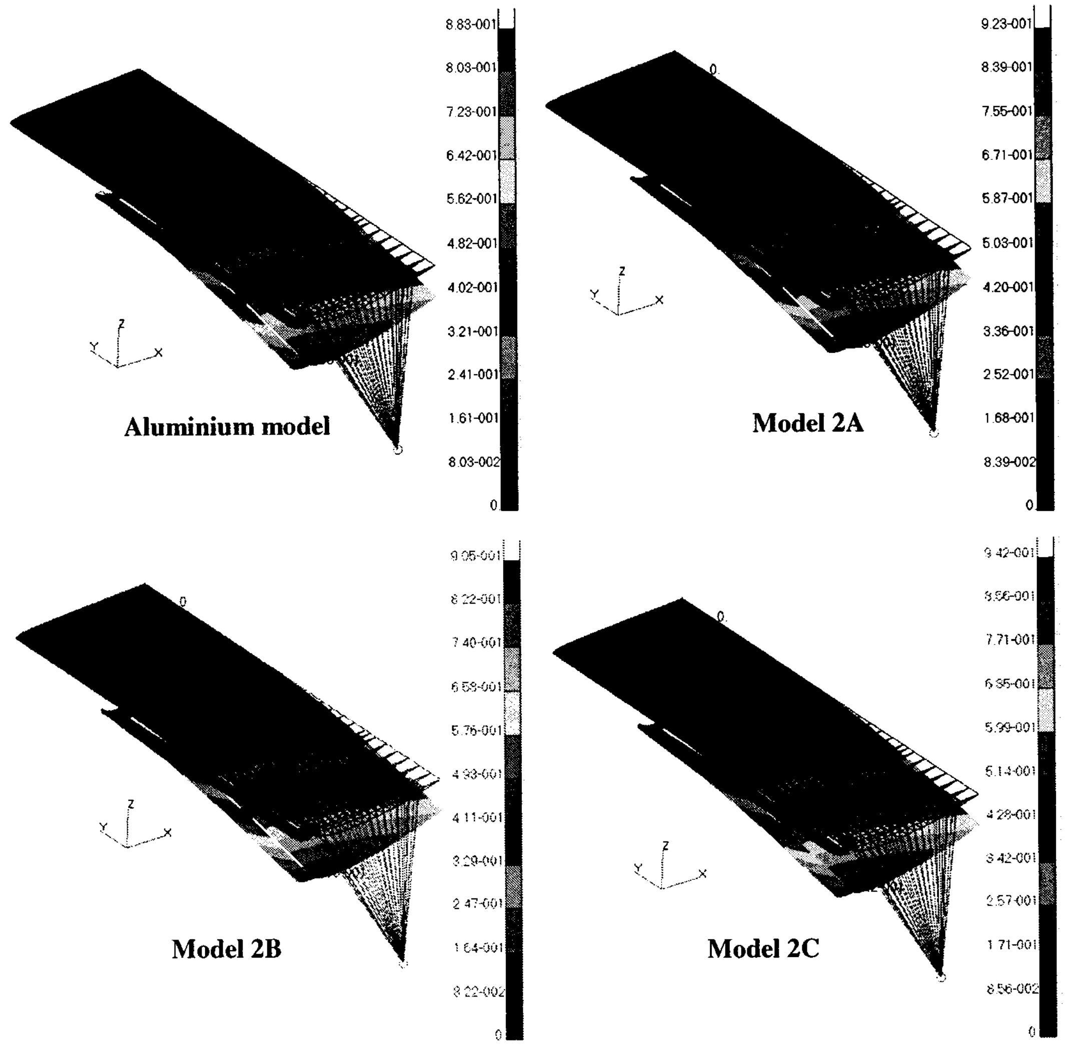

Figure A2.1: Overall deformations of the aluminium slat assembly (upper left corner), model 2A assembly (upper right corner), model 2B assembly (lower left corner) and model 2C assembly (right)

B. *Deformation results for the 3rd design stage*

Table A2.1: Maximum overall deformation values of all assembly models for the 4 different load cases (in inches)

	Load case 1	Load case 2	Load case 3	Load case 4
Original model	1.59	1.15	1.08	1.50
Model 3A	1.49	1.09	0.99	1.43
Model 3B	1.49	1.08	0.99	1.43
Model 3C	1.52	1.10	1.01	1.45
Model 3D	1.53	1.10	1.01	1.45
Model 3E	1.54	1.01	1.01	1.47
Model 3F	1.51	1.10	1.03	1.44
Model 3G	1.51	1.11	1.02	1.45
Model 3H	1.44	1.02	1.02	1.44
Model 3I	1.50	1.09	1.00	1.44
Model 3J	1.51	1.09	1.00	1.44
Model 3K	1.52	1.00	1.00	1.46
Model 3L	1.50	1.09	1.02	1.43
Model 3M	1.50	1.10	1.01	1.44
Model 3N	1.41	1.02	1.02	1.41
Model 3P	1.41	1.02	1.02	1.41

Table A2.2: Maximum deflection values at the tip of the slat for all models for the different load cases (in inches)

	Load case 1	Load case 2	Load case 3	Load case 4
Original model	1.57	0.843	1.03	1.33
Model 3A	1.46	0.768	0.941	1.25
Model 3B	1.46	0.767	0.942	1.25
Model 3C	1.52	0.795	0.980	1.31
Model 3D	1.53	0.795	0.980	1.31
Model 3E	1.54	0.897	0.988	1.33
Model 3F	1.49	0.786	0.969	1.27
Model 3G	1.48	0.788	0.960	1.27
Model 3H	1.44	0.915	0.915	1.44
Model 3I	1.49	0.794	0.974	1.28
Model 3J	1.50	0.794	0.974	1.29
Model 3K	1.52	0.897	0.986	1.31
Model 3L	1.46	0.783	0.963	1.24
Model 3M	1.45	0.784	0.955	1.25
Model 3N	1.40	0.902	0.902	1.40
Model 3P	1.40	0.905	0.905	1.40

C. <u>*Maximum failure indices results for the 3rd design stage*</u>

Table A2.3: Maximum failure indices and their location for models 3A and 3B

	Load case 1	**Load case 2**	**Load case 3**	**Load case 4**
Model 3A  90° Airfoil: 4 plies Brackets: 4 plies	0.604 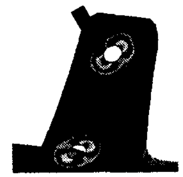 Bracket #4	0.493 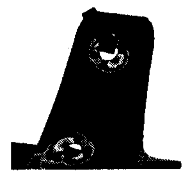 Bracket #4	0.403 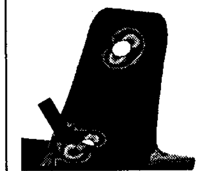 Bracket #4	0.521 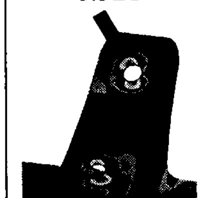 Bracket #3
Model 3B  85° Airfoil: 4 plies Brackets: 4 plies	0.577 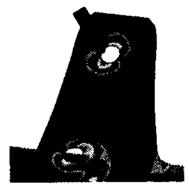 Bracket #3	0.471 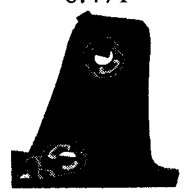 Bracket #4	0.368 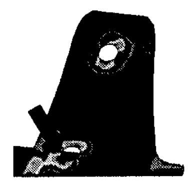 Bracket #4	0.477 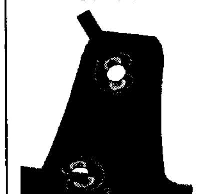 Bracket #4

Table A2.4: Maximum failure indices and their location for models 3C-3E

	Load case 1	Load case 2	Load case 3	Load case 4
Model 3C  90° Airfoil: 4 plies Brackets: 4 plies	0.684 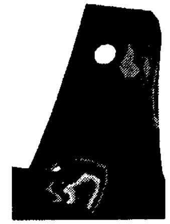 Bracket #2	0.459 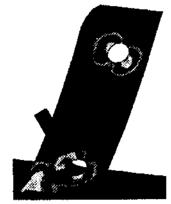 Bracket #4	0.413 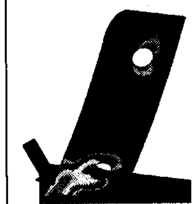 Bracket #3	0.592 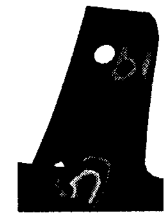 Bracket #2
Model 3D  85° Airfoil: 4 plies Brackets: 4 plies	0.693 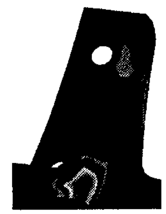 Bracket #2	0.460 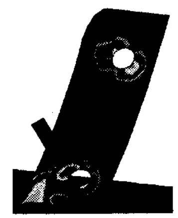 Bracket #4	0.391 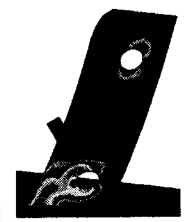 Bracket #3	0.597 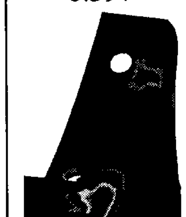 Bracket #2
Model 3E  60° Airfoil: 4 plies Brackets: 4 plies	0.839 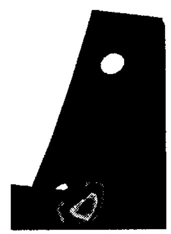 Bracket #2	0.461 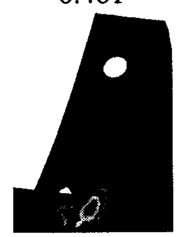 Bracket #1	0.430 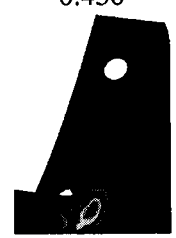 Bracket #1	0.665 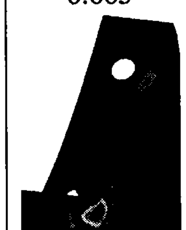 Bracket #2

Table A2.5: Maximum failure indices and their location for models 3F-3H

	Load case 1	Load case 2	Load case 3	Load case 4
Model 3F 90° Airfoil: 4 plies Brackets: 4 plies	0.711 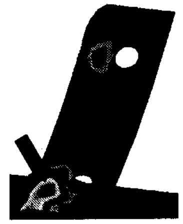 Bracket #2	0.429 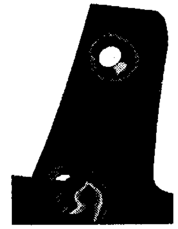 Bracket #3	0.394 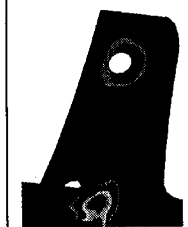 Bracket #3	0.555 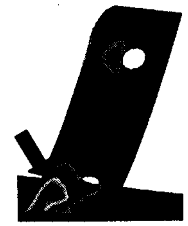 Bracket #2
Model 3G 85° Airfoil: 4 plies Brackets: 4 plies	0.673 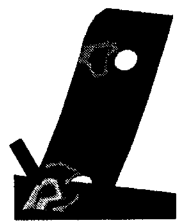 Bracket #2	0.458 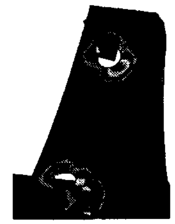 Bracket #4	0.346 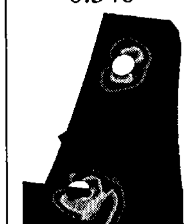 Bracket #3	0.675 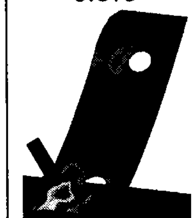 Bracket #2
Model 3H 70° Airfoil: 4 plies Brackets: 4 plies	0.563 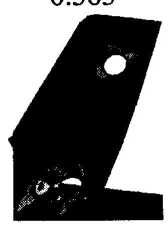 Bracket #2	0.381 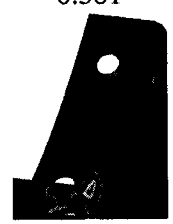 Bracket #3	0.381 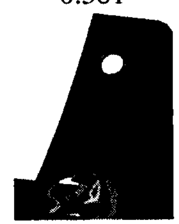 Bracket #3	0.563 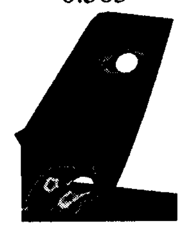 Bracket #2

Table A2.6: Maximum failure indices and their location for models 3I-3K

	Load case 1	Load case 2	Load case 3	Load case 4
Model 3I 90° Airfoil: 4 plies Brackets: 6 plies	0.562 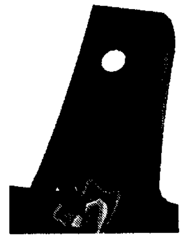 Bracket #2	0.368 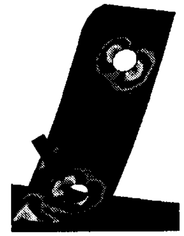 Bracket #4	0.324 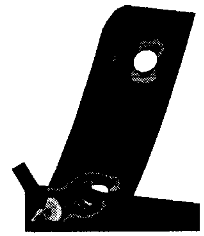 Bracket #3	0.461 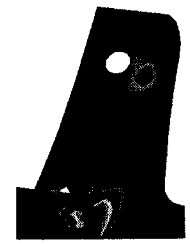 Bracket #2
Model 3J 85° Airfoil: 4 plies Brackets: 6 plies	0.562 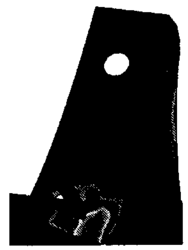 Bracket #2	0.387 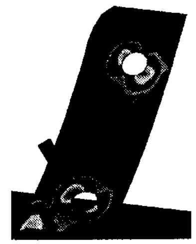 Bracket #4	0.300 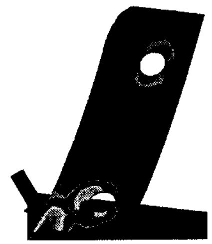 Bracket #3	0.461 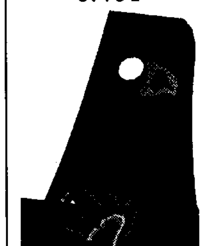 Bracket #2
Model 3K 60° Airfoil: 4 plies Brackets: 6 plies	0.609 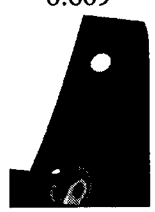 Bracket #2	0.305 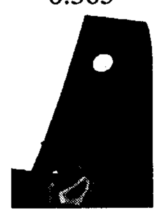 Bracket #1	0.296 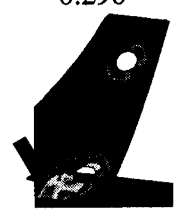 Bracket #4	0.446 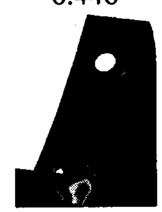 Bracket #2

Table A2.7: Maximum failure indices and their location for models 3L-3P

	Load case 1	Load case 2	Load case 3	Load case 4
Model 3L  90° Airfoil: 4 plies Brackets: 6 plies	0.540 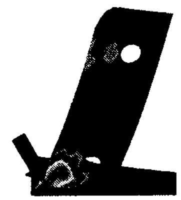 Bracket #2	0.333 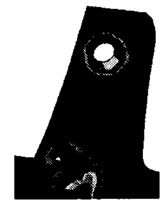 Bracket #3	0.265 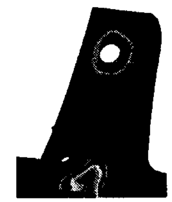 Bracket #3	0.445 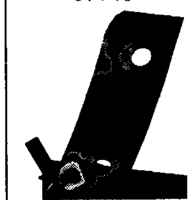 Bracket #2
Model 3M  85° Airfoil: 4 plies Brackets: 6 plies	0.478 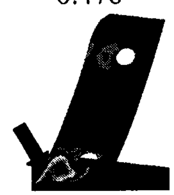 Bracket #2	0.375  Bracket #4	0.256 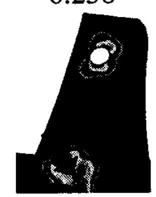 Bracket #3	0.406 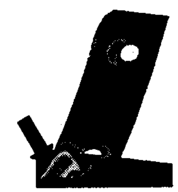 Bracket #2
Model 3N  70° Airfoil: 4 plies Brackets: 6 plies	0.361 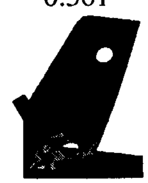 Bracket #2	0.237  Bracket #4	0.237  Bracket #4	0.361  Bracket #2
Model 3P  70° Airfoil: 4 plies Brackets: 6 plies	0.374 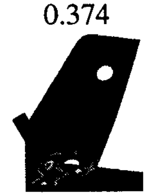 Bracket #2	0.252 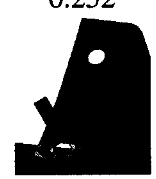 Bracket #4	0.252  Bracket #4	0.363 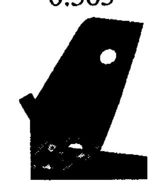 Bracket #2

Table A2.8: Maximum Von Mises stresses and their location for the original aluminium model for the third design stage (in psi)

	Load case 1	**Load case 2**	**Load case 3**	**Load case 4**
Original model 	5.33×10^4 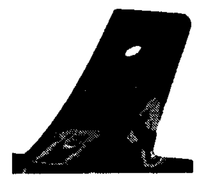 Bracket #2	2.80×10^4 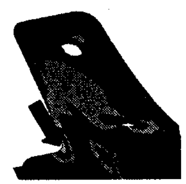 Bracket #1	2.96×10^4  Bracket #1	4.23×10^4  Bracket #2

D. *Deformation results for the 4th design stage*

Table A2.9: Maximum overall deformation values of all assembly models for the 8 different load cases and the Thermal load case (in inches)

	Load case 1	Load case 2	Load case 3	Load case 4	Load case 5	Load case 6	Load case 7	Load case 8	Load Case 9
Original model	1.55	0.999	1.04	1.37	0.931	0.409	0.387	0.808	0.126
Model 4A	1.49	1.02	1.04	1.33	0.872	0.439	0.413	0.779	0.114
Model 4B	1.48	1.02	1.05	1.33	0.868	0.441	0.419	0.771	0.114
Model 4C	1.48	1.01	1.05	1.32	0.871	0.435	0.422	0.764	0.113
Model 4D	1.48	1.01	1.05	1.32	0.871	0.435	0.422	0.764	0.113
Model 4E	1.56	1.04	1.07	1.39	0.935	0.438	0.413	0.844	0.114
Model 4F	1.54	1.05	1.08	1.37	0.912	0.449	0.426	0.830	0.114
Model 4G	1.56	1.03	1.06	1.39	0.935	0.436	0.410	0.864	0.114
Model 4H	1.56	1.12	1.07	1.52	0.929	0.438	0.416	0.868	0.114
Model 4I	1.56	1.05	1.09	1.38	0.928	0.451	0.426	0.818	0.115
Model 4J	1.55	1.05	1.09	1.38	0.925	0.452	0.428	0.817	0.115
Model 4K	1.55	1.05	1.09	1.38	0.924	0.452	0.428	0.816	0.115
Model 4L	1.55	1.06	1.09	1.38	0.918	0.457	0.435	0.809	0.115
Model 4M	1.30	0.931	0.902	1.21	0.760	0.405	0.356	0.701	0.116
Model 4N	1.30	0.936	0.908	1.21	0.757	0.409	0.360	0.700	0.117
Model 4P	1.29	0.940	0.906	1.22	0.755	0.412	0.357	0.704	0.117
Model 4Q	1.29	0.940	0.906	1.22	0.755	0.412	0.357	0.704	0.112
Model 4R	1.40	0.965	0.952	1.29	0.841	0.411	0.366	0.760	0.111
Model 4S	1.43	0.993	0.992	1.30	0.854	0.427	0.389	0.764	0.116
Model 4T	1.41	0.964	0.950	1.29	0.851	0.411	0.365	0.762	0.117
Model 4U	1.41	1.05	0.955	1.36	0.852	0.412	0.371	0.756	0.115
Model 4V	1.41	0.975	0.969	1.29	0.826	0.418	0.378	0.755	0.116
Model 4W	1.40	0.976	0.971	1.28	0.824	0.420	0.380	0.753	0.116
Model 4X	1.40	0.976	0.970	1.29	0.825	0.419	0.379	0.754	0.116
Model 4Y	1.40	0.978	0.975	1.28	0.821	0.422	0.383	0.750	0.116

Table A2.10: Maximum deflection values at the tip of the slat for all models for the different load cases (in inches)

	Load case 1	Load case 2	Load case 3	Load case 4	Load case 5	Load case 6	Load case 7	Load case 8	Load case 9
Original model	1.55	0.797	0.993	1.26	0.931	0.277	0.363	0.808	0.119
Model 4A	1.46	0.824	1.01	1.25	0.867	0.319	0.399	0.757	0.107
Model 4B	1.46	0.827	1.02	1.25	0.862	0.321	0.404	0.752	0.107
Model 4C	1.46	0.823	1.02	1.24	0.865	0.351	0.406	0.750	0.106
Model 4D	1.46	0.823	1.02	1.24	0.805	0.351	0.406	0.750	0.106
Model 4E	1.56	0.862	1.04	1.36	0.935	0.319	0.4	0.844	0.107
Model 4F	1.54	0.883	1.05	1.35	0.912	0.338	0.413	0.830	0.107
Model 4G	1.56	0.870	1.03	1.39	0.935	0.323	0.389	0.864	0.107
Model 4H	1.56	0.993	1.03	1.52	0.929	0.329	0.389	0.868	0.104
Model 4I	1.53	0.854	1.03	1.31	0.928	0.332	0.407	0.805	0.108
Model 4J	1.53	0.856	1.03	1.30	0.925	0.334	0.408	0.801	0.108
Model 4K	1.53	0.856	1.03	1.30	0.924	0.334	0.409	0.801	0.108
Model 4L	1.52	0.862	1.03	1.29	0.918	0.340	0.415	0.794	0.108
Model 4M	1.27	0.754	0.863	1.13	0.747	0.302	0.338	0.690	0.116
Model 4N	1.27	0.762	0.872	1.13	0.745	0.307	0.343	0.689	0.117
Model 4P	1.27	0.764	0.872	1.13	0.745	0.309	0.341	0.692	0.117
Model 4Q	1.27	0.764	0.872	1.13	0.745	0.309	0.341	0.692	0.108
Model 4R	1.40	0.789	0.926	1.23	0.841	0.299	0.357	0.760	0.104
Model 4S	1.43	0.822	0.969	1.25	0.854	0.317	0.382	0.763	0.116
Model 4T	1.41	0.784	0.928	1.23	0.851	0.294	0.358	0.762	0.117
Model 4U	1.41	0.891	0.934	1.34	0.852	0.296	0.365	0.756	0.114
Model 4V	1.35	0.787	0.906	1.20	0.807	0.309	0.353	0.746	0.116
Model 4W	1.34	0.788	0.907	1.20	0.802	0.310	0.354	0.741	0.116
Model 4X	1.34	0.788	0.907	1.20	0.804	0.310	0.354	0.743	0.116
Model 4Y	1.34	0.792	0.911	1.20	0.801	0.314	0.358	0.741	0.116

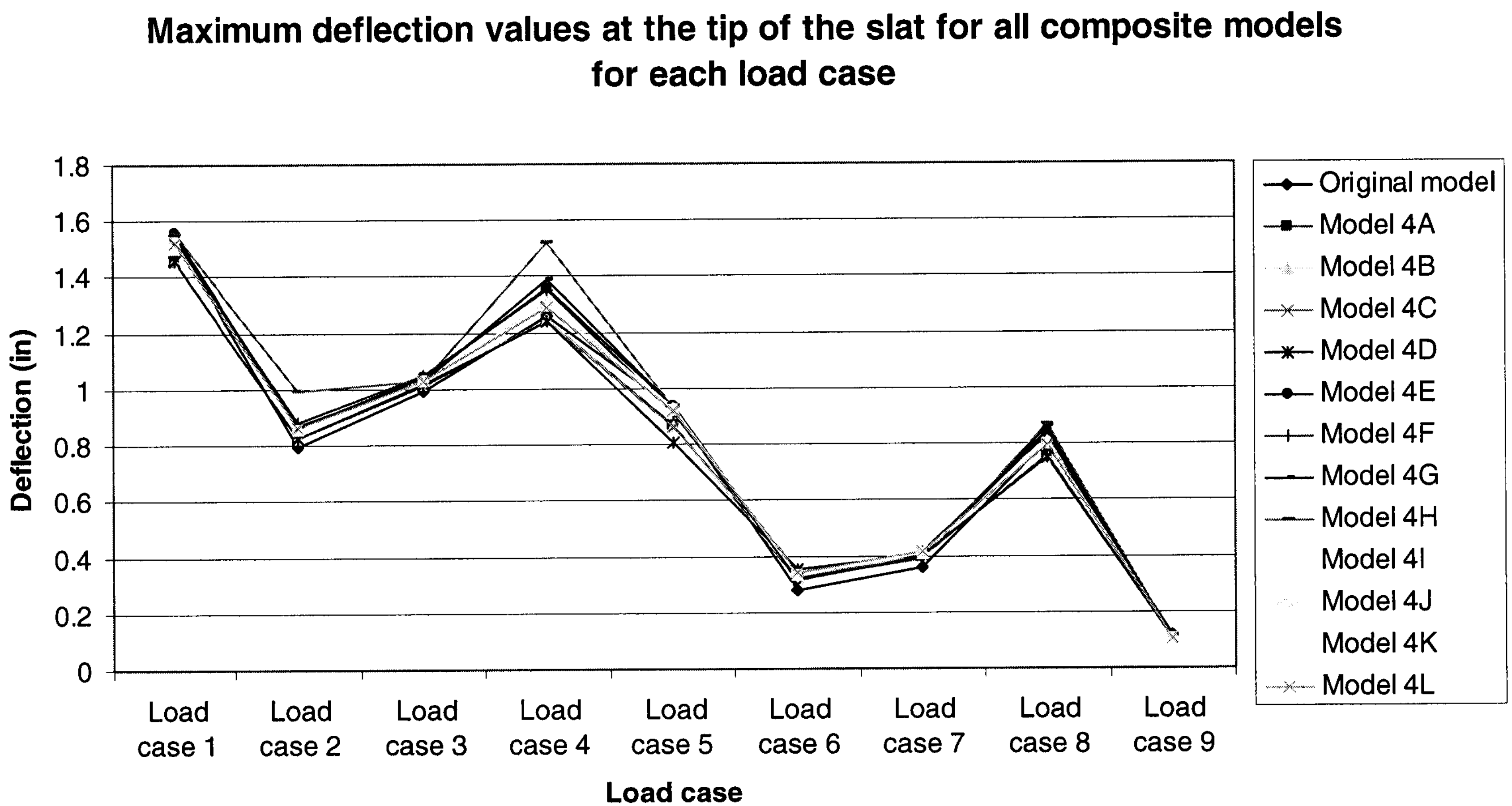

Figure A2.2: Graph of the maximum deflection values at the tip of the slat for all composite models for each load case

E. *Maximum failure indices results for the 4th design stage*

Table A2.11: Maximum failure indices and their location for models 4A-4D

	Load case 1	Load case 2	Load case 3	Load case 4	Load case 5	Load case 6	Load case 7	Load case 8	Load case 9
Model 4A 90° Airfoil: 4 plies Brackets: 6 plies	1.20  Bracket #3	0.514  Bracket #3	1.14  Bracket #4	0.892  Bracket #2	0.733 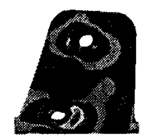 Bracket #3	0.342 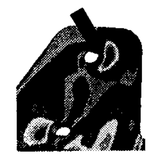 Bracket #1	0.609 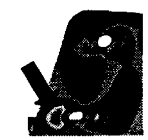 Bracket #4	0.604  Bracket #2	0.227  Bracket #1
Model 4B 80° Airfoil: 4 plies Brackets: 6 plies	1.23 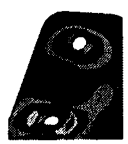 Bracket #3	0.568 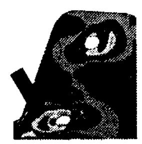 Bracket #3	1.21 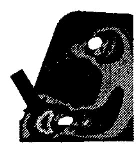 Bracket #4	0.989  Bracket #2	0.722 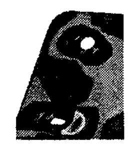 Bracket #3	0.318  Bracket #1	0.626 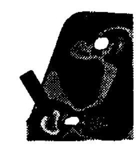 Bracket #4	0.662  Bracket #2	0.240  Bracket #1
Model 4C 70° Airfoil: 4 plies Brackets: 6 plies	1.24  Bracket #4	0.488  Bracket #4	1.23 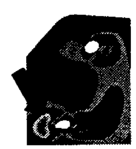 Bracket #4	1.15  Bracket #3	0.713  Bracket #4	0.299  Bracket #4	0.600  Bracket #4	0.740  Bracket #2	0.245  Bracket #1
Model 4D 60° Airfoil: 4 plies Brackets: 6 plies	1.24  Bracket #4	0.487 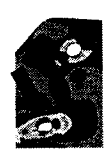 Bracket #4	1.23 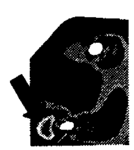 Bracket #4	1.15  Bracket #3	0.715  Bracket #4	0.299  Bracket #4	0.602 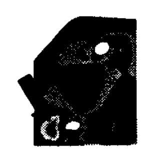 Bracket #4	0.740  Bracket #2	0.244  Bracket #1

Table A2.12: Maximum failure indices and their location for models 4E-4H

	Load case 1	Load case 2	Load case 3	Load case 4	Load case 5	Load case 6	Load case 7	Load case 8	Load case 9
Model 4E 90° Airfoil: 4 plies Brackets: 6 plies	1.04  Bracket #2	0.548 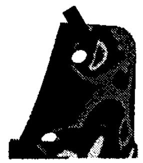 Bracket #1	1.32  Bracket #4	1.38 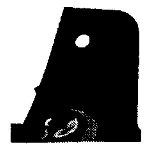 Bracket #2	0.757 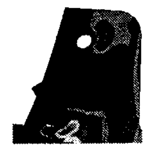 Bracket #2	0.475  Bracket #1	0.967  Bracket #4	1.12 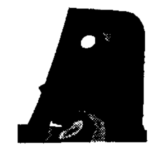 Bracket #2	0.258  Bracket #1
Model 4F 80° Airfoil: 4 plies Brackets: 6 plies	1.01 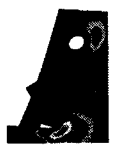 Bracket #2	0. 524  Bracket #1	1.32  Bracket #4	1.48  Bracket #2	0.705  Bracket #2	0.454  Bracket #1	0.938  Bracket #4	1.18  Bracket #2	0.281  Bracket #1
Model 4G 70° Airfoil: 4 plies Brackets: 6 plies	1.04  Bracket #2	0.558  Bracket #1	1.49 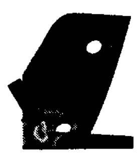 Bracket #4	1.71  Bracket #2	0.713  Bracket #2	0.484 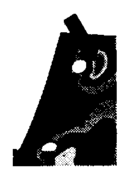 Bracket #1	1.06  Bracket #4	1.35  Bracket #2	0.283 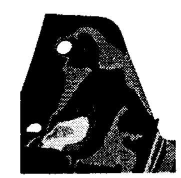 Bracket #1
Model 4H 60° Airfoil: 4 plies Brackets: 6 plies	0.956  Bracket #2	0.482  Bracket #1	1.61 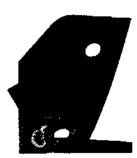 Bracket #4	2.46  Bracket #2	0.632 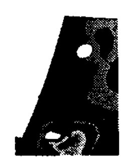 Bracket #2	0.477  Bracket #1	1.13  Bracket #4	1.43  Bracket #2	0.324 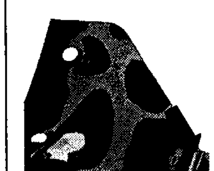 Bracket #1

Table A2.13: Maximum failure indices and their location for models 4I-4L

	Load case 1	Load case 2	Load case 3	Load case 4	Load case 5	Load case 6	Load case 7	Load case 8	Load case 9
Model 4I 90° Airfoil: 4 plies Brackets: 6 plies	1.19 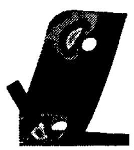 Bracket #2	0.876  Bracket #1	0.604  Bracket #4	0.759 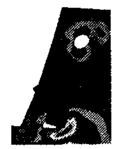 Bracket #3	1.09 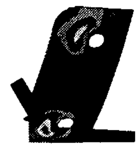 Bracket #2	0.896  Bracket #2	0.535  Bracket #3	0. 721 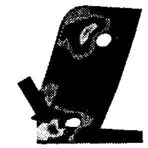 Bracket #2	0.294  Bracket #1
Model 4J 80° Airfoil: 4 plies Brackets: 6 plies	1.08 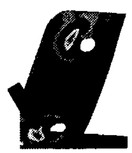 Bracket #2	1.02 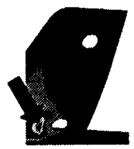 Bracket #1	0.622  Bracket #4	0.823  Bracket #3	1.01 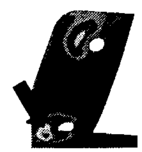 Bracket #2	0.914 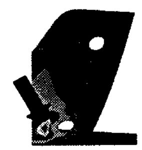 Bracket #1	0.568 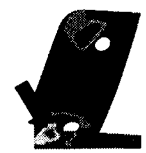 Bracket #2	0.763 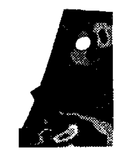 Bracket #3	0.328 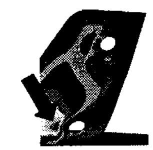 Bracket #1
Model 4K 70° Airfoil: 4 plies Brackets: 6 plies	1.10 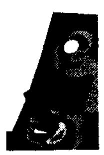 Bracket #3	0.870 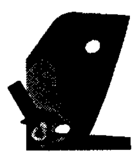 Bracket #1	0.619  Bracket #4	0.923 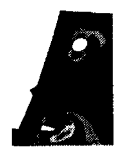 Bracket #3	0.984 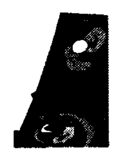 Bracket #3	0.799 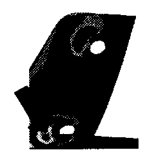 Bracket #2	0.595 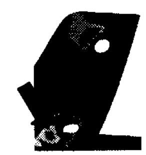 Bracket #2	0.834 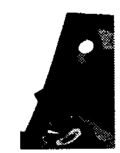 Bracket #3	0.295  Bracket #1
Model 4L 60° Airfoil: 4 plies Brackets: 6 plies	1.12  Bracket #3	1.03 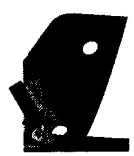 Bracket #1	0.657  Bracket #4	1.08 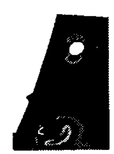 Bracket #3	0.979  Bracket #3	0.923 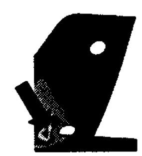 Bracket #1	0.669  Bracket #2	0.961  Bracket #3	0.337  Bracket #1

Table A2.14: Maximum Von Mises stresses and their location for the original aluminium model for the fourth design stage (in psi)

	Load case 1	Load case 2	Load case 3	Load case 4	Load case 5	Load case 6	Load case 7	Load case 8	Load case 9
Original model 	5.77 x 10^4  Bracket #2	3.20 x 10^4  Bracket #1	3.37 x 10^4  Bracket #1	4.44 x 10^4  Bracket #2	4.42 x 10^4  Bracket #2	3.08 x 10^4  Bracket #2	3.02 x 10^4  Bracket #3	4.16 x 10^4  Bracket #2	4.84 x 10^3  Bracket #4

Table A2.15: Maximum Von Mises stress values for aluminium surface models (in psi)

	Load case 1	Load case 2	Load case 3	Load case 4	Load case 5	Load case 6	Load case 7	Load case 8	Load case 9
Model 4M	1.10×10^5	6.60×10^4	7.27×10^4	9.27×10^4	7.50×10^4	3.89×10^4	3.77×10^4	6.50×10^4	1.09×10^4
Model 4N	1.06×10^5	6.56×10^4	7.42×10^4	8.95×10^4	7.17×10^4	3.82×10^4	3.79×10^4	6.25×10^4	1.17×10^4
Model 4P	1.08×10^5	6.66×10^4	7.08×10^4	8.81×10^4	7.32×10^4	3.82×10^4	3.68×10^4	6.29×10^4	1.23×10^4
Model 4Q	1.08×10^5	6.66×10^4	7.07×10^4	8.80×10^4	7.31×10^4	3.82×10^4	3.68×10^4	6.29×10^4	8.09×10^4
Model 4R	1.48×10^5	7.40×10^4	6.59×10^4	1.18×10^5	1.09×10^5	5.84×10^4	4.88×10^4	8.98×10^4	9.93×10^4
Model 4S	1.41×10^5	7.44×10^4	6.20×10^4	1.10×10^5	1.04×10^5	5.69×10^4	4.46×10^4	8.38×10^4	1.45×10^4
Model 4T	1.54×10^5	7.86×10^4	7.05×10^4	1.22×10^5	1.12×10^5	6.03×10^4	4.95×10^4	9.21×10^4	1.53×10^4
Model 4U	1.54×10^5	7.40×10^4	7.45×10^4	1.47×10^5	1.12×10^5	6.37×10^4	5.09×10^4	9.20×10^4	1.58×10^4
Model 4V	1.26×10^5	6.33×10^4	7.62×10^4	1.10×10^5	9.96×10^4	5.45×10^4	5.57×10^4	9.29×10^4	7.82×10^3
Model 4W	1.18×10^5	7.16×10^4	8.77×10^4	1.02×10^5	9.39×10^4	5.14×10^4	6.06×10^4	8.62×10^4	8.34×10^3
Model 4X	1.15×10^5	6.10×10^4	7.44×10^4	1.02×10^5	9.37×10^4	5.32×10^4	5.30×10^4	8.75×10^4	7.74×10^3
Model 4Y	1.01×10^4	6.99×10^4	8.64×10^4	9.13×10^4	8.37×10^4	5.07×10^4	6.06×10^4	7.99×10^4	8.40×10^3

Table A2.16: Minimum margin of safety values for all models of the fourth design stage for all 9 load cases

	Load case 1	Load case 2	Load case 3	Load case 4	Load case 5	Load case 6	Load case 7	Load case 8	Load case 9
Model 4A	-0.109	0.719	-0.0792	0.118	0.279	1.22	0.474	0.502	2.17
Model 4B	-0.123	0.571	-0.118	0.0348	0.283	1.37	0.447	0.391	2.55
Model 4C	-0.136	-0.808	-0.127	-0.0759	0.288	1.51	0.497	0.274	2.52
Model 4D	-0.138	0.81	-0.128	-0.075	0.285	1.9	0.491	0.274	2.52
Model 4E	-0.0141	0.558	-0.117	-0.195	0.258	0.74	0.0362	-0.0673	1.91
Model 4F	0.0125	0.605	-0.158	-0.231	0.33	0.792	0.0648	-0.099	2.04
Model 4G	-0.0122	0.531	-0.232	-0.304	0.324	0.703	-0.0322	-0.18	2.04
Model 4H	0.593	0.678	-0.272	-0.453	0.467	0.709	-0.076	-0.214	1.61
Model 4I	-0.102	0.112	0.514	0.244	-0.046	0.1	0.639	0.304.	1.72
Model 4J	-0.0444	-0.0131	0.483	0.163	0.00382	0.0731	0.543	0.232	1.48
Model 4K	-0.0601	0.117	0.483	0.072	0.0245	0.204	0.489	0.154	1.7
Model 4L	-0.0547	-0.0249	0.417	-0.0285	0.045	0.0647	0.373	0.0535	1.43
Model 4M	-0.500	-0.167	-0.243	-0.407	-0.267	-1.000	0.459	-0.154	4.046
Model 4N	-0.481	-0.162	-0.259	-0.385	-0.233	0.440	0.451	-0.120	3.701
Model 4P	-0.491	-0.174	-0.223	-0.376	-0.249	0.440	0.495	-0.126	3.472
Model 4Q	-0.491	-0.174	-0.222	-0.375	-0.248	0.440	0.495	-0.126	-0.320
Model 4R	-0.628	-0.257	-0.165	-0.534	-0.495	-0.058	0.127	-0.388	-0.446
Model 4S	-0.610	-0.261	-0.113	-0.500	-0.471	-0.033	0.233	-0.344	2.793
Model 4T	-0.643	-0.300	-0.220	-0.549	-0.509	-0.088	0.111	-0.403	2.595
Model 4U	-0.643	-0.257	-0.262	-0.626	-0.509	-0.137	0.081	-0.402	2.481
Model 4V	-0.563	-0.131	-0.278	-0.500	-0.448	0.009	-0.013	-0.402	6.033
Model 4W	-0.534	-0.232	-0.373	-0.461	-0.414	0.070	-0.092	-0.362	5.595
Model 4X	-0.522	-0.098	-0.261	-0.461	-0.413	0.034	0.038	-0.371	6.106
Model 4Y	4.446	-0.213	-0.363	-0.398	-0.343	0.085	-0.092	-0.312	5.548

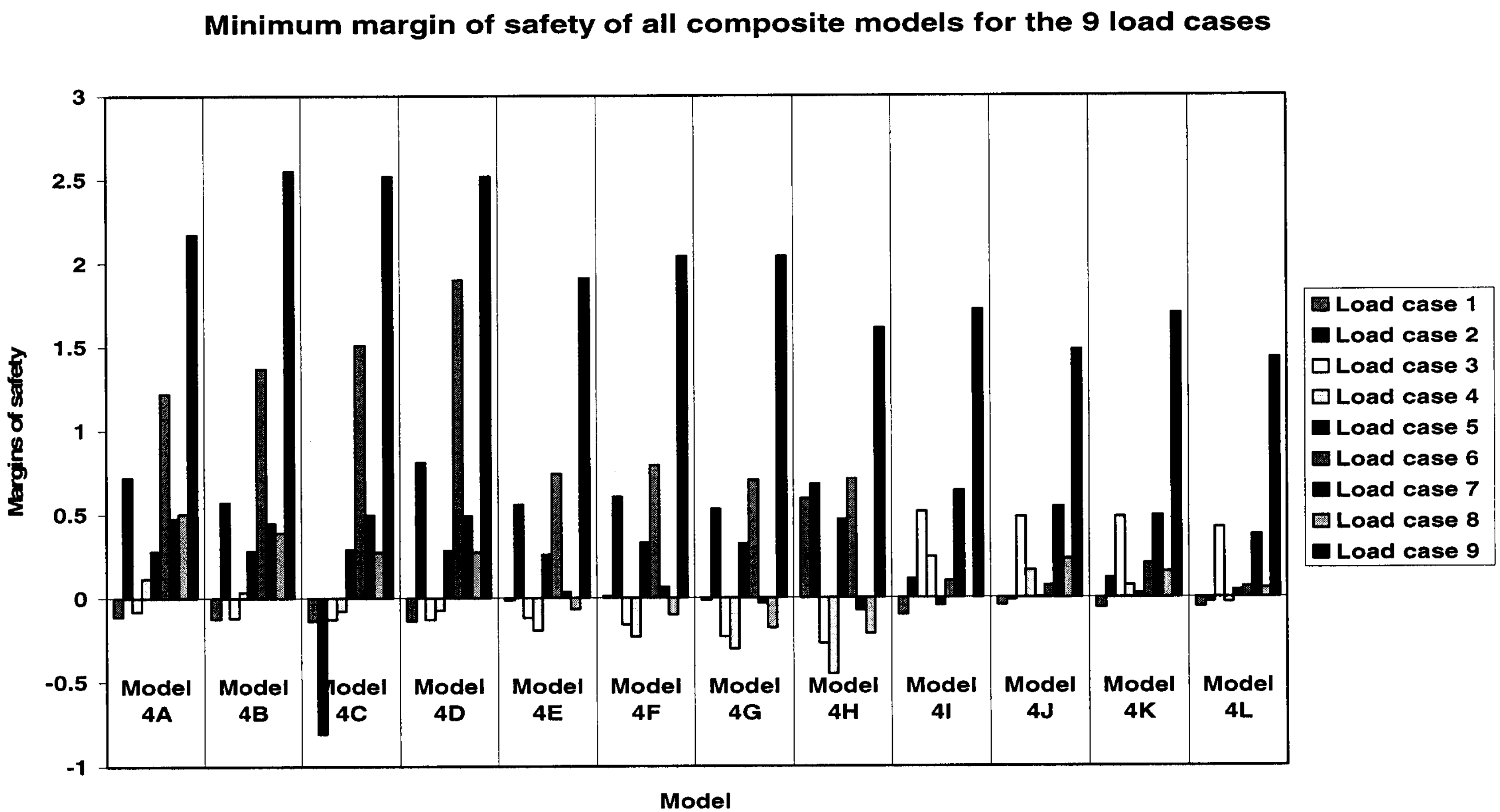

Figure A2.3: Comparative graph of the minimum margin of safety of all composite models for the 9 load cases

Minimum margin of safety of all aluminium surface models for the 9 load cases

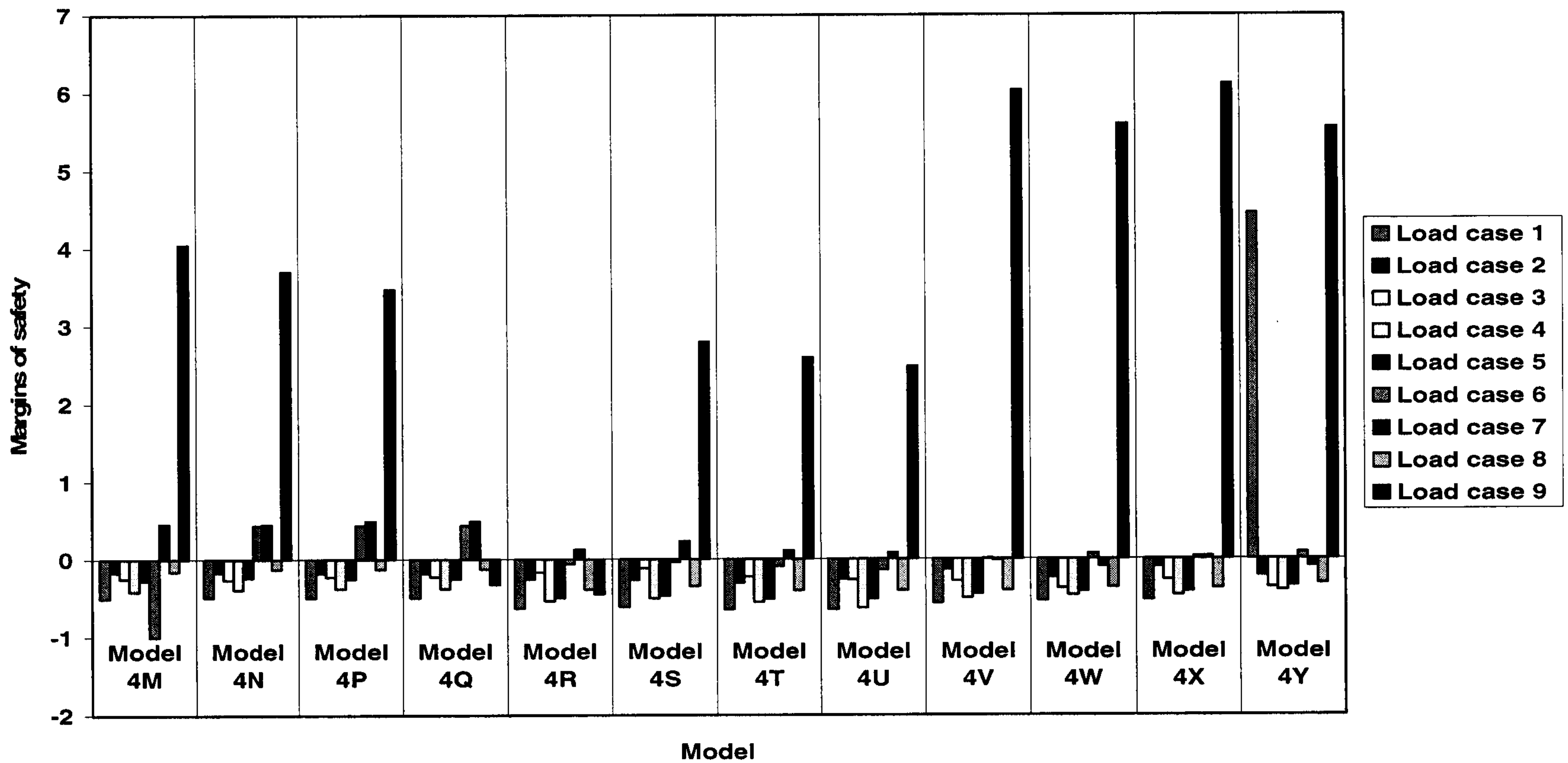

Figure A2.4: Comparative graph of the minimum margin of safety of all aluminium surface models for the 9 load cases